LBL-1403
c.2

DIFFUSION AND PHASE RELATIONSHIP STUDIES IN THE ALUMINA-SILICA SYSTEM

Ilhan A. Aksay

(Ph. D. Thesis)

April 1973

Prepared for the U. S. Atomic Energy Commission
under Contract W-7405-ENG-48

TWO-WEEK LOAN COPY

This is a Library Circulating Copy which may be borrowed for two weeks. For a personal retention copy, call Tech. Info. Division, Ext. 5545

LOAN COPY
Circulates
For 4 weeks
EP Blg 50 Lib Rm 4014
Lawrence Berkeley National Laboratory
c.2
LBL-1403
Copy 2

LAWRENCE BERKELEY LABORATORY
UNIVERSITY OF CALIFORNIA
BERKELEY

DISCLAIMER

This document was prepared as an account of work sponsored by the United States Government. While this document is believed to contain correct information, neither the United States Government nor any agency thereof, nor the Regents of the University of California, nor any of their employees, makes any warranty, express or implied, or assumes any legal responsibility for the accuracy, completeness, or usefulness of any information, apparatus, product, or process disclosed, or represents that its use would not infringe privately owned rights. Reference herein to any specific commercial product, process, or service by its trade name, trademark, manufacturer, or otherwise, does not necessarily constitute or imply its endorsement, recommendation, or favoring by the United States Government or any agency thereof, or the Regents of the University of California. The views and opinions of authors expressed herein do not necessarily state or reflect those of the United States Government or any agency thereof or the Regents of the University of California.

DIFFUSION AND PHASE RELATIONSHIP STUDIES IN THE ALUMINA-SILICA SYSTEM

Contents

Abstract v

I. Introduction 1

II. Mathematics of Diffusion 7

A. Concentration Dependent Diffusion in a Multi-Phase System 11

B. Concentration Independent Diffusion in a Multi-Phase System 16

C. Temperature Dependence of the Diffusion Coefficient . . 20

III. Experimental Work 21

A. Diffusion Experiments 21

1. Sapphire-Fused Silica Couples 21

2. Sapphire-Mullite-Liquid Couples 22

3. Diffusion Cell 23

4. Diffusion Anneals 23

B. Phase Equilibrium Studies by Static Method of Quenching 26

C. Electron Microprobe Analysis 29

D. Densities of SiO_2-Al_2O_3 Melts 31

E. Computer Analysis 33

IV. Results and Analysis 37

A. Densities of SiO_2-Al_2O_3 Melts 37

B. Diffusion Profiles and Phase Equilibria 43

1. Sapphire-Fused Silica Couples 43

2. Sapphire-Mullite-Liquid Couples 47

3. Phase Equilibria 52

C. Diffusion Zone Microstructure of the Sapphire-Fused Silica Couples 56

D. Phase Equilibria by Static Method of Quenching 64

E. Melting Behavior of Mullite 73

F. Stable and Metastable Phase Equilibria 76

G. Diffusion Data 78

1. Diffusion in SiO_2-Al_2O_3 Melts 78

2. Diffusion in Mullite 85

V. Discussion 88

A. Structure of SiO_2-Al_2O_3 Melts 88

B. Diffusion Mechanism in SiO_2-Al_2O_3 Melts 95

C. Diffusion Mechanism in Mullite 100

VI. Conclusions 102

Acknowledgements 105

Appendix: Computer Program for Boltzmann-Matano Analysis 106

References 113

DIFFUSION AND PHASE RELATIONSHIP STUDIES IN THE ALUMINA-SILICA SYSTEM

Ilhan A. Aksay

Inorganic Materials Research Division, Lawrence Berkeley Laboratory
and Department of Materials Science and Engineering,
College of Engineering; University of California,
Berkeley, California 94720

ABSTRACT

Sapphire-fused silica diffusion couples annealed in air or sealed Mo crucibles in the temperature range of 1678° to 2003°C were analyzed by electron beam microprobe. The diffusion profiles were analyzed by the Boltzmann-Matano analysis to determine the diffusion parameters for aluminum-silicate melts and mullite ($3Al_2O_3 \cdot 2SiO_2$). Interfacial compositions across the phase boundaries were used to determine the stable composition range of the mullite phase field, ranging from 70.5 to 74.0 wt% Al_2O_3, and the alumina liquidus. Incongruent melting of mullite, at 1828±10°C, as originally determined by Bowen and Greig (1924) was confirmed. Experiments by the static method of quenching also confirmed the incongruent melting of mullite. However, metastable extension of the mullite field above the peritectic temperature and the metastable solidification of mullite with alumina contents up to 83.2 wt% were easily realized. The extension of the alumina liquidus below the peritectic temperature provided a direct evidence for the metastable existence of a SiO_2-Al_2O_3 binary phase diagram without any mullite phase.

The activation energy for diffusion in the aluminum-silicate melts, above the softening temperature of fused silica, decreased from 211 kcal/mole

for pure silica to 42 kcal/mole at 63.1 mole% Al_2O_3. This substantial change in activation energy for diffusion is attributed to the gradual increase in the ratio of AlO_6/AlO_4 groups with increasing alumina content and thus the formation of non-bridging oxygens. Below the softening point, the activation energy for diffusion in fused silica increases to 338 kcal/mole due to the tightening of the network structure. At 45 mole% Al_2O_3 content, the continuous network structure of fused silica is completely broken down to form discrete anionic groups. High activation energies in fused silica and high-silica melts are attributed to the rupture of M-O bonds of tetrahedrally coordinated silicon and aluminum. Diffusion in high alumina liquids, on the other hand, is by mutual rotation of anionic groups involving only coulombic interaction and thus requires a lower activation energy. The structural model for the SiO_2-Al_2O_3 melts is further supported by the viscosity and density data.

An activation energy of 168±7 kcal/mole was determined for diffusion in mullite.

I. INTRODUCTION

Diffusion studies in condensed phases are of interest because many kinetic processes at elevated temperatures are transport-controlled and thus are governed by diffusion phenomena. A continuum approach to diffusion phenomena[1] neglects the atomistic nature of the diffusion process and provides macroscopic parameters, such as diffusion coefficients, for use in rate equations. An atomistic approach[2-6] provides a broader picture of the diffusion process since it relates these macroscopic parameters to atomic parameters, but a prior understanding of the structure of the phases involved in the diffusion process is required in order to complete the picture by the atomistic approach. However, should this structural information be lacking, the macroscopic parameters determined by the continuum approach, when incorporated with other physical properties, may provide some of the missing information about the structure.

When a diffusion couple is annealed at a sufficiently high temperature, atom mobility is enhanced, and the components of the end phases interdiffuse to achieve a state of chemical equilibrium. The diffusion of the components is in such a direction as to eliminate any chemical potential gradient. At constant T and P, under equilibrium conditions, all the phase fields intersected by the corresponding isotherm and the isobar between the end phases will form as layers in the diffusion zone. The thickness of each layer is dependent upon the growth rate of the corresponding phase. Regardless of its thickness, however, each phase must exist in the diffusion zone in order to provide a continuous and monotonic chemical potential gradient throughout the zone. If diffusion

transport is the rate controlling mechanism, a local chemical equilibrium will exist at each interface. These interfacial compositions, then, correspond to either a liquidus or a solidus composition[7] and can be used to construct the equilibrium phase diagram involving the end phases of the diffusion couple.[8,9]

Having thus outlined the extent of the information one can obtain from a diffusion study, the reason for the choice of the SiO_2-Al_2O_3 system for such a study becomes apparent since (1) limited structural information and diffusion data are available on the binary aluminum silicates, and (2) although this system has been the subject of numerous phase equilibrium studies during the last half century, questions about the melting behavior and about the solid solution range of its intermediate compound, mullite ($3Al_2O_3 \cdot 2SiO_2$), still remain to be answered.

The first systematic study of the SiO_2-Al_2O_3 system was conducted in 1924 by Bowen and Greig[10] who showed that, under atmospheric pressure, mullite ($3Al_2O_3 \cdot 2SiO_2$) but not sillimanite ($Al_2O_3 \cdot SiO_2$) was the only stable compound of this system. Furthermore, it was shown that mullite melted incongruently at 1828°C. The findings of Bowen and Greig were generally accepted without any serious question until 1950, when Bauer et al.[11] were successful in growing mullite single crystals by the Verneuil method. Since single crystals of incongruently melting compounds are not ordinarily produced by this method, the incongruency of mullite was thus questioned. Subsequently in 1951, Toropov and Galakhov[12] provided additional evidence that mullite melted congruently. Since then, numerous conflicting investigations[13-28] have been conducted, some of which supported the incongruency[13-21] as originally determined by Bowen

and Greig and some of which supported the congruency of mullite decomposition.[21-28] Among these, the studies by Trömel et al.[15] and Aramaki and Roy[26] should be mentioned as the most extensive ones. The findings of Trömel et al., in general, are in agreement with those of Bowen and Greig.[10] Aramaki and Roy's[26] diagram (Fig. 1), however, supports the congruent melting of mullite; and, at the present, their study stands out as the generally accepted one. The details of these studies will not be discussed here since this subject matter has been covered by several reviews.[31-35]

In addition to the melting behavior of mullite, a second outstanding problem of the SiO_2-Al_2O_3 system has been the determination of the stable solid solution range of mullite. As shown in the Aramaki and Roy diagram (Fig. 1), mullite, normally, corresponds to a composition of $3Al_2O_3 \cdot 2SiO_2$, and its solid solution range extends from 71.8 wt% to ∿74.3 wt% Al_2O_3. This range, however, is only realized when mullite is prepared by solid state reactions in the presence of alumina. When solidified from a melt, the composition of mullite may extend up to 77.3 wt% Al_2O_3 ($2Al_2O_3 \cdot SiO_2$), a fact which raises the question of metastability.[26] No satisfactory explanation for the fact that high alumina mullite is formed only from a melt has yet been presented.

Most phase equilibrium studies on the SiO_2-Al_2O_3 system have been conducted either by the static method of quenching[36] or by differential thermal analysis (DTA). Difficulties of obtaining accurate phase equilibrium data by these techniques, especially in a silicate system with an incongruently melting compound, have been discussed both by Bowen[37] and Eitel.[38] Because of the sluggish nature of reactions in

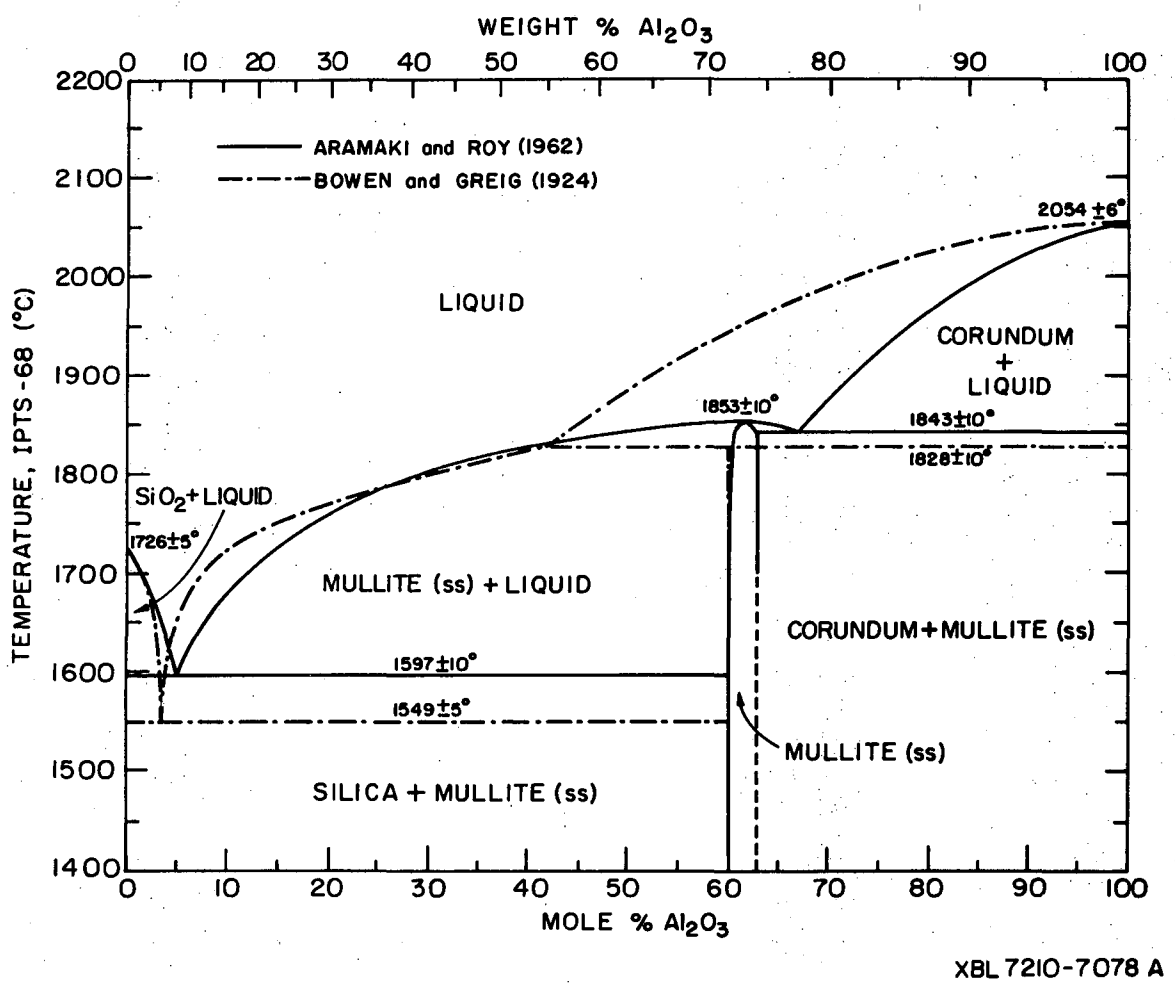

Fig. 1. SiO_2-Al_2O_3 phase diagram as determined by Bowen and Greig[10] and by Aramaki and Roy.[26] The melting temperatures of SiO_2 (cristobalite) and Al_2O_3 (corundum) are by Greig[29] and by Schneider and McDaniel (30), respectively.

silicates, often non-equilibrium crystal phases also occur which have their own metastable equilibrium diagrams. Among the investigators of the SiO_2-Al_2O_3 system, this concept was first indirectly considered by Trömel et al.[15] who argued that although the original work of Bowen and Greig reflected the stable equilibrium, it was possible to obtain a metastable congruent liquidus by means of supercooling of the liquids without any alumina precipitation. This concept was strongly rejected by Aramaki and Roy[26] on the grounds that precipitation of corundum with a relatively simple structure would occur readily when it is the equilibrium phase. Aramaki and Roy's[26] argument, however, should now be considered with reservation since recent studies have shown that liquid alumina itself can be supercooled as much as 200°C.[39-41] Furthermore, if supercooling of the silicates with high alumina contents is indeed a possibility, any data obtained by the conventional quenching technique or DTA should be reviewed critically.

In a recent diffusion study, Davis and Pask,[42] utilizing semi-infinite couples of silica and alumina and the electron microprobe for determining composition profiles, demonstrated the power of this technique for obtaining not only diffusion data but accurate stable and metastable phase equilibrium data as well. These studies, however, were confined to the temperature range of 1552° to 1803°C (Fig. 1), below the melting point of mullite, with particular emphasis on the diffusion kinetics in the high-silica liquids.

The objectives of the present study were to extend the studies of Davis and Pask above the melting temperature of mullite in order (1) to obtain diffusion data not only on the high-silica liquids, but also on

the high-alumina liquids, and (2) to determine the phase equilibria in this portion of the system by a technique not handicapped by the deficiencies of the techniques utilized in the previous phase equilibria studies. Furthermore, diffusion studies below the melting temperature of mullite were also conducted in order (1) to determine the stable solid solution range of mullite, and (2) to study diffusion kinetics in the mullite phase.

II. MATHEMATICS OF DIFFUSION

The kinetics of diffusion can be interpreted by means of the well-known Fick's first and second laws for the one-dimensional case:

$$J = - D\left(\frac{\partial c}{\partial x}\right) \tag{1}$$

$$\frac{\partial c}{\partial t} = \frac{\partial}{\partial x}\left(D\frac{\partial c}{\partial x}\right) \tag{2}$$

where J is the net flux of the diffusing species passing through unit area of a plane normal to the x-direction in unit time (gm/cm^2-sec), c is the concentration of this species per unit volume (gm/cm^3), t is the time (sec), and D is the diffusion coefficient (cm^2/sec). In these relationships, concentration rather than the chemical potential gradient is generally used because of the ease in determining the former.

In a diffusion couple of non-ionic substances, when two species intermingle, the rate of mixing is dependent upon the self-diffusion rates of both species. In such a case, D as determined from the above equations is the interdiffusion coefficient and can be related to the self-diffusion coefficients through Darken's equations.[43] Diffusion in ionic substances, however, has a restriction since a local space charge neutrality has to be maintained. The measured interdiffusion coefficient, then, is not only dependent on the self-diffusion rates but also on the ionic charge of the diffusing species. The relationship between self-diffusion and the interdiffusion coefficients in ionic systems has been

discussed by Cooper and Heasley.[44]

As expressed in Eq. (2), D is concentration dependent. In the SiO_2-Al_2O_3 system, diffusion in the liquid phase above the melting temperature of mullite extends over a wide concentration range (Fig. 2); thus D would normally be expected to be concentration dependent. Davis and Pask[42] have shown that D is concentration dependent in the high silica liquids of the SiO_2-Al_2O_3 system. The solid solution range of the mullite phase, however, is very small ($\sim$3 mole%) (Fig. 3); the assumption that D is independent of composition in this case thus is satisfactory. Diffusion mathematics of these two cases is outlined in the following sections.

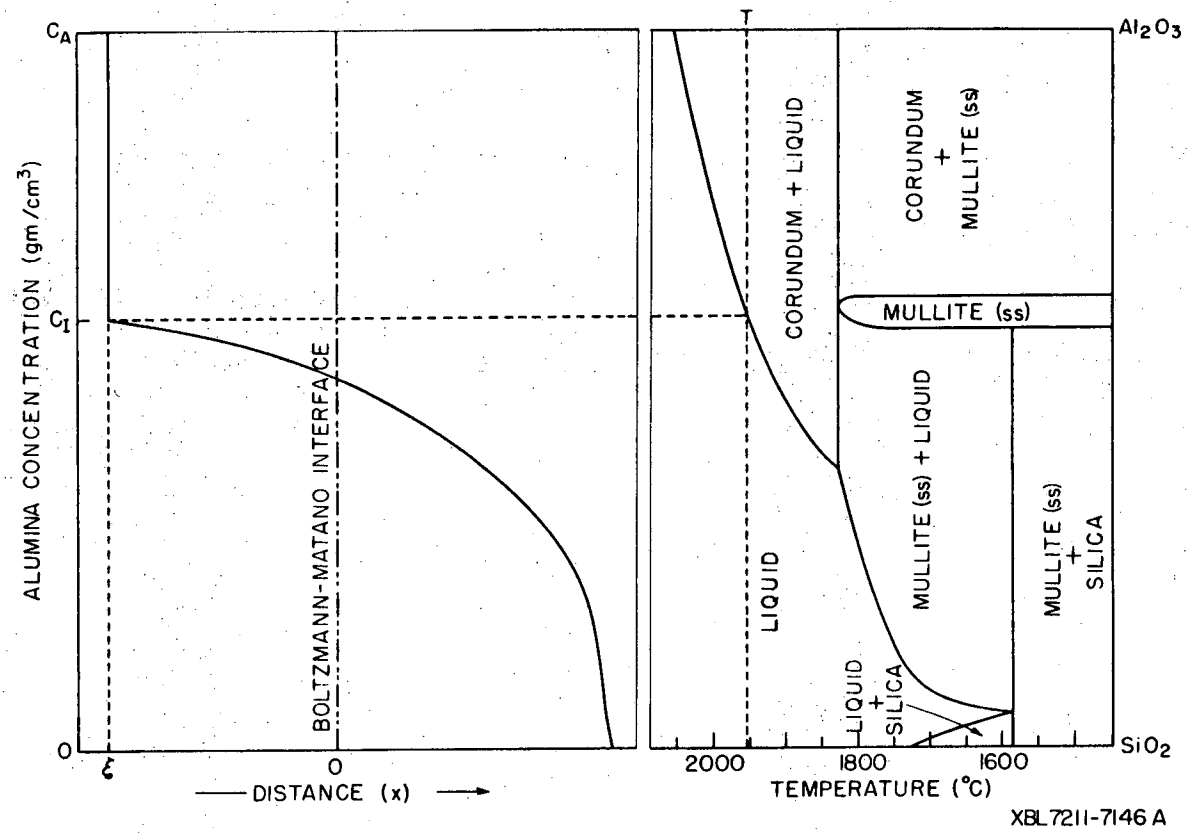

Fig. 2. The relationship between the concentration profile of a semi-infinite SiO_2-Al_2O_3 diffusion couple and the phase diagram, at temperature T above the melting point of mullite. Boltzmann-Matano interface corresponds to the phase boundary at t = o.[45-46]

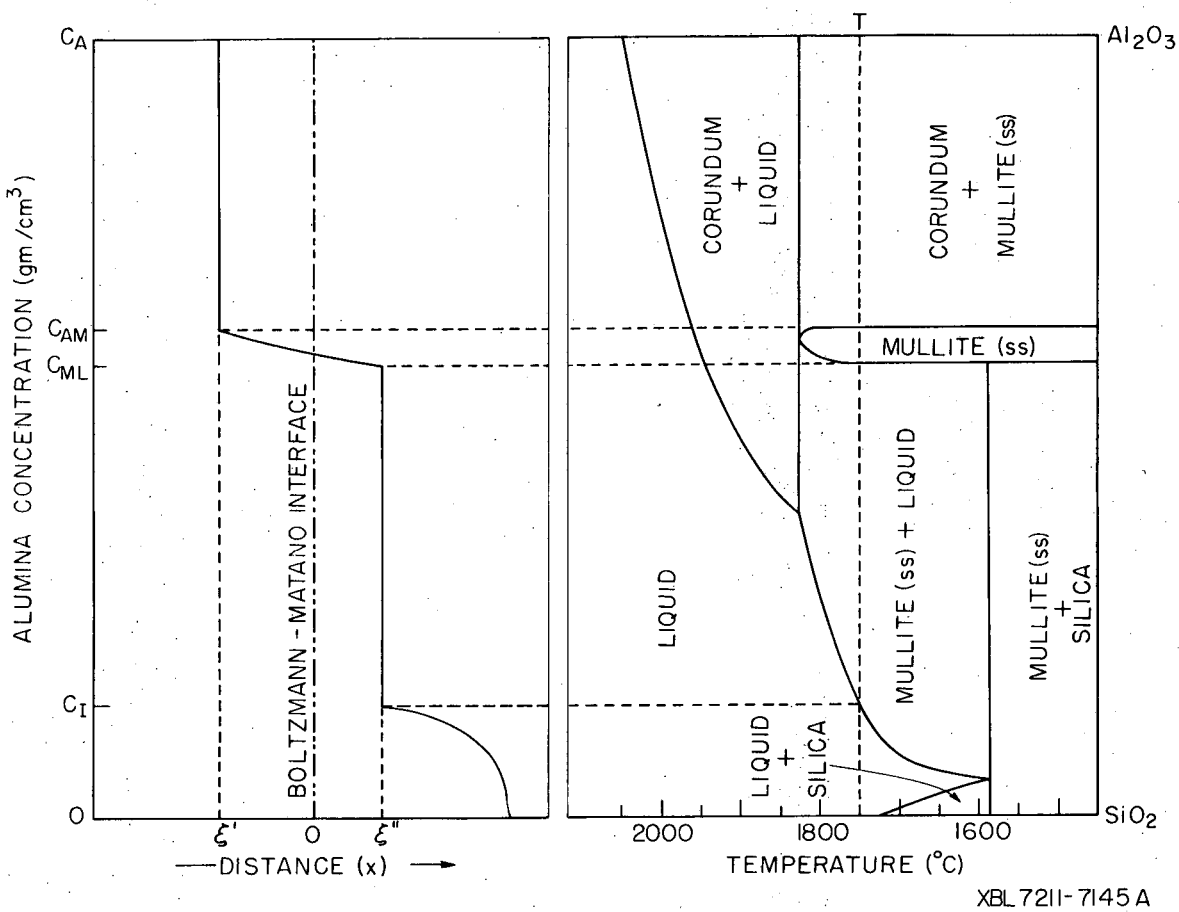

Fig. 3. The relationship between the concentration profile of a semi-infinite SiO_2-Al_2O_3 diffusion couple and the phase diagram, at temperature T below the melting point of mullite. Boltzmann-Matano interface corresponds to the phase boundary at t = o.[45-46]

A. Concentration Dependent Diffusion in a Multi-Phase System

Boltzmann[45] has treated the case where a pair of semi-infinite media form one phase so that $c(x,t)$ is a continuous function with continuous derivatives for all $t>o$ and $-\infty<x<+\infty$. If diffusion transport is rate controlling, $c \equiv c(xt^{-1/2})$ only, then by substituting $\lambda = xt^{-1/2}$, Eq. (2) can be transformed into an ordinary homogeneous differential equation:

$$\frac{\partial c}{\partial t} = \left(\frac{\partial c}{\partial \lambda}\right)\left(\frac{\partial \lambda}{\partial t}\right) = -\frac{x}{2t^{3/2}}\left(\frac{\partial c}{\partial \lambda}\right) \tag{3}$$

$$\frac{\partial c}{\partial x} = \left(\frac{\partial c}{\partial \lambda}\right)\left(\frac{\partial \lambda}{\partial x}\right) = \frac{1}{t^{1/2}}\left(\frac{\partial c}{\partial \lambda}\right), \text{ and} \tag{4}$$

$$\frac{\partial}{\partial x} = \frac{\partial}{\partial x}\left(\frac{\partial \lambda}{\partial x}\right) = \frac{1}{t^{1/2}}\left(\frac{\partial}{\partial \lambda}\right). \tag{5}$$

Substituting Eqs. (3) to (5) into Eq. (2), one obtains

$$-\frac{\lambda}{2}\left(\frac{\partial c}{\partial \lambda}\right) = \frac{\partial}{\partial \lambda}\left(D\frac{\partial c}{\partial \lambda}\right). \tag{6}$$

Experimentally, $c(x)$ is always determined at a constant time, t, thus

$$-\frac{xdc}{2} = d\left(Dt\frac{dc}{dx}\right). \tag{7}$$

Now, if $c(x)$ is continuous with continuous derivatives over the entire range, $-\infty<x<+\infty$ (Fig. 4), Eq. (7) may be integrated with respect to c

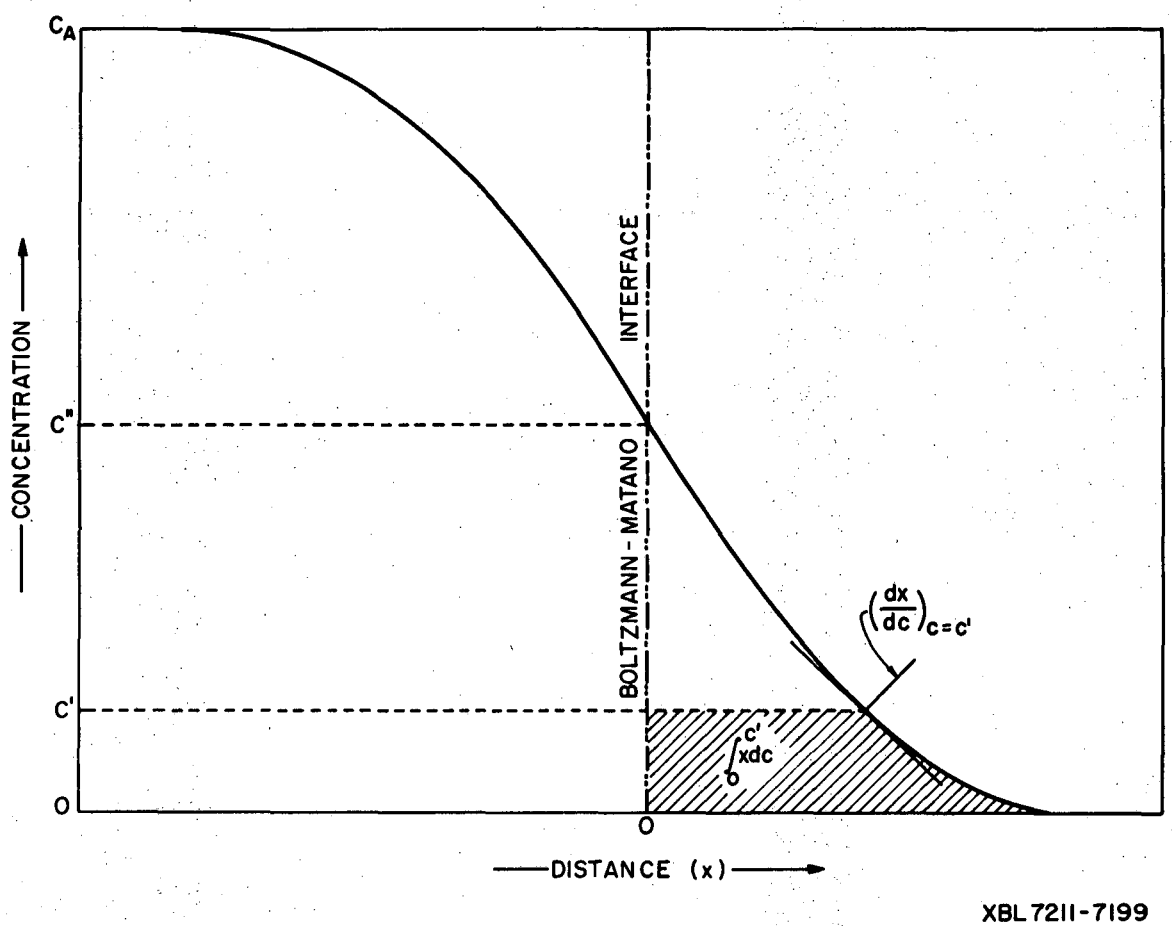

Fig. 4. A continuous concentration vs distance profile and the parameters that have to be determined graphically for the solution of Eq. (12).

from o to c', where $o<c'<c_A$ and the initial conditions are

$$c = c_A \text{ for } -\infty<x<o \tag{8}$$

$$c = o \text{ for } o<x<\infty \ , \tag{9}$$

$$\int_o^{c'} -\frac{xdc}{2} = t\left[D(c')\left(\frac{dc}{dx}\right)_{c=c'}\right] - t\left[D(o)\left(\frac{dc}{dx}\right)_{c=o}\right] . \tag{10}$$

Since

$$\left(\frac{dc}{dx}\right)_{c=o} = \left(\frac{dc}{dx}\right)_{c=c_A} = o, \tag{11}$$

$$D(c') = -\frac{1}{2t}\left(\frac{dx}{dc}\right)_{c=c'} \int_o^{c'} xdc \ . \tag{12}$$

If the above integration is carried from c = o to $c = c_A$,

$$\int_o^{c_A} xdc = o \tag{13}$$

where $-\infty<x<+\infty$. Equation (13) sets the condition for x = o for the evaluation of the integral in Eq. (12), i.e.

$$\int_o^{c''} xdc = \int_{c''}^{c_A} (-x)dc \tag{14}$$

where $c=c''$ at $x=o$ (Fig. 4). This $x=o$ interface is usually called the Boltzmann-Matano interface,[46] which corresponds to the plane of mass balance of the diffusing species. Thus, if a pair of semi-infinite media is annealed at a constant T and P for a certain time interval and the concentration profile is obtained by experimental means, $D(c')$ of Eq. (12) can be determined by measuring $\left(\frac{dx}{dc}\right)$ and $\int_o^{c'} xdc$ graphically (Fig. 4). Furthermore, since c is a function of λ only, at a constant composition, $\lambda=xt^{-1/2}$ must also be a constant. Then, the basic requirement of the Boltzmann-Matano analysis, i.e. that diffusion is rate controlling, may be verified by plotting values of x at a given composition versus the corresponding values of $t^{1/2}$. If the process is diffusion controlled, a straight line relationship has to be obtained.

The Boltzmann-Matano analysis as presented above, however, is not applicable to a multi-phase system since $c(x)$ is not continuous with continuous derivatives over the entire range, $-\infty<x<+\infty$ (Fig. 5). A modified solution of the above method for a pair of semi-infinite media of two different phases has been first presented by Jost[47] and more recently by Appel.[48] In this case, the condition which determines the $x=o$ interface (Fig. 5) becomes

$$\int_o^{c_1} xdc + (c_2-c_1)\xi + \int_{c_2}^{c_3} xdc = o \qquad (15)$$

where ξ is measured from $x=o$. Thus, up to the discontinuity, i.e. for $c'<c_1$, Eq. (12) applies, and for $c'>c_1$ including the discontinuity

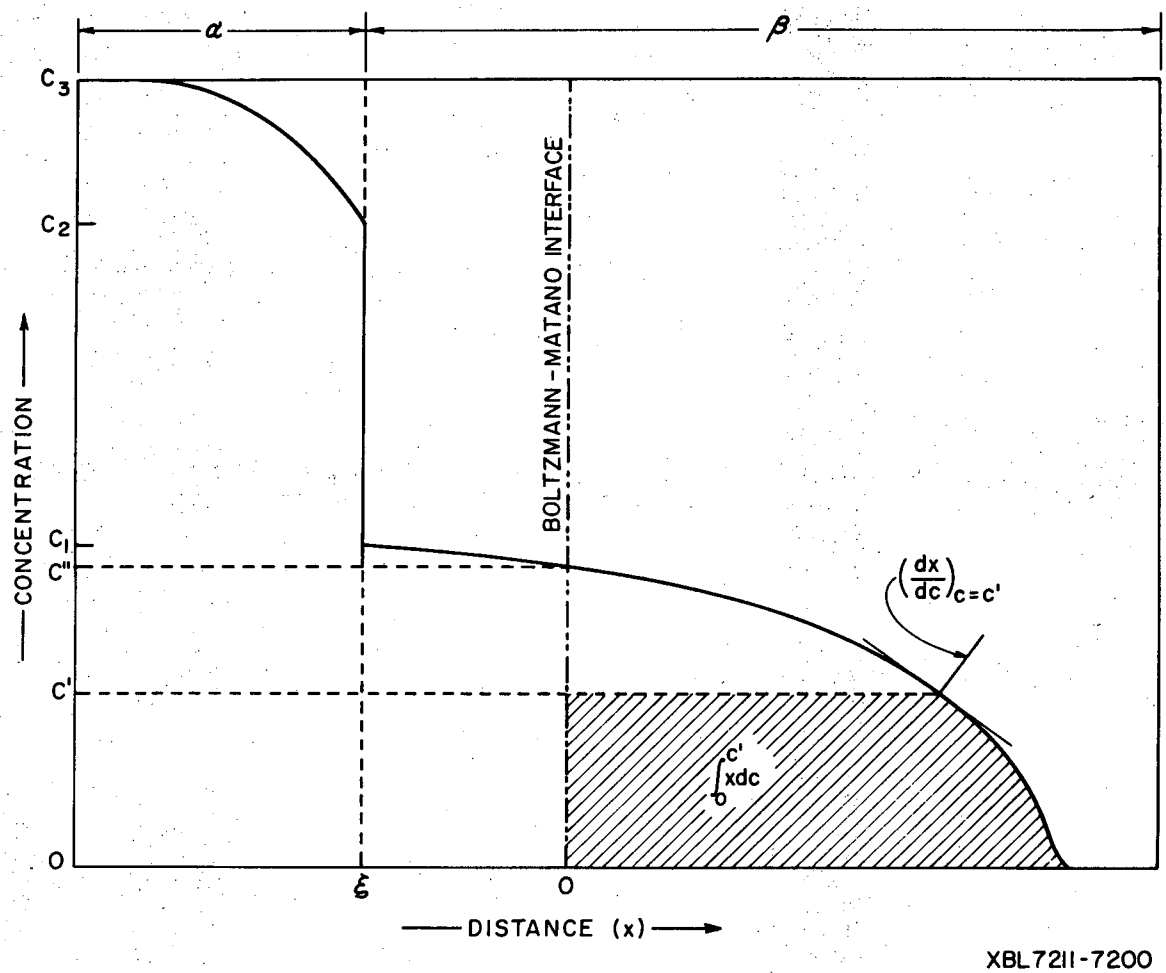

Fig. 5. A discontinuous concentration vs distance profile of a semi-infinite diffusion couple between phases α and β and the parameters that have to be determined graphically for the solution of Eq. (16).

$$D(c') = -\frac{1}{2t}\left(\frac{dx}{dc}\right)_{c=c'}\left[\int_{o}^{c_1} xdc + (c_2-c_1)\,\xi + \int_{c_2}^{c'} xdc\right]. \quad (16)$$

The interdiffusion coefficient, $D(c')$ is again determined graphically (Fig. 5).

B. Concentration Independent Diffusion in a Multi-Phase System

The Boltzmann-Matano solution as presented above is also applicable to this case. When the interdiffusion coefficient, D, however, is concentration independent, a more straightforward approach can be followed without an explicit determination of the concentration profile $c(x,t)$ through the phases. A solution to this case was first presented by Gibbs[49] based on a more general solution of Kidson.[50,51]

In a three-phase system with two moving boundaries (Fig. 6), the movement of the phase interfaces ξ' and ξ'' with respect to the Boltzmann-Matano interface is described by

$$(c_4-c_3)\,\frac{d\xi'}{dt} = D_\beta\left(\frac{\partial c}{\partial x}\right)_3 - D\alpha\left(\frac{\partial c}{\partial x}\right)_4 \quad (17)$$

$$(c_2-c_1)\,\frac{d\xi''}{dt} = D_\gamma\left(\frac{\partial c}{\partial x}\right)_1 - D_\beta\left(\frac{\partial c}{\partial x}\right)_2 \quad . \quad (18)$$

Wagner[52] has shown that the plane of discontinuity is shifted in proportion to $t^{1/2}$,

$$\xi' = 2\gamma_A\,(D_\beta t)^{1/2} \quad (19)$$

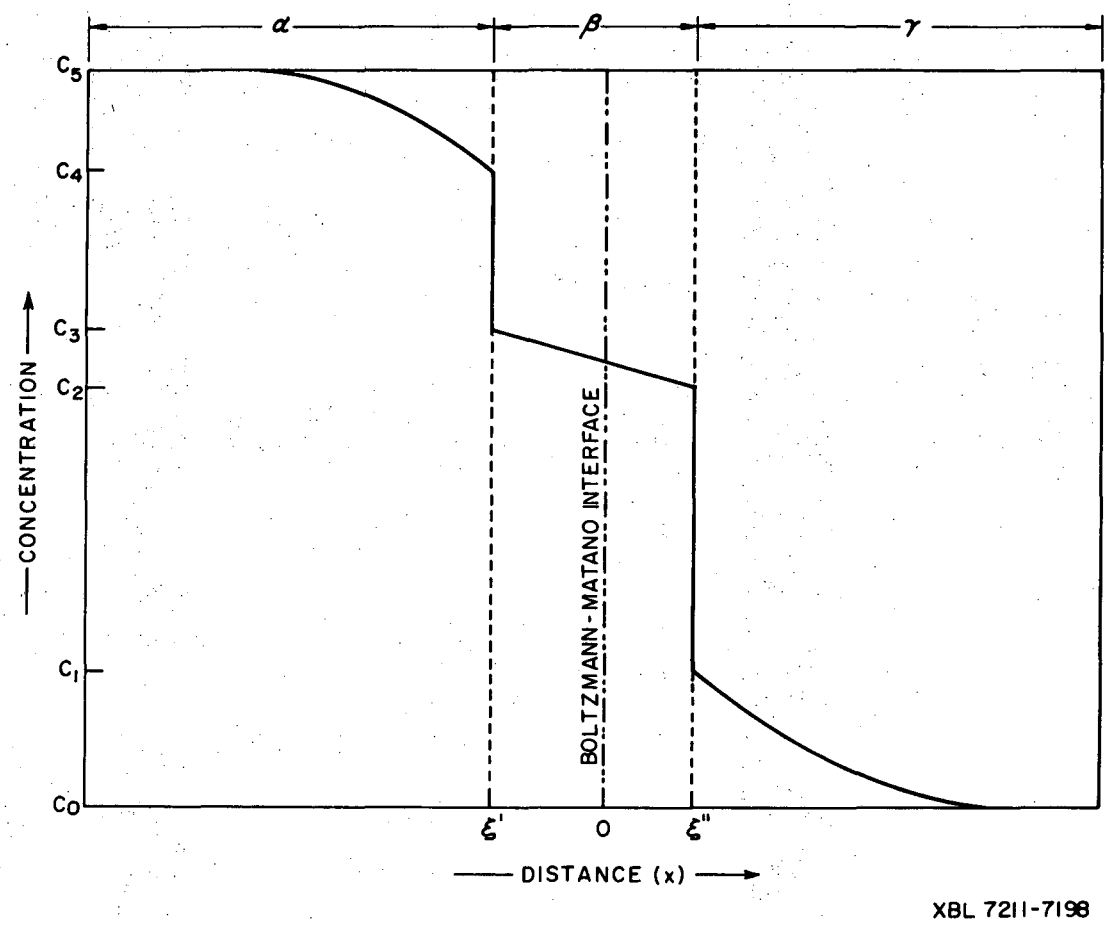

Fig. 6. Concentration vs distance profile of a semi-infinite diffusion couple between phases α and γ where the growth of an intermediate phase β is realized.

$$\xi'' = 2\gamma_B \, (D_\beta t)^{1/2}, \tag{20}$$

where γ_A and γ_B are constants. Particular integrals of Eq. (2) are:

(1) in the α-phase

$$c = c_5 - \frac{(c_5 - c_4)}{1 + \operatorname{erf} \gamma_A \, (D_\beta/D_\alpha)^{1/2}} \left\{ 1 + \operatorname{erf} x \, (4D_\alpha t)^{-1/2} \right\} \tag{21}$$

(2) in the β-phase

$$c = c_3 - \frac{(c_3 - c_2)}{\operatorname{erf} \gamma_B - \operatorname{erf} \gamma_A} \left\{ \operatorname{erf} x \, (4D_\beta t)^{-1/2} - \operatorname{erf} \gamma_A \right\} \tag{22}$$

(3) in the γ-phase

$$c = c_0 + \frac{(c_1 - c_0)}{1 - \operatorname{erf} \gamma_B (D_\beta/D_\gamma)^{1/2}} \left\{ 1 - \operatorname{erf} x \, (4D_\gamma t)^{-1/2} \right\} . \tag{23}$$

Substituting $\frac{d\xi}{dt}$ and $\frac{\partial c}{\partial x}$ from Eqs. (19) to (23) into Eqs. (17) and (18),

$$(c_4 - c_3)\gamma_A = \left(\frac{D\alpha}{D\beta}\right)^{1/2} \left\{ \frac{(c_5 - c_4)}{1 + \operatorname{erf} \left[\gamma_A (D_\beta/D_\alpha)^{1/2} \right]} \right\} \left\{ \pi^{-1/2} \exp \left[-\gamma_A^2 \left(\frac{D\beta}{D\alpha} \right) \right] \right\}$$

$$+ \frac{(c_2 - c_3)}{\operatorname{erf} \gamma_B - \operatorname{erf} \gamma_A} \left\{ \pi^{-1/2} \exp \left(-\gamma_A^2 \right) \right\} \tag{24}$$

$$(c_2-c_1)\gamma_B = \left(\frac{D\gamma}{D\beta}\right)^{1/2} \left\{\frac{(c_0-c_1)}{1 - \text{erf}\ \gamma_B(D_\beta/D_\gamma)^{1/2}}\right\} \left\{\pi^{-1/2} \exp\left[-\gamma_B^2\left(\frac{D\beta}{D\gamma}\right)\right]\right\}$$

$$+ \frac{(c_3-c_2)}{\text{erf}\ \gamma_B - \text{erf}\ \gamma_A} \left\{\pi^{-1/2} \exp\ (-\gamma_B^2)\right\} . \qquad (25)$$

When the particular emphasis is on the diffusion kinetics in the intermediate phase, i.e. mullite, Eqs. (24) and (25) can be simplified if $c_4 = c_5$ and $c_0 = c_1$ (Fig. 6). Then,

$$\frac{c_2-c_3}{c_5-c_3} = \gamma_A\pi^{1/2} \exp\ (\gamma_A^2)(\text{erf}\ \gamma_B - \text{erf}\ \gamma_A) \qquad (24a)^*$$

$$\frac{c_3-c_2}{c_2-c_1} = \gamma_B\pi^{1/2} \exp\ (\gamma_B^2)(\text{erf}\ \gamma_B - \text{erf}\ \gamma_A) . \qquad (25a)^*$$

Equations (24a) and (25a) may be solved graphically to determine γ_A and γ_B. From Eqs. (19) and (20),

$$D_\beta = \frac{(\xi''-\xi')^2}{4(\gamma_B-\gamma_A)^2\ t} . \qquad (26)$$

---

*Solutions to this limiting case have also been provided by Wagner and presented by Jost,[2] p. 75, Eqs. (1.332) and (1.333). However, typographical errors appear in Wagner's solutions.

Concentration independent diffusivity in the β-phase can then be determined from Eq. (26) by directly measuring the thickness of the intermediate layer if the equilibrium solution limits are known.

C. Temperature Dependence of the Diffusion Coefficient

Interdiffusion coefficient values to be generated by the methods of the previous sections are of practical importance since they can be directly used to predict the kinetic processes in industrial applications. A greater importance of interdiffusion coefficients, however, lies in the information they yield about the migration mechanism of the diffusing species. Generally, the diffusion coefficients are expressed in the form of an Arrhenius equation,[53,54]

$$D = D_o \exp(-\frac{Q}{RT}) \tag{27}$$

where D_o is the temperature independent pre-exponential constant, Q is the activation energy, R is the gas constant, and T is the absolute temperature. D_o and Q have different meanings for different diffusion mechanisms. The pre-exponential factor D_o contains the mean free path of atomic movement, the lattice vibration frequency, and the entropy of activation as $\exp(\Delta S/R)$. Converting Eq. (27) to logarithmic form gives

$$\ln D = \ln D_o - \frac{Q}{RT}, \tag{28}$$

thus Q and D_o can be determined by plotting ln D versus 1/T.

III. EXPERIMENTAL WORK

A. Diffusion Experiments

1. Sapphire-Fused Silica Couples

Sapphire-fused silica couples have been used to study the diffusion kinetics in the liquid phase. The couples were prepared from single crystals (8.7 mm in diameter by 1.6 mm) of Al_2O_3 (sapphire)* and fused silica disks (9 mm in diameter by ∿7 mm) of lowest water content, sold under the trade name "Amersil."† The sapphire single crystals were cut with the c-axis oriented ∿30° from the vertical and had an as-received surface finish of ∿0.27 μm. The fused silica disks were subjected to a standard ceramographic polishing on one surface. Polishing consisted of approximately 10 min each on 45, 30, 15, and 6 μm metal-bonded diamond laps,** 24 h of vibratory≠ polishing in a slurry of 6 μm diamond particles and 24 h of final vibratory polishing in a slurry of 1 μm diamond particles.

---

*Union Carbide Corp., Torrance, Calif. Spectrographic analysis by American Spectrographic Labs., San Francisco, Calif.: as oxides (wt%) Si 0.210, Na 0.050, Sn 0.005, B 0.005, Fe 0.004, Ba 0.001, Ca 0.001, Ti 0.001, Mg 0.0005, Cu 0.0005.

†Amersil, Division of Engelhard Industries, Inc., Hillside, N.J. Spectrographic analysis by American Spectrographic Labs., San Francisco, Calif.: as oxides (wt%) Al 0.045, Fe 0.015, Mg 0.0007, Ca 0.0005, Cu 0.0005.

**Minnesota Mining and Manufacturing Co., So. San Francisco, Calif.

≠Syntron Division, FMC Corp., Homer City, Pa.; Vibratory polishing machine.

2. Sapphire-Mullite-Liquid Couples

Aluminum-silicate glasses of 10.9, 22.8, and 42.2 wt% Al_2O_3 were prepared using high purity powders of Alcoa XA-16* reactive α-Al_2O_3 and -325 mesh Corning 7940 fused silica.≠ The powders were intimately mixed in isopropyl alcohol, dried at 90°C, calcined at 1000°C for 10 h, vacuum melted in open molybdenum crucibles at 1900°C for 30 to 60 min and quenched in He to room temperature in less than 5 min. The calcination stage at 1000°C and a slow heating rate to the fusion temperature were necessary to decompose the hydroxyls of the fused silica powder. Formation of a melt before the elimination of the hydroxyls resulted in excessive bubble formation. Rods, 9 mm in diameter, were core-drilled, cut into 7 mm thick sections and polished on one side. A representative section of each glass was analyzed by electron microprobe, and the compositions were found to be within 1 wt% of the starting value.

These glasses are in equilibrium with mullite at 1678°, 1753°, and 1813°C according to the mullite liquidus of Davis and Pask.[42] Thus, the alumina-glass diffusion couples of these compositions at the corresponding annealing temperatures could be used to study the growth kinetics of mullite as an intermediate phase, without any dissolution in the end phases (Section IIB).

---

*Aluminum Co. of America, Pittsburgh, Pa. Chemical analysis (wt%) Na_2O 0.08, SiO_2 0.05, CaO 0.03, MgO 0.05, Fe_2O_3 0.01, MnO 0.0015, B_2O_3 <0.001, Cr_2O_3 0.0002.

≠Corning Glass Works, Corning, N.Y. Produced by hydrolyzation of $SiCl_4$ when spraying into an oxygen-hydrogen flame. Practically free from metallic impurities, but contains a high amount of OH (∿1000 ppm) and Cl (∿100 ppm).

3. Diffusion Cell

The diffusion cell arrangement consisted of molybdenum or alumina crucibles containing a fused silica or aluminum-silicate glass disk on a sapphire substrate (Fig. 7). Molybdenum crucibles with 9.1 mm ID and ∿11 mm internal height were machined from high purity rods 12.7 mm in diameter. Some of the runs at 1678°C were done in air with covered alumina crucibles* of comparable dimensions. Prior to a cell assemblage, the polished surfaces of the diffusion couple parts were checked for flatness against their counterparts to effect good bonding and prohibit the entrapment of helium or air in an irregular surface. The crucibles and the diffusion couple parts were cleaned ultrasonically in ethyl alcohol. The molybdenum crucibles were sealed around the lid by electron beam welding (Fig. 7) and He leak checked. This sealing was necessary to eliminate silica losses by evaporation during annealing. An assembly of as many as six couples could be run during each annealing by stacking the crucibles with spacers in between. The crucible assembly was covered with a thick wall Mo crucible to ensure temperature uniformity. A similar arrangement of alumina crucibles was used at 1678°C in air runs.

4. Diffusion Anneals

A tantalum resistance heating furnace** with a heating zone 10 cm in diameter by 20 cm was used for all the anneals above 1700°C. The diffusion cell assembly as shown in Fig. 7 was placed on a Mo support

---

*Coors Porcelain Company, Golden, Colo. Crucible CN-2, AD998 (99.8 wt% Al_2O_3).
**Richard D. Brew and Co., Inc., Concord, N.H.; Model 1466S-4.

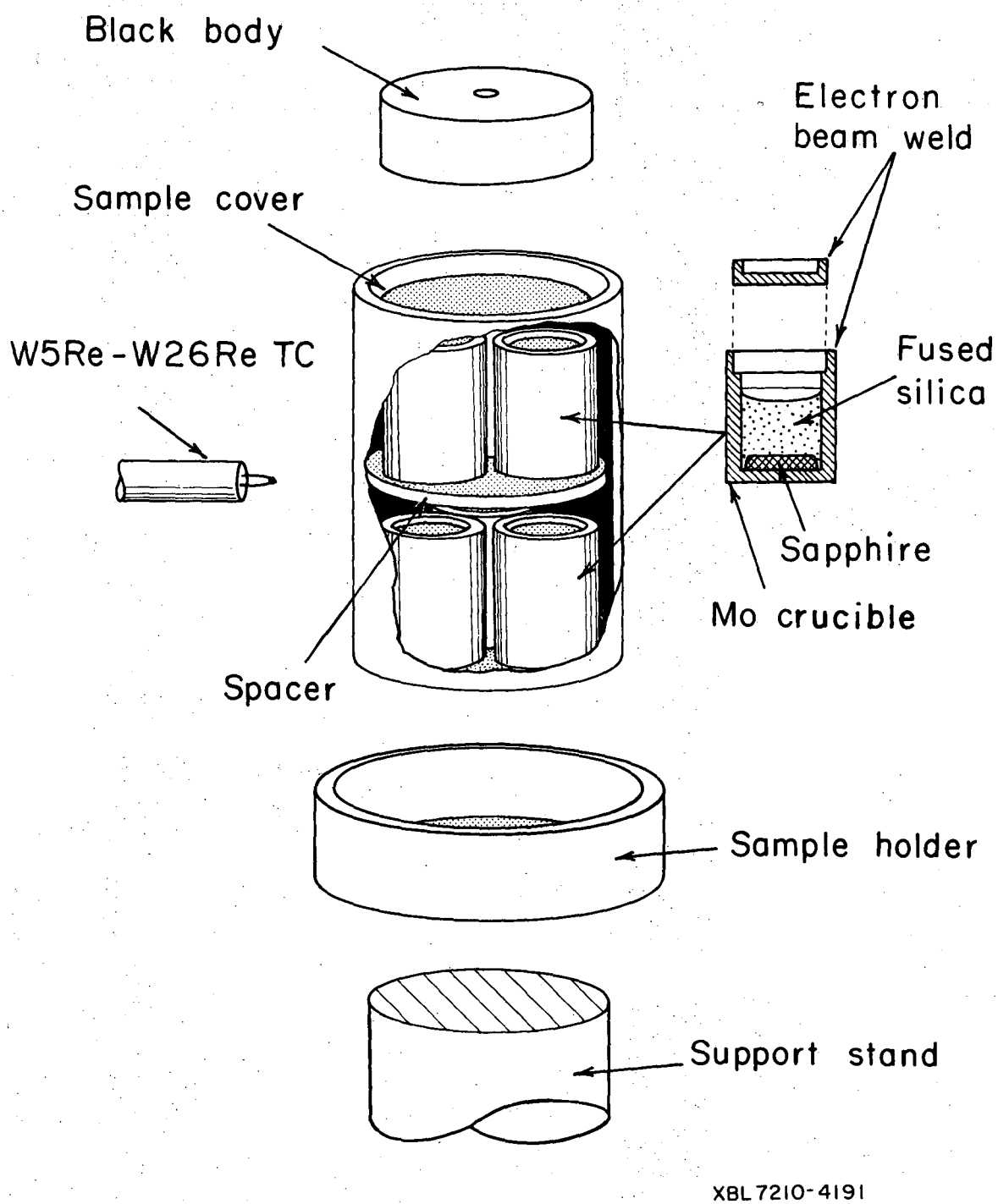

Fig. 7. Diffusion cell assembly. All of the container parts are molybdenum.

stand and heated to 1200°C at 10^{-6} mm Hg. The chamber was then filled with helium slightly below atmospheric pressure, and the temperature was rapidly raised (2-3 min) to the annealing point to avoid chemical bond formation at the interface at lower temperatures and subsequent cracking of the sapphire due to thermal expansion differences between sapphire and fused silica.

The diffusion anneals ranged from 15 min to a month, depending on the diffusion zone length. The principal temperature range was from 1753° to 2003°C. The temperature of the tantalum chamber was monitored and controlled by a Leeds and Northrup Speedomax-H Recorder-Controller* (precision ± 1°C) through a W5Re-W26Re thermocouple (accuracy ± 7° at 1800°C). The specimen temperature, however, was measured separately with two Leeds and Northrup optical pyrometers* (accuracy ± 10° at 2000°C) utilizing black body conditions. The pyrometers were frequently calibrated against an NBS secondary standard pyrometer (No. 8632-C, NBS No. 4172312; accuracy ± 3°C) and at the melting point of platinum≠ (1772°C)[55] and Al_2O_3 (2054°C).[30] The melting temperature of Al_2O_3 was verified within 2° utilizing black body conditions with a hole core-drilled directly into a sapphire crystal. Furthermore, the pyrometers themselves were frequently checked against each other to detect any malfunction. All the temperatures reported here are based on the 1968 International Practical Temperature Scale (IPTS-68).[55]

---

*Leeds & Northrup Co., Philadelphia, Pa.

≠NBS standard platinum was provided by K. S. Mazdiyasni, Air Force Materials Lab., Wright-Patterson Air Force Base, Ohio.

A Kanthal Super 33* resistance heating furnace was used for the air runs at 1678°C. The furnace was loaded at 1200°C and raised to the annealing temperature in ∿45 min. The furnace temperature was monitored and controlled by a Honeywell Electro-O-Volt 18 Recorder-Controller** (precision ± 1°C) through a Pt6Rh-Pt30Rh thermocouple (accuracy ± 5° at 1650°C). The specimen temperature was separately measured and recorded with a Honeywell Electronik 193 Recorder** through a Pt6Rh-Pt30Rh thermocouple.

The diffusion anneals were completed by rapidly cooling the furnaces down to 1500°C (∿1 min) to prevent excessive crystallization in the diffusion zone. Continued cooling to room temperature, however, was very slow (up to 4 days) to avoid loss of integrity at the interface as a result of the difference in thermal expansion. The couples were subsequently sectioned in half parallel to the direction of diffusion, mounted in polyester resin and polished as described in Section IIIA1.

B. Phase Equilibrium Studies by Static Method of Quenching

Concentration profile discontinuities across the phase boundaries provide very accurate information about the stable composition range of the phase fields.[8,9] Normally, this information alone would be sufficient to complete a phase diagram. However, due to the great controversy about the melting behavior of mullite, quench experiments were also performed to supplement the diffusion experiments of the previous section.

---

*The Kanthal Corp., Bethel, Conn.

**Honeywell, Industrial Div., Fort Washington, Pa.

The compositions of the specimens used in the quenching experiments were 42.2, 60.0, 71.8, 78.3, and 80.0 wt% Al_2O_3. The aluminum-silicate mixtures of 42.2, 60 and 80 wt% Al_2O_3 were prepared (as in section IIIA2) by intimately mixing Alcoa XA-16 reactive α-Al_2O_3 and -325 mesh Corning 7940 fused silica in isopropyl alcohol. The mixtures were subsequently dried at 90°C, calcined at 1000°C for 10 h to reduce the hydroxyl content of the fused silica and melted in Mo crucibles at 1953° or 2003°C for 15 to 30 min. The composition of a representative section was analyzed by electron microprobe, and the crucibles were sealed by electron beam welding before the heat treatment. The sealing of the crucibles, as before, was necessary to avoid silica losses during long anneals. Heat treatment was done in the tantalum resistance heating element furnace in the temperature range of 1753° to 1953°C The specimens were quenched by turning off the power to the furnace and allowing He to flow rapidly through the furnace.

The 78.3 wt% Al_2O_3 specimen was a commercial grade fused cast aluminum-silicate* prepared by the arc fusion process. Specimens 9 mm in diameter by 10 mm were core-drilled from a pore-free portion of a fused cast ingot, for the heat treatment as described above. A ceramographic (reflected light) examination of the as-received specimens showed mullite grains surrounded by a continuous glassy phase.

---

*Carborundum Corp., Niagara Falls, N.Y. Sold as fused cast mullite. Wet chemical analysis was performed by Coors Spectro Chemical Lab., Golden, Colorado. Spectrographic analysis by American Spectrographic Lab., San Francisco, Calif.: as oxides (wt%) Na 0.12, Fe 0.02, Mg 0.01, Zr 0.01, Ca 0.006, Ti 0.005, Cr 0.003, Cu <0.005, Mn <0.001.

The 71.8 wt% Al_2O_3 specimens used in these quenching experiments were the by-products of the efforts made to synthesize stoichiometric mullite ($3Al_2O_3 \cdot 2SiO_2$). Highly reactive γ-Al_2O_3* and amorphous SiO_2† powders were mixed in isopropyl alcohol, dried (90°C), calcined (700°C) and vacuum hot pressed in graphite dies at 3.5×10^6 Nt/m^2 up to 1500°C. X-ray diffraction analysis of the hot pressed and annealed (1300°C) specimens always revealed some unreacted α-Al_2O_3 and cristobalite. The presence of a glassy film would be expected from the findings of DeKeyser,[56] Staley and Brindley,[57] and Davis and Pask.[42] These specimens, as before, were core-drilled and sealed in Mo crucibles for quenching experiments.

The melting behavior of mullite was studied using polycrystalline stoichiometric 3:2 mullite (71.8 wt% Al_2O_3) specimens≠ synthesized by vacuum hot pressing mixed high-purity, submicron oxide powders.[58] The mixed oxide powders were prepared by the hydrolytic decomposition of mixed metal alkoxides. Translucent and completely reacted specimens, 99-99.5% of the theoretical density, could easily be obtained by hot pressing at 1500°C and 3.5×10^6 Nt/m^2 for 30 min. The reported composition of the specimens was verified by electron microprobe analysis. The specimens (5 mm x 5 mm x 8 mm), placed in Mo crucibles, were melted in vacuum in the tantalum resistance heating element furnace. The

---

*Cabot Corp., Boston, Mass. Alon-C, a colloidal γ-Al_2O_3 made by the hydrolysis of $AlCl_3$ in a flame.
†Cabot Corp., Boston, Mass. Cab-O-Sil, produced by the hydrolysis of $SiCl_4$ at 1100°C.
≠The specimens were provided by K. S. Mazdiyasni, Air Force Materials Lab., Wright-Patterson AFB, Ohio.

specimen temperature was measured with an optical pyrometer utilizing black body conditions with a hole core-drilled directly into the specimen. Since the melting temperature of mullite was expected to be between 1800° and 1900°C, the heating rate to 1800°C was fast (5-10 min) followed by a 5°C/min heating rate from thereon in order to maintain thermal equilibrium. The melting temperature was assumed to be that at the first instant of the specimen slumping. Some specimens were only partially melted and quenched by turning off the power to the furnace and allowing He to flow rapidly through the furnace. Cross sections of these partially melted specimens were subjected to ceramographic examination of their microstructure just in and just out of the melting zone. Similarly all the other specimens of the quenching experiments were subjected to ceramographic examination, and the composition of the phases, when necessary, was determined by electron microprobe analysis.

C. Electron Microprobe Analysis

The aluminum and silicon concentration profiles of the diffusion couples and the microstructure specimens of the quenching experiments were determined using an electron microprobe analyzer.* The electron microprobe is a combination of a conventional X-ray tube, an X-ray emission spectrograph, a light microscope, and an electron microscope all in a common vacuum chamber. The specimen to be analyzed is bombarded by a monoenergetic beam of electrons to excite the characteristic X-radiation of the elements present in the specimen. The primary characteristic X-ray intensities emitted from the specimen and a standard

*Model 400, Materials Analysis Co., Palo Alto, Calif.

may then be compared to obtain quantitative data on the concentration of each element in the specimen. Corrections for absorption, fluorescence, atomic number, dead time, drift, and background have to be made to improve the accuracy of the analysis.[59,60]

Prior to the electron microprobe analysis, the highly polished surfaces of the specimens were made electrically conductive by vapor depositing a carbon film of about 200 Å thickness and by painting the mounting material and the corners of the specimen with a slurry of carbon in ethanol. All the measurements were made with an accelerating voltage of 15 kV and a specimen current of 0.03 μA. The diameter of the electron beam was 1 μm, although the volume affected by it was probably in the order of 5-10 cu μm.[59] Two spectrometers were used to record the intensities of the AlK_α and SiK_α peaks simultaneously. The analyzers were curved KAP (potassium acid phthalate) crystals bent and ground in the Johansson mode. The detectors were of the flow proportional type containing a mixture of 93% argon and 7% methane and utilizing 3 μm thick mylar windows.

The concentration profiles were obtained by traversing the electron beam along a desired path perpendicular to the diffusion couple interface or the phase boundaries. An integrated count per 10 s at a location was monitored by logic circuit counters and simultaneously punched on IBM cards for the introduction of corrections by computer. The beam was then advanced automatically by a fixed distance (0.5 to 10 μm to repeat the same procedure.

Extensive crystallization of alumina and/or mullite occurred in the liquid portion of the sapphire-fused silica diffusion couples during

cooling. Thus, the concentration profiles obtained by the point-beam technique were extremely rough and difficult to analyze. Davis and Pask[42] overcame this difficulty by rapidly scanning the electron beam parallel to the interface of the couple in order to obtain an average composition over an area affected by localized solidification. When the standards are also analyzed by the same method, inaccuracies introduced by the decreased X-ray intensity as the beam deviates from the center of the cross hairs may be eliminated. This method was used in the analysis of all the diffusion couples that showed extensive crystallization during cooling. The scanning span ranged from 40 to 150 μm depending on the size of crystals in the diffusion zone.

D. Densities of SiO_2-Al_2O_3 Melts

The concentration profiles obtained by the electron microprobe analysis are expressed as wt% oxides or cations after the introduction of the correction factors. For the use of the diffusion equations, however, the concentration units have to be expressed as weight per volume of the diffusing species unless the density of the matrix does not change with the introduction of the diffusing species into the matrix. Over a wide concentration range, as in the sapphire-fused silica couples (e.g. 0-78.2 mole % Al_2O_3 at 2003°C), the densities would be expected to vary. Thus, the densities of the SiO_2-Al_2O_3 melts had to be determined in order to convert the wt% values to gm/cm^3.

The SiO_2-Al_2O_3 melts up to about 30 mole % Al_2O_3 form glasses when quenched by conventional techniques.[61] The densities of these glasses may then be used for the above conversion although these densities would correspond to a fictive temperature somewhat lower than the annealing

temperature of the diffusion runs. In the diffusion studies of Davis and Pask[42] this method was used since the highest alumina concentration dealt with had only 29 mole % Al_2O_3. The densities of the melts with higher alumina contents had to be measured at temperature since they readily crystallized during quenching.

An X-radiographic technique developed by Rasmussen and Nelson[62] was used to determine the densities of the SiO_2-Al_2O_3 melts in the temperature range of 1700° to 2000°C for the entire binary system. The technique consisted of measuring the volume of a melt at temperature from its radiographed image obtained with a 300 kV X-ray source and of relating this volume to its density. This technique was especially suitable for the SiO_2-Al_2O_3 melts since the specimens could be sealed in their containers to eliminate silica loses during measurements.

The compositions chosen for this study contained 22.8, 42.2, 60.0, and 80.0 wt% Al_2O_3 which were mixtures used in the diffusion and the phase equilibrium studies of Sections IIIA and B. These mixtures were melted in Mo capsules at 1953°C in vacuum for ∿30 to 60 min. The Mo capsules with a wall thickness of 0.4 mm and 7.6 cm high were machined from high purity Mo rods with 1.27 cm OD. The weight of the fused cast material in each capsule was determined prior to the sealing of the crucibles by electron beam welding the lids. Subsequently, each crucible was He leak checked for possible cracks.

The X-radiographic measurements were performed by Rasmussen* using the system described by Rasmussen and Nelson.[62] The specimens were

---

*Rasmussen, J. J., Battelle Pacific Northwest Labs., Ceramics and Graphite Section, Richland, Wash.

melted in a W-mesh resistance heating element vacuum furnace. The specimen temperature was varied in the temperature range of 1700° to 2000°C with a 3°C/min rate, and the specimen images were radiographed on film at ∿25°C intervals. The temperature was measured continuously with a two-color optical pyrometer with an accuracy of ± 10°C. The volume of the melt was determined from its height and the crucible diameter, and corrected for thermal expansion.[63] In most instances, the column length could be measured reproducibly to give a density variation of ± 0.004 gm/cm^3. A typical set of radiographs used in these measurements is shown in Fig. 8.

E. Computer Analysis

A computer program written by Frazer, et al.[64] was modified for use with the CDC-7600 computer system of this laboratory and used to correct the electron microprobe data for dead time, drift, background, absorption, and fluorescence. Atomic number correction was not necessary since the difference between the atomic number of Al and Si is very small.

The output of this electron microprobe program given in wt% of the elements or their oxides in the melt was converted to gm/cm^3 of the elements and their oxides with an additional program utilizing the density data of Section IIID. The density vs wt% relationship used in this second program was

$$\rho_{1900} = 2.106 + 0.0085\ (\text{wt\% } Al_2O_3) \qquad (29)$$

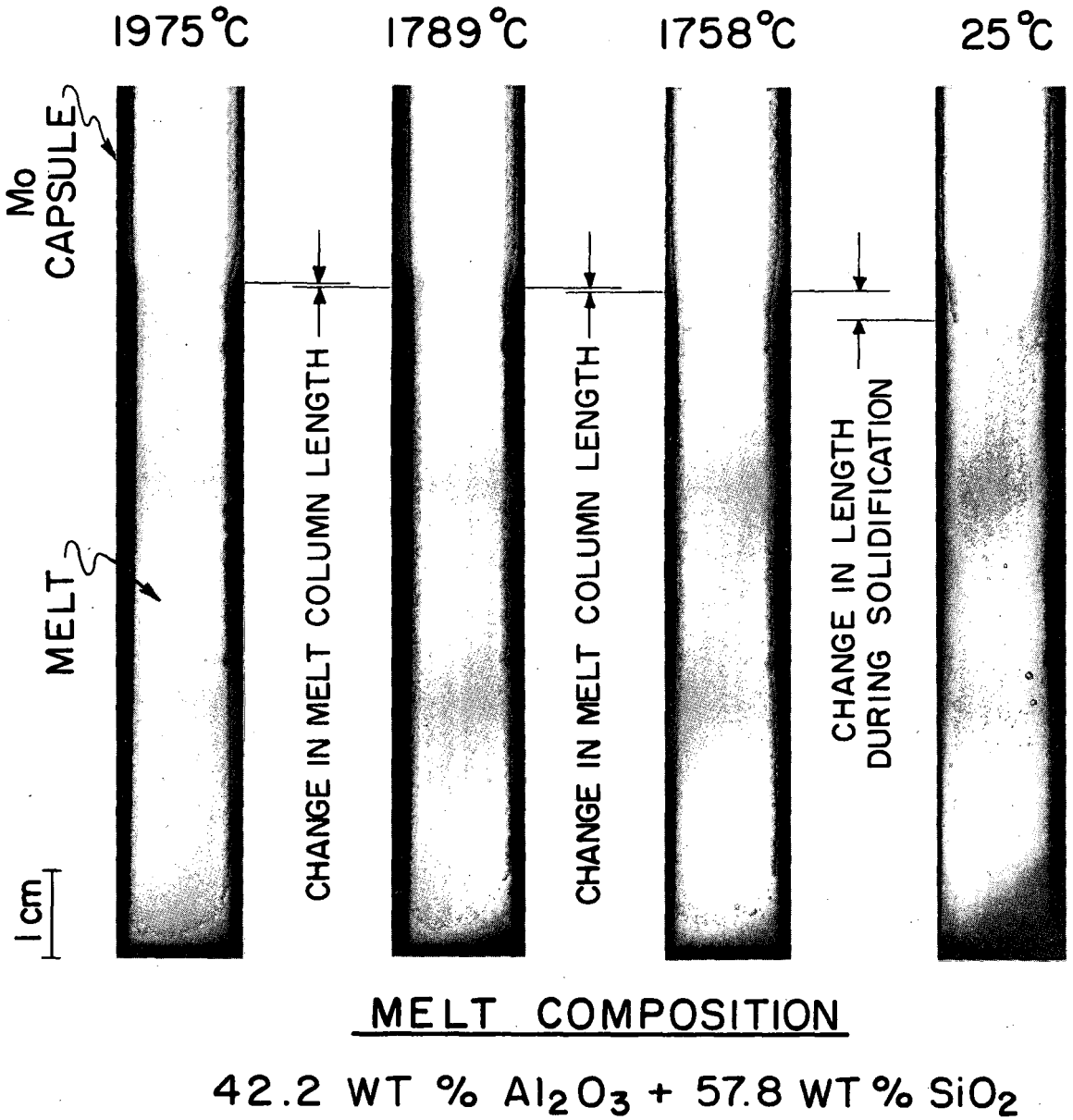

MELT COMPOSITION

42.2 WT % Al_2O_3 + 57.8 WT % SiO_2

XBB 728-4233

Fig. 8. Radiographs of molten and solidified aluminum-silicate columns used in the determination of densities.

where ρ_{1900} is the density of the melt at 1900°C. This single relationship rather than a separate equation for each temperature anneal was used since the differences in the densities were too small (± 0.003 gm/cm^3 at 1800°–2000°C) to introduce any significant change in the diffusivity values. The relationship between Al and Al_2O_3 concentration (gm/cm^3) in the melt vs mole and wt% Al_2O_3, based on Eq. (29), is shown in Fig. 9. Similarly, the conversion for the diffusion profiles through the mullite layer was made by substituting the theoretical density of mullite,[58] 3.19 gm/cm^3, for Eq. (29). Cal-Comp programs were incorporated into the above programs to plot the concentration of Al vs distance profiles on graph paper.

The Boltzmann-Matano interface defined by Eq. (15) and the interdiffusivities of Eq. (16) were determined by inserting the concentration of Al(gm/cm^3) vs distance coordinates of the smoothed diffusion profiles into the programs written by Appel[65] (Appendix). These programs were also incorporated with additional Cal-Comp subroutines to plot the diffusivity (D) or ln D vs concentration values on graph paper.

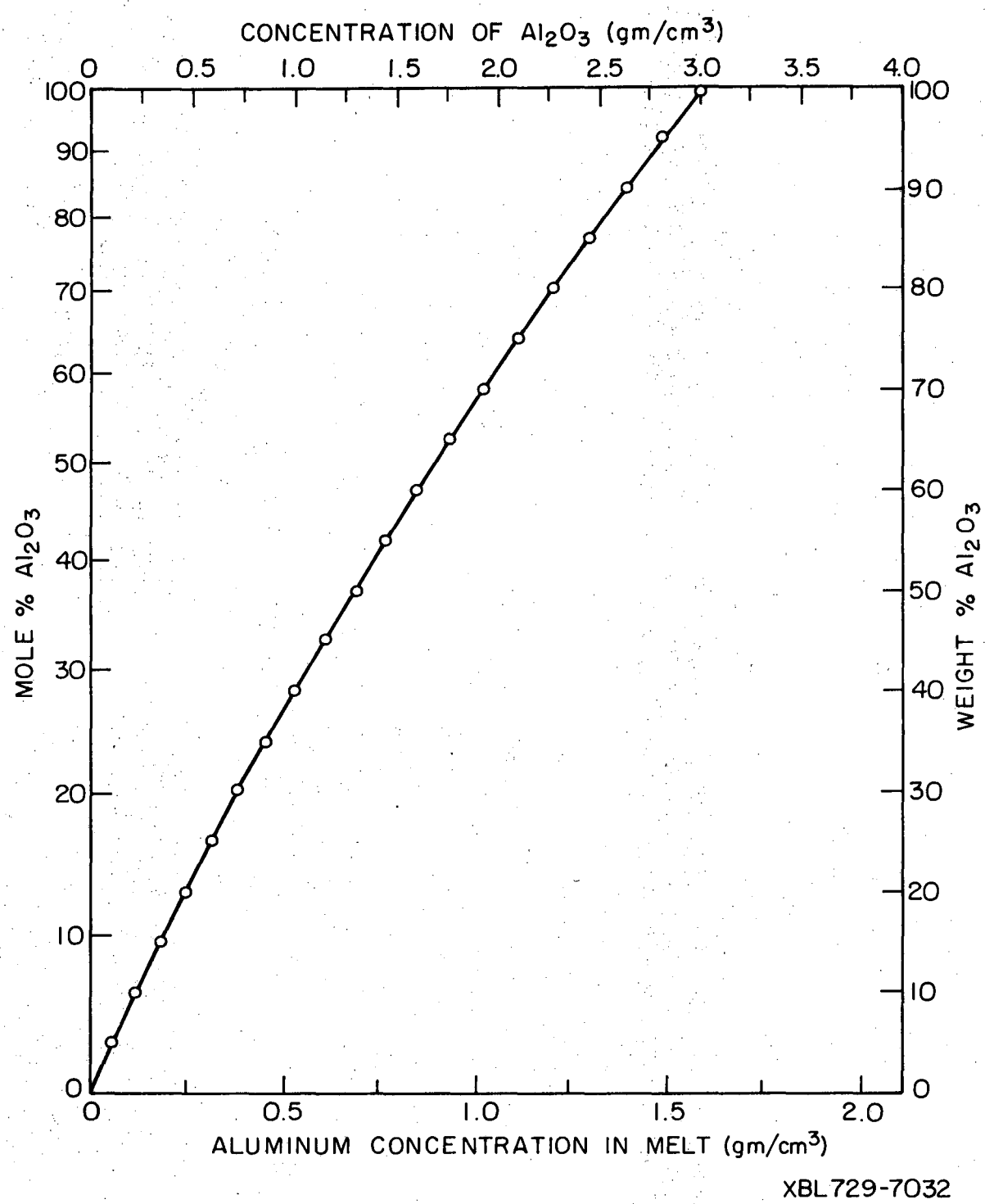

Fig. 9. Relationship between Al and Al_2O_3 concentration in aluminum-silicate melts vs mole and wt% Al_2O_3.

IV. RESULTS AND ANALYSIS

A. Densities of SiO_2-Al_2O_3 Melts

The densities of the aluminum-silicate melts are tabulated in Table I. The values reported here are those obtained during the cooling cycle only. The measurements obtained during the initial heating cycle were considered erroneous due to the formation of bubbles and the presence of cores in the melts. However, consistent results could be obtained during a subsequent reheating. This phenomenon has also been observed with $MgAl_2O_4$ and Al_2O_3[66] during the formation of initial melts from single crystals which are usually grown in the presence of H_2 or Ar.

The densities varied linearly with temperature within the temperature range studied, as illustrated in Fig. 10. The solidification temperatures for the 46.92 and 70.21 mole % Al_2O_3 melts were determined during the cooling cycle when an abrupt volume change occurred due to the precipitation of mullite or alumina. Because the 14.82 and 30.08 mole % Al_2O_3 melts formed glasses during cooling, they showed no abrupt volume change during cooling.

The density of liquid alumina has been measured by various investigators.[66-71] The results of Mitin and Nagibin[70] who made their measurements by hydrostatic weighing technique and obtained a linear density temperature relationship between the melting point and 2550°C are reproduced in Fig. 10. The density of solid alumina up to its melting point was calculated using the coefficient of expansion data of Wachtman et al.[72] and the room temperature density of 3.965 gm/cm^3.[73]

The density data of liquid silica also shown in Fig. 10 are by Bacon et al.[74] who reported five density values between 1938° and 2326°C.

Table I. Densities of the SiO_2-Al_2O_3 melts.

22.8 wt% Al_2O_3 (14.82 mole%)		42.2 wt% Al_2O_3 (30.08 mole%)		60.0 wt% Al_2O_3 (46.92 mole%)		80.0 wt% Al_2O_3 (70.21 mole%)	
Temp. (°C)	ρ (gm/cm^3)	Temp. (°C)	ρ (gm/cm^3)	Temp. (°C)	ρ (gm/cm^3)	Temp. (°C)	ρ (gm/cm^3)
1707	2.319	1758	2.475	1755	2.736	1966	2.811
1752	2.319	1789	2.466	1773	2.732	1993	2.799
1813	2.320	1813	2.461	1803	2.724	1995	2.791
1858	2.316	1838	2.465	1808	2.724		
1907	2.313	1858	2.460	1835	2.629		
1909	2.313	1880	2.454	1859	2.627		
1963	2.305	1881	2.455	1882	2.626		
1988	2.302	1909	2.448	1910	2.625		
2008	2.302	1913	2.449	1938	2.615		
		1941	2.445	1959	2.612		
		1975	2.446	1985	2.608		

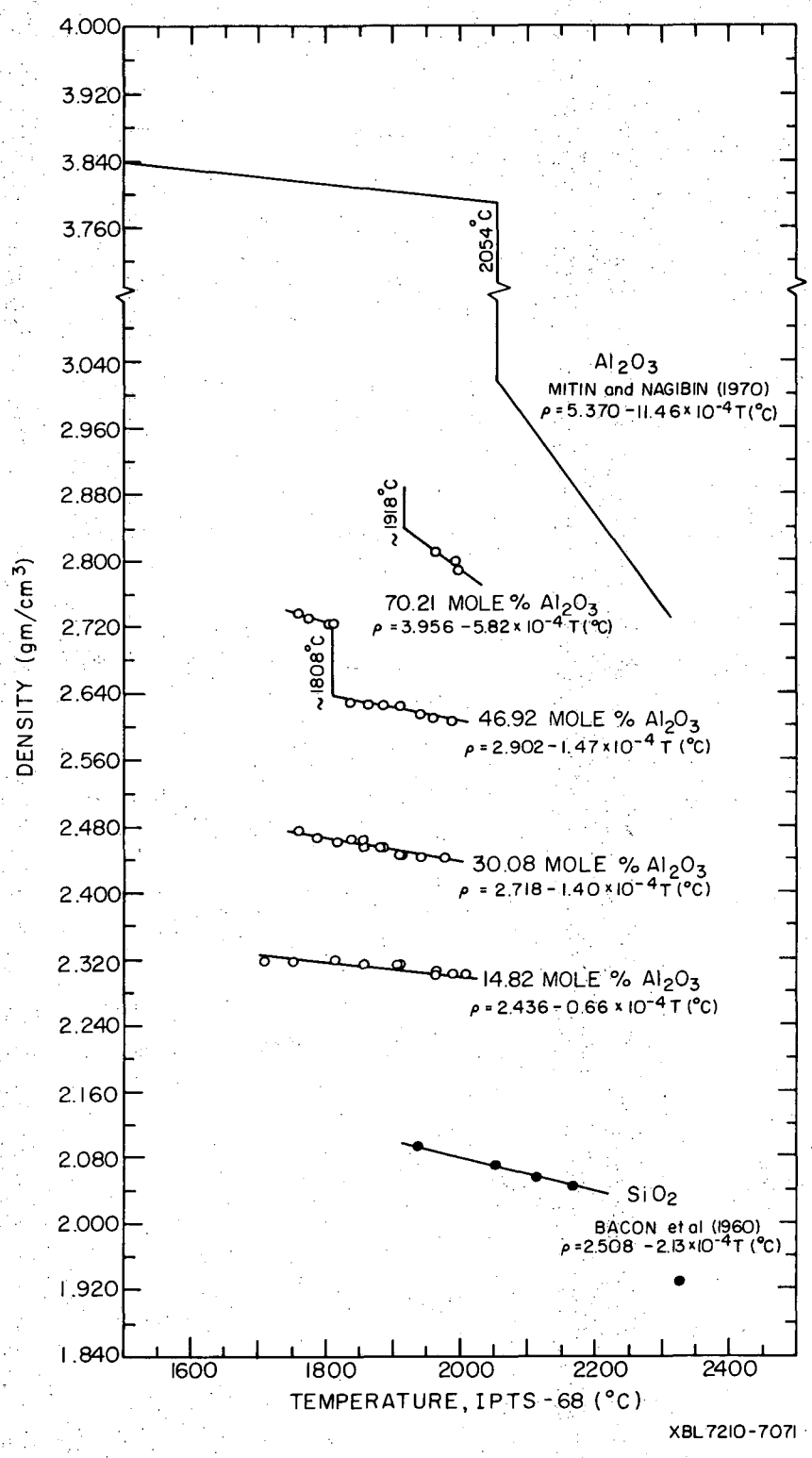

Fig. 10. Variation of the aluminum-silicate melt densities with temperature.

A least squares fit[75] to a straight line including all the data points has a poor correlation, while a correlation factor of 0.998 is obtained when the last data point at 2326°C is excluded from the set. Furthermore, when this last point is included in the set, the extrapolated value of the liquid density at the melting temperature of cristobalite is higher than that of the solid. Thus, it is concluded that either the density of liquid silica varies linearly only up to ∿2200°C (Fig. 10) and deviates from linearity from thereon or the value reported at 2326°C is erroneous.

The variation of the melt densities with alumina content in the temperature range of 1800° to 2200°C is illustrated in Fig. 11. In this temperature range, the densities increase linearly only up to ∿45 mole % Al_2O_3. The negative deviation from linearity at higher alumina contents is indicative of the formation of a looser structure.

Also illustrated in Fig. 11 are the room temperature densities of the glasses quenched from 1803°C.[42] On the basis of the data of Fig. 10, these room temperature densities correspond to a fictive temperature of ∿1200°C.

No attempt has been made to calculate the partial molar volume of Al_2O_3 and SiO_2 in the melt. The partial molar volume data of the components of silicate melts are useful in estimating the densities of complex silicate and magmatic liquids that are of interest to ceramists and petrologists but are difficult to study directly at high temperatures. The partial molar volumes, in general, are composition, temperature, and pressure dependent. However, the data compiled by Huggins and Sun,[76] Bottinga and Weill,[77] and others [78-81] indicate that partial

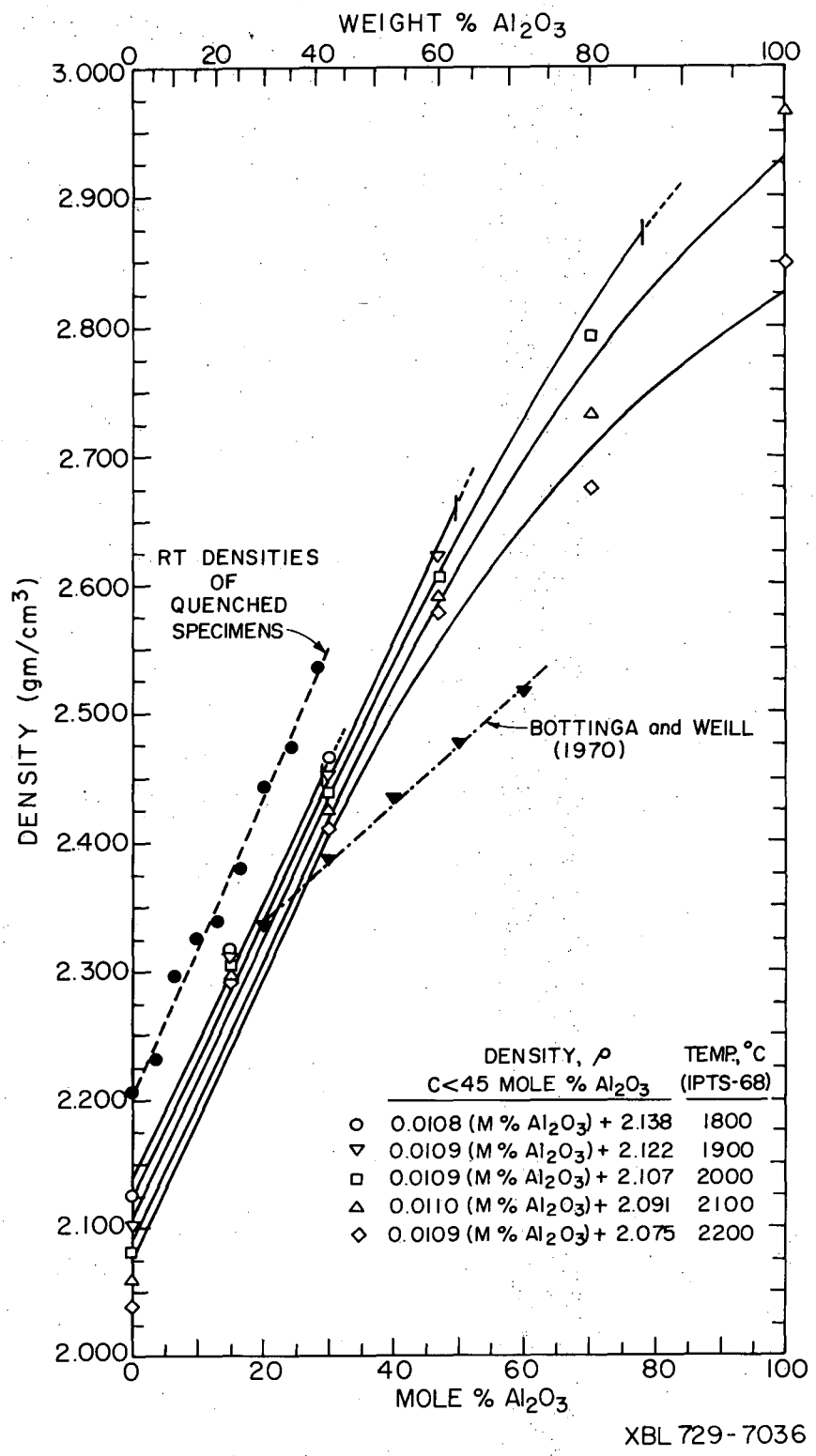

Fig. 11. Variation of the aluminum-silicate melt densities with Al_2O_3 content.

molar volumes are constant in a certain range of silicate composition. These data may then be used to calculate the density of any silicate liquid within that range.

The only partial molar volume data available on Al_2O_3 are those obtained from ternary alkali or alkaline earth aluminum-silicates.[76,77] The values reported by Bottinga and Weill[77] were extrapolated to 1900°C and used to calculate the densities of binary aluminum-silicate melts in the range of 20 to 60 mole % Al_2O_3. As shown in Fig. 11, the agreement between these calculated values and the measured ones is poor, especially at higher alumina contents. Similar results are also obtained if the values compiled by Huggins and Sun[76] are used. Then it appears that the partial molar volumes obtained from ternary aluminum-silicates may only be satisfactorily used to predict the densities of other ternary or more complex silicates of similar composition but not those of binary aluminum-silicates since a denser structure is present in the latter case.

The density data presented above may also be used to determine the fractional volume change of mullite and alumina upon melting or solidification. A search of the literature showed that the only information available on the fractional volume change of mullite during solidification is that by Tyrolerova and Lu[82] who reported a volume decrease of 10.3% during solidification for a fused-cast mullite specimen of 75.1 wt% Al_2O_3. The density of stoichiometric mullite (71.8 wt% Al_2O_3) at its metastable congruent melting temperature, 1890°C (Section IVE), is 3.10 gm/cm^3 when calculated from the expansion data of mullite.[58] The density of the corresponding melt at the same temperature is 2.774 gm/cm^3

based on the data presented in Fig. 11. Thus, the fractional volume decrease of mullite on solidification is 10.28% which agrees with the value reported by Tyrolerova and Lu.

The fractional volume decrease of alumina on solidification based on the data of Fig. 10 is 20.7% which is much higher than the corresponding value for mullite. Similar values for the fractional volume change of alumina melts on solidification have been reported by Kingery[68] as 20.4%* and by Tyrolerova and Lu[83] as 19.9-20.1%. The values reported by Kirshenbaum and Cahill[69] and Bates et al.[66] on melting are 22.0 and 24.0%. For comparison, however, these values should also be expressed as fractional volume change on solidification not melting. Then, the new values are 18.2 and 19.4%, respectively, and compare well with the values reported by Kingery[68] and Tyrolerova and Lu.[83]

B. Diffusion Profiles and Phase Equilibria

1. Sapphire-Fused Silica Couples

The experimental conditions of the diffusion anneals in the temperature range of 1803° to 2003°C are outlined in Table II. The annealing times were at least 15 min in order to ensure that the annealing time was considerably longer than the time needed to attain thermal stability in the furnace (∿30-60 sec). Above 1913°C, however, a 15 min anneal was also the maximum limit since at longer time the diffusion profiles were extremely long (>2000 μm); thus their analysis by the electron microprobe was not feasible.

---

*This value was erroneously reported by Kingery[68] as fractional volume change on melting instead of solidification.

Table II. Experimental conditions and data for sapphire-fused silica runs.

Temp. IPTS-68 (°C)	Time (sec × 10^{-3})	Sample Designation	Interfacial Composition, C_I		
			Al^{3+} (gm/cm^3)	Al_2O_3 (mole%)	Al_2O_3 (wt%)
1803	3.6	8.71.7A	0.547	29.0	40.9
1803	3.6	8.71.7B			
1803	3.6	8.71.7C			
1803	14.4	8.71.1A			
1803	14.4	8.71.1B			
1803	14.4	8.71.2			
1803	14.4	039*	0.547	29.0	40.9
1803	21.6	040*			
1803	28.8	041*			
1803	602.1	1.72.2B	0.547	29.0	40.9
1853	0.9	8.71.9A	0.752	40.9	54.0
1853	0.9	8.71.9B			
1853	1.8	8.71.11A			
1853	3.6	8.71.4			
1853	3.6	8.71.5			
1853	3.6	8.71.6A			
1853	3.6	8.71.6B			
1853	7.2	9.71.1			
1853	65.7	7.70.4			
1903	0.9	5.72.3AM	0.893	49.6	62.5
1903	0.9	5.72.3M			
1903	0.9	5.72.3A			
1903	1.8	9.71.4			
1903	3.6	4.71.2			

*R. F. Davis and J. A. Pask (1972).[42]

Table II. Experimental conditions and data for sapphire-fused silica runs. (continued)

Temp. IPTS-68 (°C)	Time (sec × 10^{-3})	Sample Designation	Interfacial Composition, CI		
			Al^{3+} (gm/cm^3)	Al_2O_3 (mole%)	Al_2O_3 (wt%)
1913	0.9	9.71.2	0.919	51.2	64.0
1913	1.8	9.71.3			
1953	0.9	9.71.5	1.048	59.6	71.5
1953	0.9	5.72.8			
1953	0.9	6.72.1			
2003	0.9	7.72.1	1.313	78.2	85.9

Also outlined in Table II is the composition of the melt at the sapphire interface as obtained from the diffusion profiles. The composition of sapphire at the same interface always corresponded to that of pure Al_2O_3 since the solubility limit of silica in the sapphire substrate was below the detection limit of the electron microprobe. These interfacial compositions remained constant with time at a temperature, indicating that the diffusion in the liquid phase was slower than the dissolution rate of sapphire.[7] The diffusion-controlled nature of the dissolution of sapphire, then, satisfies the basic requirement of the Boltzmann-Matano analysis as discussed in Section IIA. Although no time studies could be performed at 1953° and 2003°C, it is assumed that the diffusion in the liquid phase is still the rate controlling step at these temperatures. These interfacial compositions, then, correspond to a liquidus composition.[7]

Mullite growth at the sapphire-fused silica interface at temperature was observed at 1803°C but not at 1853°C (Section IVC), indicating that the stable range of the mullite field lies below 1853°C. Thus the interfacial compositions of Table II correspond to the liquidus of alumina at 1853° to 2003°C while the one at 1803°C corresponds to that of mullite.

Extremely long anneals were necessary to grow the mullite layer at 1803°C to a feasible thickness for microprobe analysis. This difficulty was also encountered by Davis and Pask[42] who, by optical methods, were unable to observe any mullite growth at 1803°C due to insufficient annealing times (Table II). However, their kinetic data on mullite growth obtained in the temperature range of 1653° to 1753°C, when

extrapolated to 1803°C, predicts that interfacial mullite would grow to a thickness of 12 μm when a sapphire-fused silica couple is annealed at 1803°C for seven days. This prediction was in excellent agreement with the data of this study since approximately seven days (602.1×10^3 sec) were required to grow a mullite layer of ∿10 μm in thickness at 1803°C. The composition of this layer ranged from 71.1 wt% Al_2O_3 at the melt interface to 74.0 wt% Al_2O_3 at the sapphire interface.

Typical computer plotted diffusion profiles used in the determination of the interfacial compositions and the diffusion parameters are shown in Fig. 12. The choice of the diffusing species was abritrary because there is no information on the nature of the actual diffusing unit. Thus, the diffusion profiles were expressed as concentration of aluminum ions vs distance rather than as concentration of Al_2O_3 or other Al-O species.

The Boltzmann-Matano or the original interface is located at x=o. The basic requirement of the Boltzmann-Matano analysis, i.e., that diffusion is the rate controlling process, could be verified once more by ascertaining that at a given temperature the distance from x=o for a given concentration is directly proportional to the square root of time. Such straight line plots are shown in Figs. 13-15.

2. Sapphire-Mullite-Liquid Couples

When the fused silica portion of the couples of the previous section were substituted by melts with compositions corresponding to that of the mullite liquids,[42] the intermediate mullite layer could be grown to a thickness (>10 μm) suitable for electron microprobe

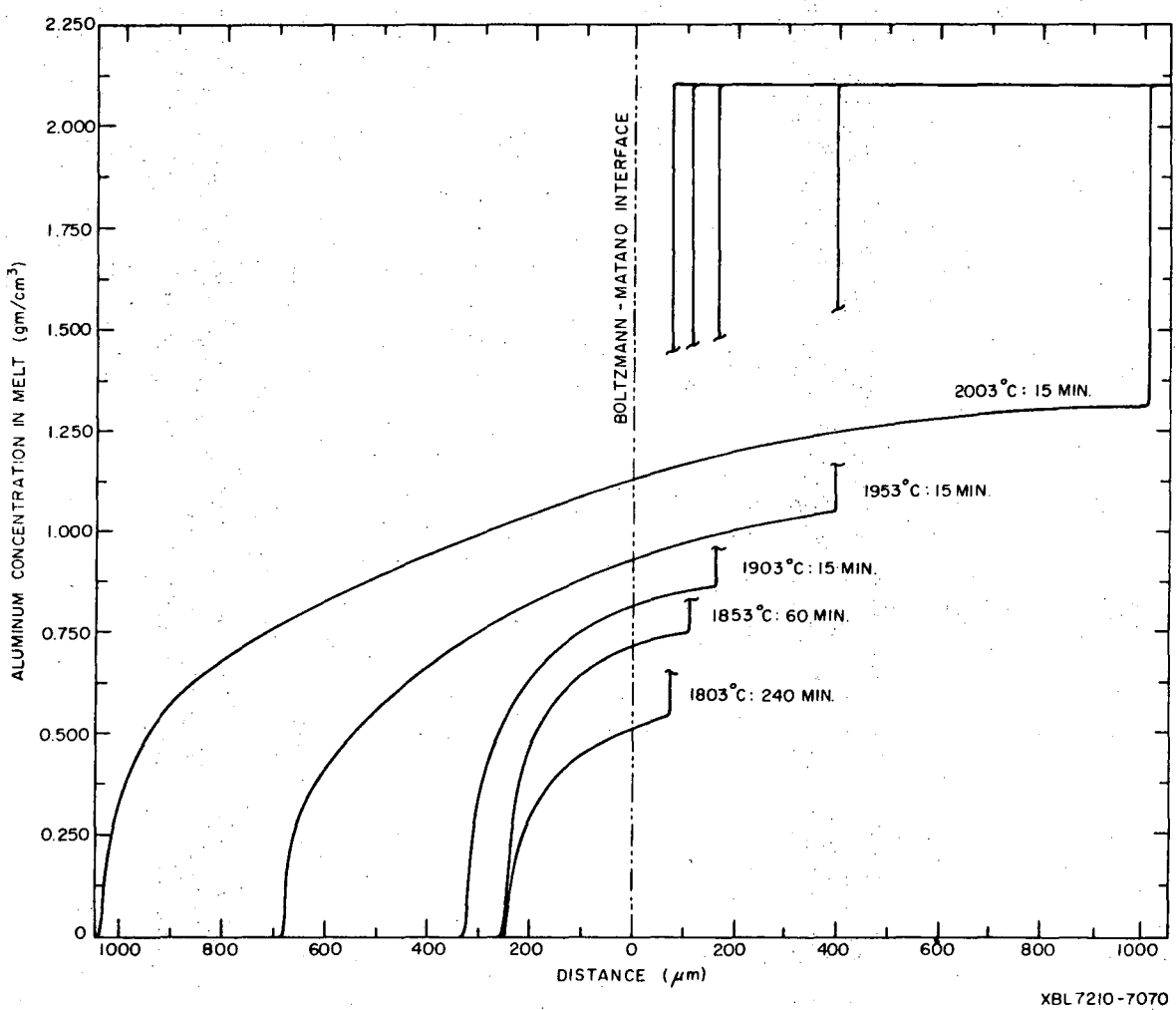

Fig. 12. Typical computer plotted concentration profiles of sapphire-fused silica couples in the temperature range of 1803° to 2003°C arranged with a common Boltzmann-Matano interface.

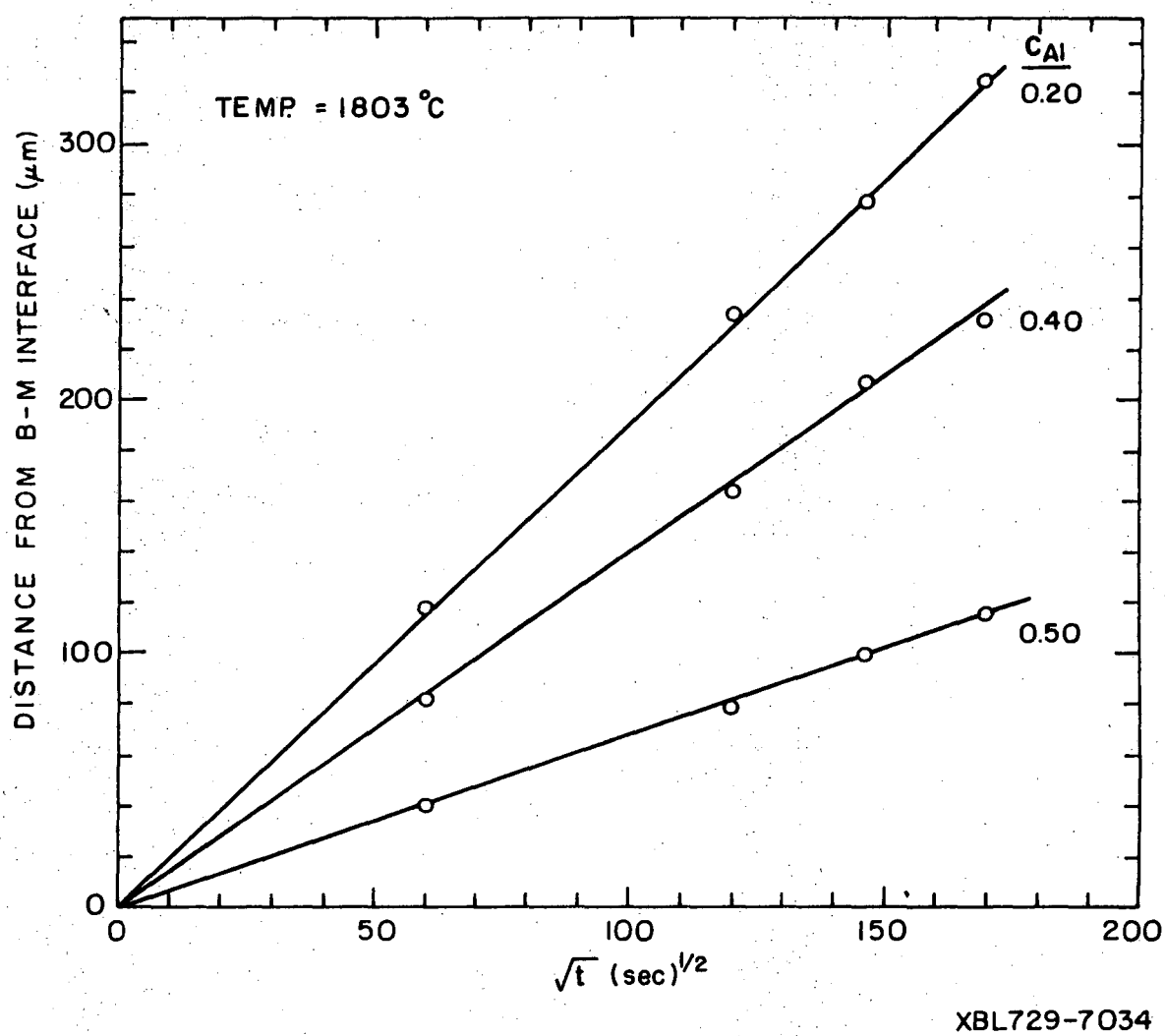

Fig. 13. Variation of distance from Boltzmann-Matano interface at a given concentration, C_{Al}(gm/cm^3), with square root of time at 1803°C.

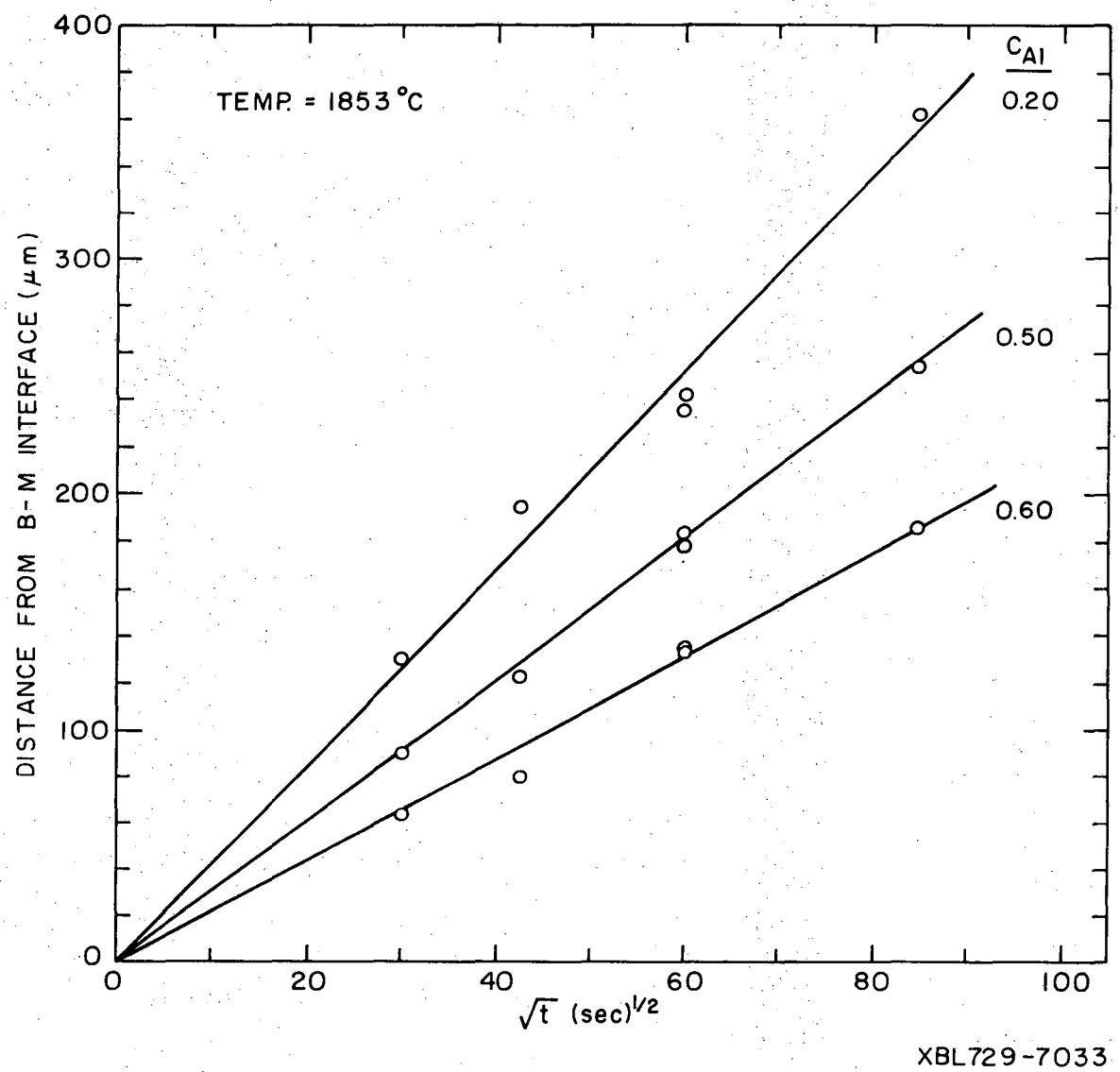

Fig. 14. Variation of distance from Boltzmann-Matano interface at a given concentration, C_{Al} (gm/cm^3), with square root of time at 1853°C.

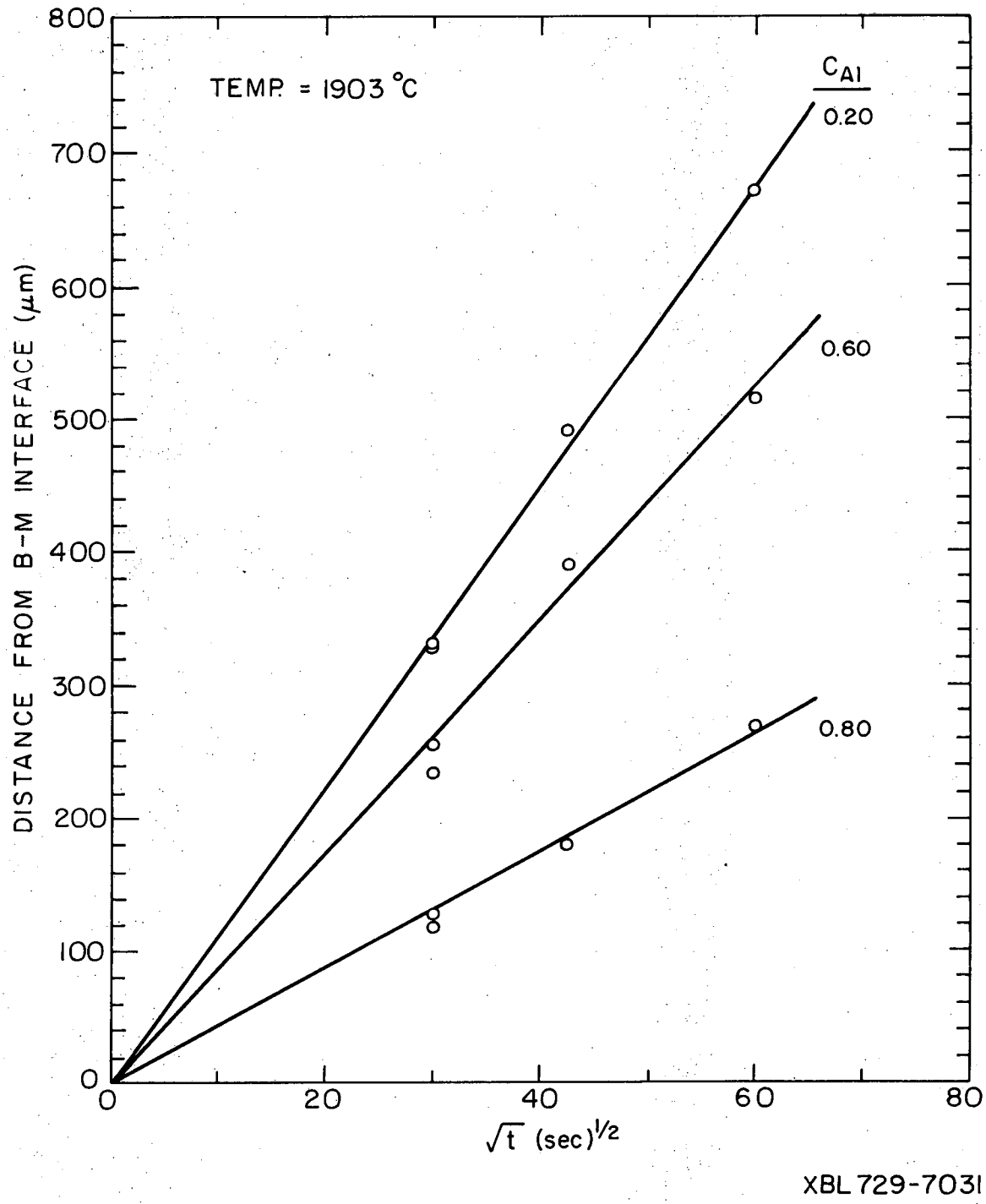

Fig. 15. Variation of distance from Boltzmann-Matano interface at a given concentration, C_{Al}(gm/cm^3), with square root of time at 1903°C.

analysis (Fig. 16).* The results of these runs in the temperature range of 1678° to 1813°C are tabulated in Table III. The experimental results of Davis[84] who conducted similar runs with a non-equilibrium liquid at 1653°, 1703° and 1753°C are also included in this table for comparison. The 15.0 wt% Al_2O_3 containing liquid used in his studies is at equilibrium with mullite at 1718°C.[42] The use of this liquid then creates a condition of some mullite dissolution into the liquid at 1753°C while some additional growth occurs at 1653° and 1703°C. The runs at 1703°C, however, may be approximated to an equilibrium case since the equilibrium liquid at 1703°C contains 13 wt% Al_2O_3, which is quite close in composition to the liquid used by Davis.[84]

The thickness of the mullite layer increased linearly with the square root of time, indicating that the growth mechanism is diffusion controlled. The diffusion profiles across the mullite layer were quite similar to that of Fig. 3. The interfacial composition of the mullite layer obtained from these profiles, then, correspond to equilibrium solidus compositions.

3. Phase Equilibria

The interfacial compositions reported in Table II and III may now be used to construct a portion of the equilibrium binary SiO_2-Al_2O_3 phase diagram in the temperature range of 1678° to 2003°C. The complete diagram, as shown in Fig. 17, is constructed after these interfacial compositions are incorporated with the data on the mullite

*All the micrographs are by reflected light, Nomarski differential interference-contrast microscopy utilizing a Zeiss Ultraphot II metallograph.

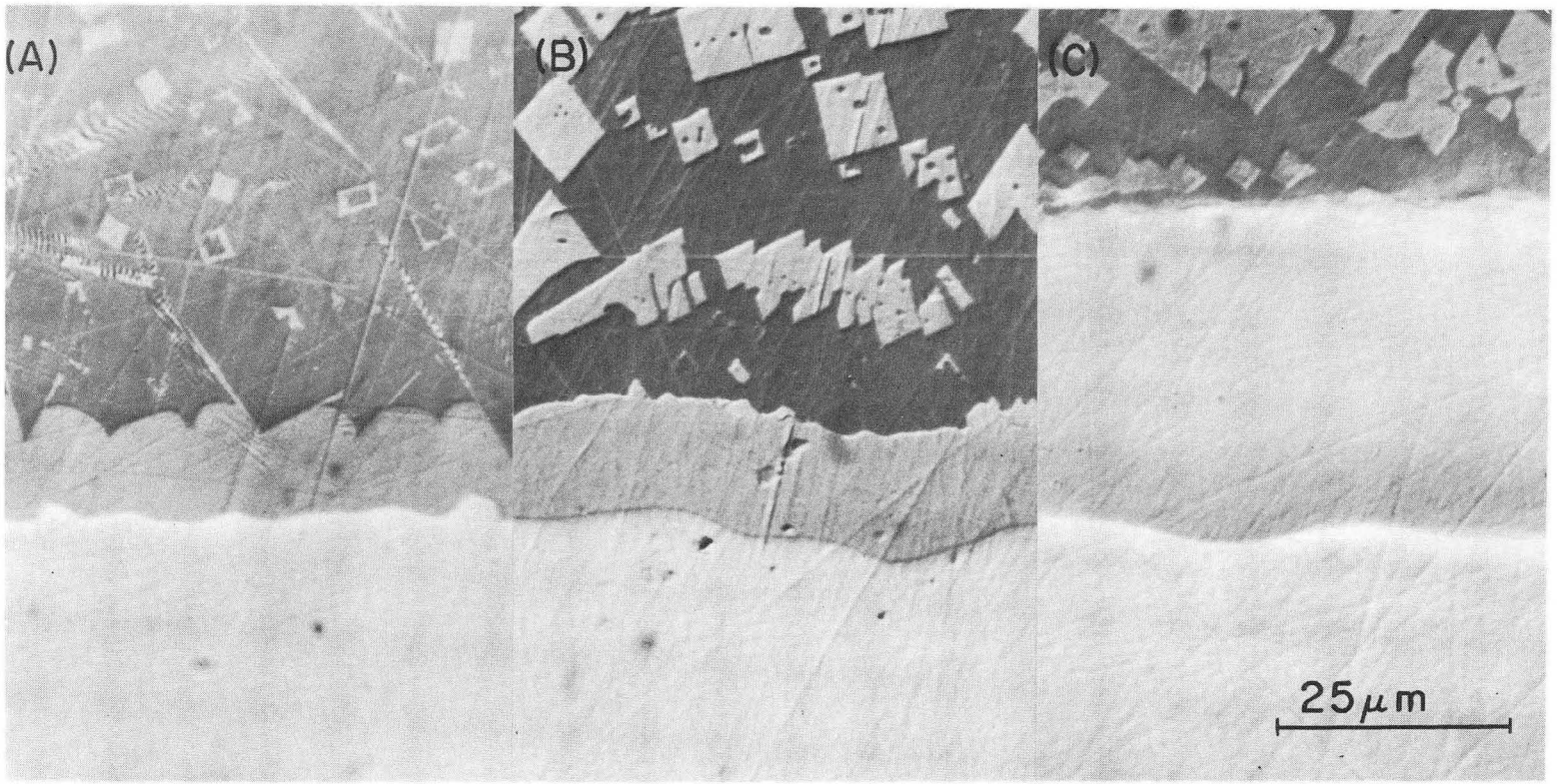

XBB 7210-5301

Fig. 16. Interference-contrast micrographs of the diffusion zone between a couple of sapphire and (A) 10.9 wt% Al_2O_3 containing silicate at 167°C for 7.309×10^5 sec (1.72.1), (B) 22.8 wt% Al_2O_3 containing silicate at 1753°C for 3.965×10^5 sec (2.72.1A), and (C) 42.2 wt% Al_2O_3 containing silicate at 1813°C for 6.015×10^5 sec (1.72.2A). The prismatic precipitates in the top portion of the diffusion zone in the silicate are mullite that crystallized during cooling.

Table III. Experimental conditions and data for sapphire-mullite-liquid diffusion runs.

Temp. IPTS-68 (°C)	Time (sec × 10^{-5})	Sample Designation	Interfacial Composition (wt% Al_2O_3) Melt	Mullite	Mullite Thickness (μm)
1653	6.048		15.0		7.65
1653	7.776		15.0		8.83
1653	9.504		15.0		10.00
1678	7.309	1.72.1	10.9*	70.5-74.0	10.00
1678	28.428	2.72.3A	10.9*	70.5-74.0	18.00
1703	3.456		15.0		8.53
1703	6.048		15.0		11.30
1703	7.776		15.0		13.35
1703	9.504		15.0	70.5-73.5	15.10
1753	1.728		15.0		6.62
1753	2.592		15.0		8.42
1753	3.456		15.0		9.43
1753	3.965	2.72.1A	22.8*	70.5-74.0	13.00
1813	6.015	1.72.2A	42.2*	71.6-74.0	36.00

*Equilibrium liquid compositions. All the other runs with a non-equilibrium melt composition of 15.0 wt% Al_2O_3 were conducted by Davis.[84]

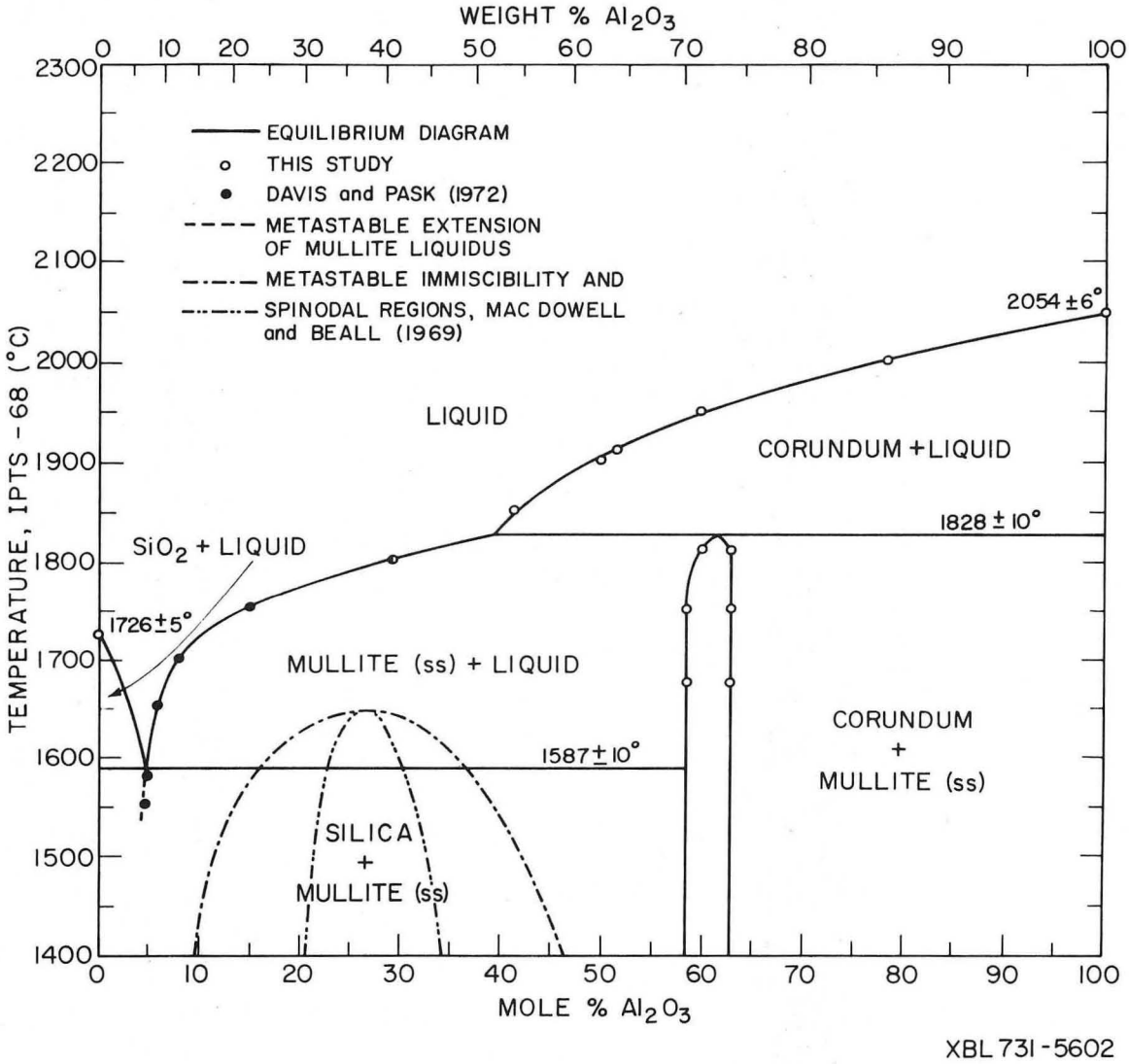

Fig. 17. Revised SiO_2-Al_2O_3 phase diagram.

liquidus by Davis and Pask,[42] the melting temperatures of cristobalite[29] and alumina[30] and the eutectic temperature of cristobalite-mullite.[85] The metastable immiscibility and spinodal regions were reported by MacDowell and Beall.[61]

The most important feature of this diagram is that mullite melts incongruently to form a silica rich liquid and solid alumina. The incongruent melting temperature was determined to be 1828 ± 10°C from the intersection of the extrapolated liquidus lines of mullite and alumina. Although this transition temperature is identical to the one measured by Bowen and Grieg,[10] its accuracy should be verified by conducting additional diffusion runs between 1813° and 1853°C, the temperatures used in this study.

C. Diffusion Zone Microstructure of the Sapphire-Fused Silica Couples

The microstructure developing in the diffusion zone during cooling was greatly dependent upon the cooling rate followed. Thus, in addition to the diffusion data obtained from these couples, information on stable and metastable equilibria could also be obtained from a study of the diffusion zone microstructure.

Typical diffusion zone microstructures of the sapphire-fused silica couples annealed at 1803° and 1853°C are shown in Fig. 18. Extensive crystallization of mullite in the melt (top portion of the micrographs) could not be eliminated although the couples were cooled down to 1500°C in less than a minute. The alumina content of these prismatic mullite grains as determined by the electron microprobe analysis almost never corresponded to the stable solidus composition of mullite as presented

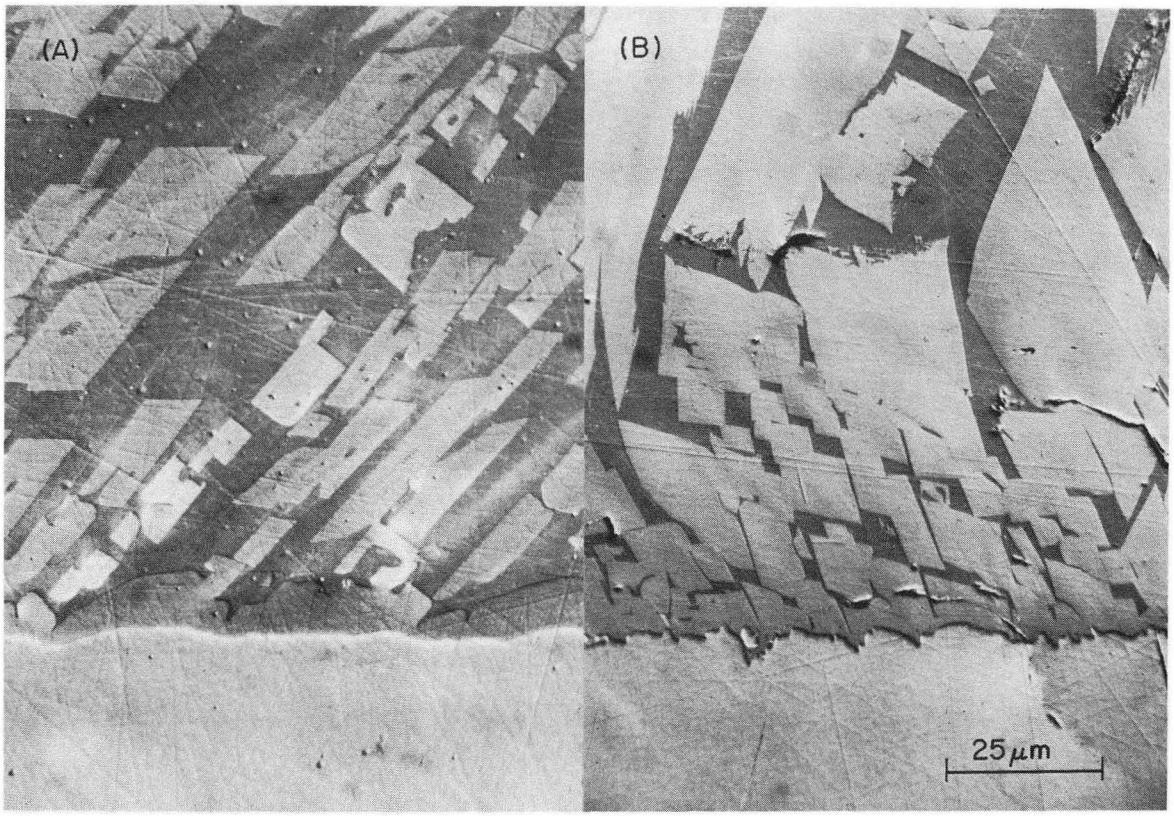

XBB 7210-5300

Fig. 18. Interference-contrast micrographs of the diffusion zone between a couple of sapphire (bottom) and fused silica (top) annealed at (A) 1803°C for 602.1×10^3 sec (1.72.2B) and (B) 1853°C for 7.2×10^3 sec (9.71.1). The prismatic precipitates (light gray) in the top portion of the diffusion zone are mullite that crystallized during cooling. However, the mullite layer at the sapphire-melt interface of microstructure (A) has an isomorphic texture since it grew at the interface at temperature.

in Fig. 17 but was always rich in alumina and varied between 73-79 wt% Al_2O_3. The composition of the isomorphic mullite layer at the sapphire interface of the couple annealed at 1803°C, however, distinctly differed from that of the precipitates; and its composition was not constant through but varied, as shown in Fig. 3, from 71.1 wt% Al_2O_3 at the melt interface to 74.0 wt% Al_2O_3 at the sapphire interface. Similarly, mullite that precipitated in the diffusion zone of the sapphire-mullite-liquid couples annealed at 1678°C, 1753°C and 1813°C (Fig. 16) was always richer in alumina (73-79 wt% Al_2O_3) than the equilibrium solidus composition determined from the interfacial mullite layer grown at temperature (Fig. 17).

Formation of mullite with alumina contents higher than the limits outlined in Fig. 17 occurs only when it is solidified from a melt cooled from above the melting temperature of mullite.[26] The composition of this mullite generally is close to 77.3 wt% Al_2O_3 ($2Al_2O_3 \cdot SiO_2$), although values as high as 82.57 wt% Al_2O_3 have also been reported.[86] Precipitation of mullite with alumina contents (74.0 wt% Al_2O_3) higher than the solidus composition outlined in Fig. 17 was also observed by Davis and Pask[42] in the diffusion zones of sapphire-fused silica couples annealed at 1803°C. They, by analogy to the mullite grown from a melt at higher temperatures, suggested that the composition of the melt was responsible for the composition of the precipitated mullite. A discussion on this subject will be provided in Section V; however, for the purposes of this section, the fact that the composition of the precipitated mullite clearly differs from that of the mullite layer grown at the sapphire interface serves as a useful criterion in the

differentiation of mullite grown at temperature from mullite precipitated during cooling.

The sapphire interface of the couple annealed at 1853°C is also covered with essentially a continuous mullite layer (Fig. 18B). The composition of this layer was constant throughout and identical to that of the precipitates in the adjoining diffusion zone. Furthermore, the prismatic morphology of this layer is similar to that of the precipitates away from the interface and differs from that of the layer grown at 1803°C (Fig. 18A). Therefore, it is concluded that this layer did not grow at temperature but precipitated at the sapphire interface during cooling. As discussed in the previous section, the growth of mullite at 1803°C but not at 1853°C indicates a transition point between these temperatures (Fig. 17).

The composition of the liquid in the diffusion zone at 1853°C varies from 0 to 54.0 wt% Al_2O_3 (Figs. 12 and 17). A portion of the diffusion zone adjacent to the sapphire becomes oversaturated with respect to alumina just below 1853°C. If an equilibrium path were followed, alumina would precipitate in the liquid during cooling, and at the transition temperature, 1828°C, alumina would be completely resorbed to form a mixture of mullite and liquid. A similar mixture of mullite and liquid, however, would also form if the liquid were supercooled below the transition temperature without any precipitation of alumina. Thus, the absence of alumina in the diffusion zone of Fig. 18B does not necessarily imply that any precipitated alumina was resorbed at the transition temperature and an equilibrium cooling path was followed. In fact, the realization of an equilibrium of this nature,

especially in silicates, is rare since the crystal phase to be resorbed becomes unavailable for a complete reaction through incrustation,[37] i.e., formation of a mullite layer zone around alumina. The absence of alumina in the diffusion zone, then, is actually an indication that the liquid was supercooled below the transition temperature.

The direct evidences for supercooling of the liquid in the diffusion zone were clearly brought out in the couples that were annealed at 1903° and 1913°C. The diffusion zone microstructures of three separate couples that were annealed at 1903°C for 15 min each but cooled at different rates are shown in Fig. 19. The microstructures obtained differed drastically although the diffusion profiles were identical to the one shown in Fig. 12. The precipitated crystalline phase was either only mullite when the couple was quenched (Fig. 19A) or only alumina when the couple was cooled relatively slowly (Fig. 19C), while at a moderate cooling rate both alumina and mullite precipitated (Fig. 19B). The composition of the diffusion zone at 1903°C ranges from 0 to 62.5 wt% Al_2O_3 (Figs. 12 and 17). The liquidus composition at the transition temperature is 52.3 wt% Al_2O_3. Thus, the portion of the diffusion zone to be affected by alumina precipitation during an equilibrium-cooling is ∿350 μm, as determined from the diffusion profile of Fig. 12. The absence of alumina in this portion of the diffusion zone of a quenched couple (Fig. 19A), while slowly cooled couples clearly show alumina precipitation, can only be explained by the supercooling of the liquid but not by the alumina resorption at the transition temperature.

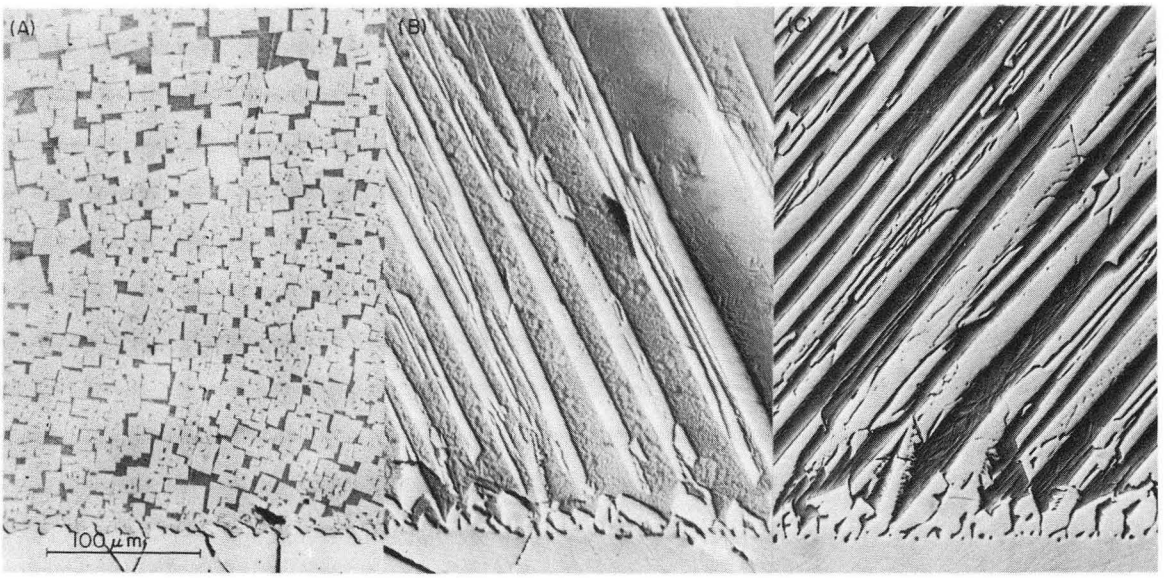

XBB 7210-5192

Fig. 19. Interference-contrast micrographs of the diffusion zone between a couple of sapphire (bottom) and fused silica (top) annealed at 1903°C for 0.9×10^3 sec and (A) quenched (5.72.3M), (B) cooled at a relatively moderate rate (5.72.3AM), and (C) cooled relatively slowly. The precipitates in the top portion of the diffusion zone are (A) mullite (light gray), (B) alumina (light gray needles) and mullite (fine precipitates between the alumina needles), and (C) alumina (light gray needles). The precipitates along the interface in (B) and (C) are also alumina.

The coexistence of alumina, mullite and liquid (glass) in the diffusion zone of the moderately cooled couple (Fig. 19B) is in violation of the phase rule. However, as already pointed out[37,38] in systems showing incongruency, complete equilibrium is rarely attained on cooling. At the transition point, the residual liquid, instead of reacting with alumina, may simply behave independently, and mullite may crystallize from it upon further cooling. Therefore, the phase rule is only observed locally, while the entire mixture itself is unstable.

Davis and Pask,[42] who observed the formation of an interfacial non-equilibrium liquid in the cristobalite-sapphire couples at subsolidus temperatures, suggested the existence of a metastable SiO_2-Al_2O_3 phase diagram with an eutectic and no mullite phase. The diffusion zone microstructure shown in Fig. 19C, then, is in further support of their observations since the total absence of mullite in this slowly cooled couple would also necessitate the metastable extension of the alumina liquidus below the transition temperature.

The diffusion zone microstructures of the 1953° and 2003°C couples showing only alumina precipitates in a glassy matrix are shown in Fig. 20. Similarly, the absence of mullite in these couples would be explained by the existence of a metastable SiO_2-Al_2O_3 phase diagram with no mullite phase.

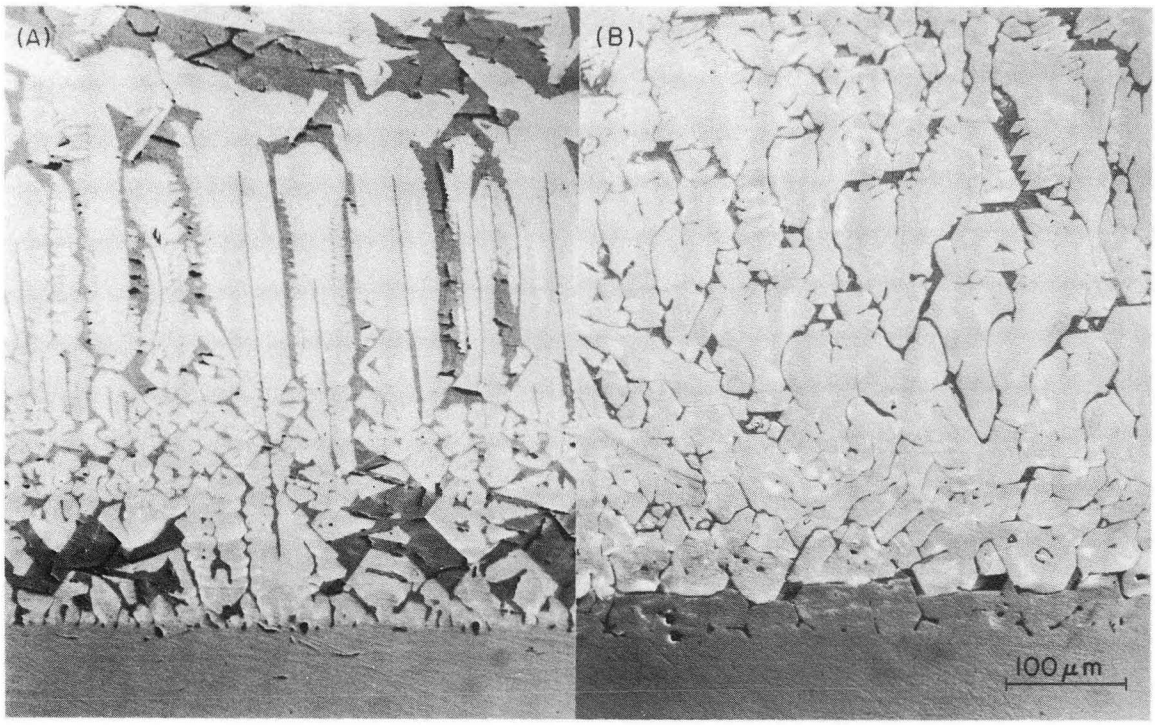

XBB 7210-5191

Fig. 20. Interference-contrast micrographs of the diffusion zone between a couple of sapphire (bottom) and fused silica (top) annealed at (A) 1953°C for 0.9×10^3 sec (5.72.8) and (B) 2003°C for 0.9×10^3 sec (7.72.1), and quenched. The light gray precipitates in the diffusion zone are alumina.

D. Phase Equilibria by Static Method of Quenching

The interpretation of the microstructures obtained by the static method of quenching would be quite difficult if the facts that have been established in the previous sections were not kept in mind: (1) mullite melts incongruently, not congruently, (2) a metastable SiO_2-Al_2O_3 phase diagram can exist without the mullite phase, and (3) the liquid phase can be supercooled through the alumina-liquid field without any alumina crystallization with increasing ease as silica increases. Numerous quenching experiments were conducted in order to test these conclusions. The results were in good agreement. Thus, only some of the typical microstructures and the ones that provided additional data are presented below.

The microstructure shown in Fig. 21 corresponds to an overall composition of 42.2 wt% Al_2O_3 that was homogenized above the mullite liquidus (Fig. 17) at 1953°C, cooled slowly below the mullite liquidus to 1753°C and quenched. The extent of mullite precipitation was highly dependent on the cooling rate due to the glass forming tendencies of the melt at this composition.[61] The mullite precipitates showed dendritic morphology, and their composition, as determined by point-beam microprobe analysis, varied from 73.0 to 78.5 wt% Al_2O_3. The formation of mullite in this melt during cooling is in agreement with the equilibrium phase diagram of Fig. 17; however, its formation with higher alumina contents than that of the equilibrium mullite solidus indicates metastability.

The microstructure of a 60.0 wt% Al_2O_3 containing mixture that was homogenized above the alumina liquidus at 1953°C and cooled slowly

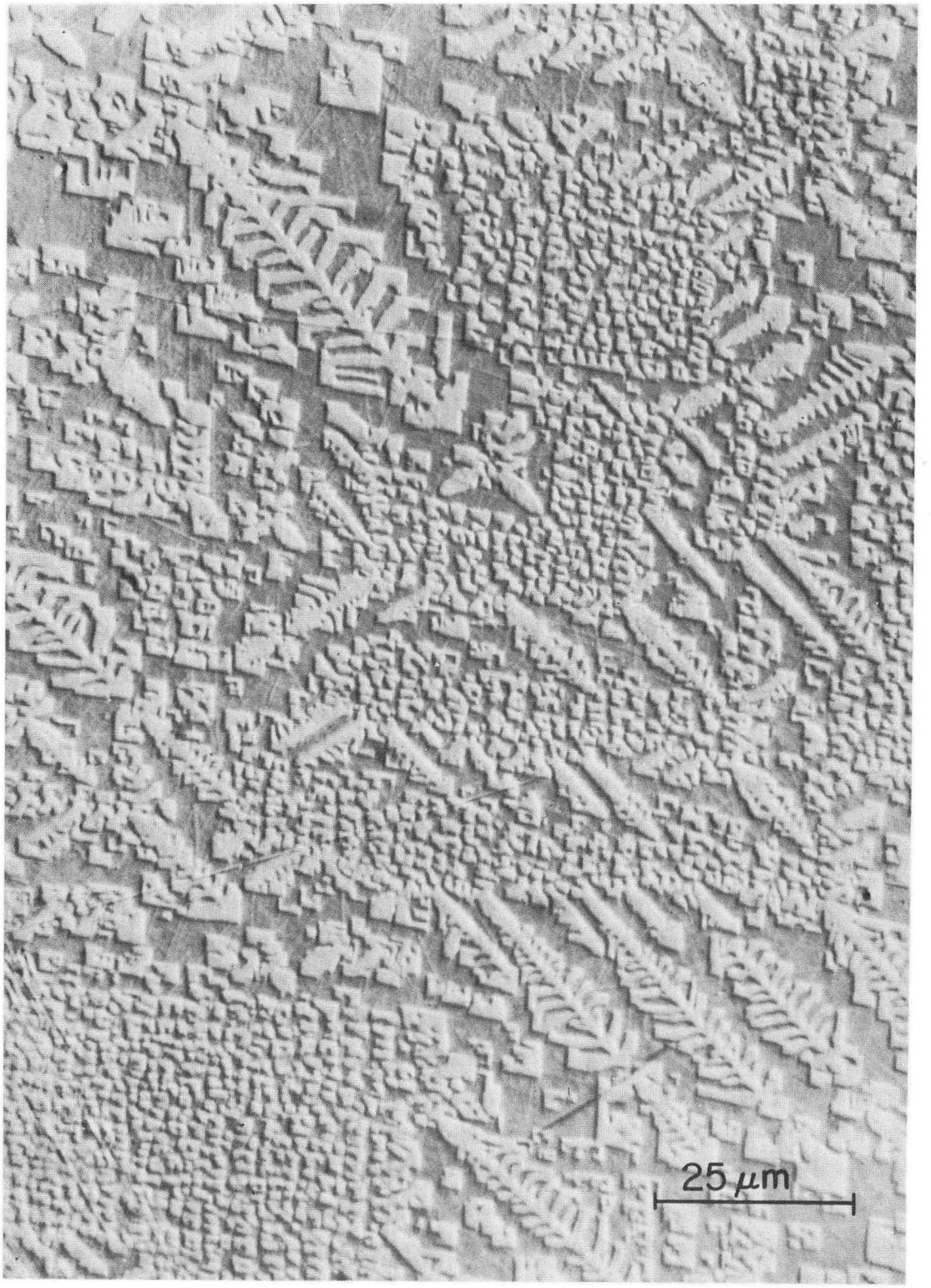

XBB 7210-5184

Fig. 21. Microstructure of the 42.2 wt% Al_2O_3 containing silicate melted in a sealed Mo crucible at 1953°C for 30 min, cooled to 1753°C in 30 min, and quenched in He from 1753°C (4.72.2). The light gray precipitates surrounded by a glassy matrix are mullite.

(∿60 min) below the transition temperature before quenching showed only mullite but no alumina (Fig. 22). The absence of alumina in this slowly cooled specimen, then, suggests the supercooling of the melt below the transition temperature. For comparison, it should be pointed out that melts of similar composition (∿60.0 wt% Al_2O_3) also formed to a large extent in the diffusion zone of the sapphire-fused silica couples that were annealed at 1903°C (Fig. 12 and 17). However, when these couples were cooled relatively slowly, the diffusion zone melts could not be supercooled since alumina precipitated out readily (Figs. 19B and C); and supercooling in the diffusion zone was only achieved by quenching (Fig. 19A). This comparison, then, suggests that the ease in precipitation of alumina in a diffusion zone but not in a homogenized melt would be attributed to the presence of the sapphire substrate in the former as a site for heterogeneous nucleation of alumina; the appearance of the microstructure supports this suggestion.

The precipitation of alumina, however, was observed in a mixture of 71.8 wt% Al_2O_3 ($3Al_2O_3 \cdot 2SiO_2$) that was homogenized at ∿1953°C, cooled slowly (∿30 min) to 1753°C, and annealed at 1753°C for approximately 29 days (Fig. 23). The formation of alumina in a melt of this composition clearly illustrates the incongruency of mullite. Although this mixture was annealed at 1753°C for approximately 29 days, the peritectic reaction was still incomplete due to the diffusion controlled nature of the reaction through the mullite layer that grew around each alumina precipitate. The composition profile through these mullite layers corresponded to the stable mullite solid solution range of 70.5-74.0 wt% Al_2O_3 (Fig. 17) indicating that local equilibrium existed

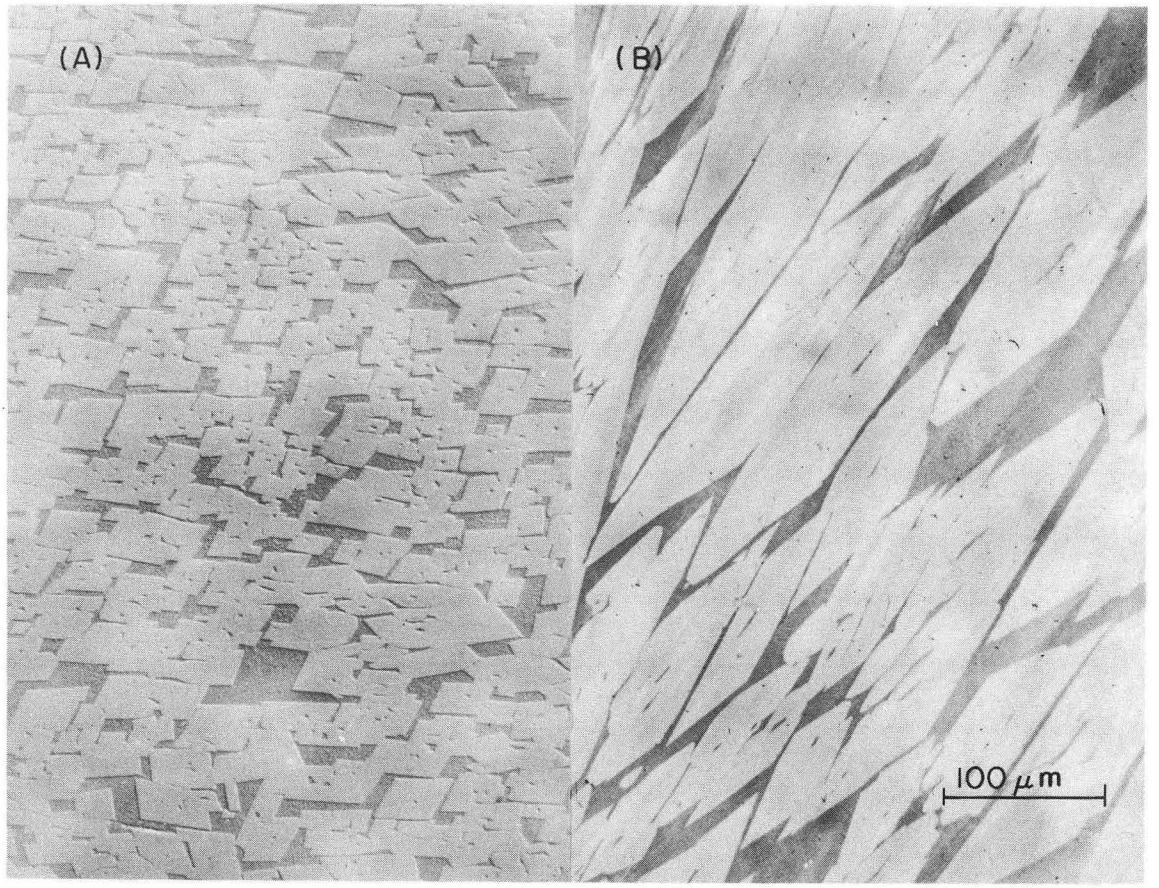

XBB 7210-5303

Fig. 22. Microstructure of the 60.0 wt% Al_2O_3 containing silicate melted in a sealed Mo crucible at 1953°C for 30 min, cooled to 1703°C in 60 min, and quenched from 1703°C (12.71.3). The light gray prismatic precipitates surrounded by a glassy matrix are mullite with their elongated direction (A) perpendicular and (B) parallel to the polished surface.

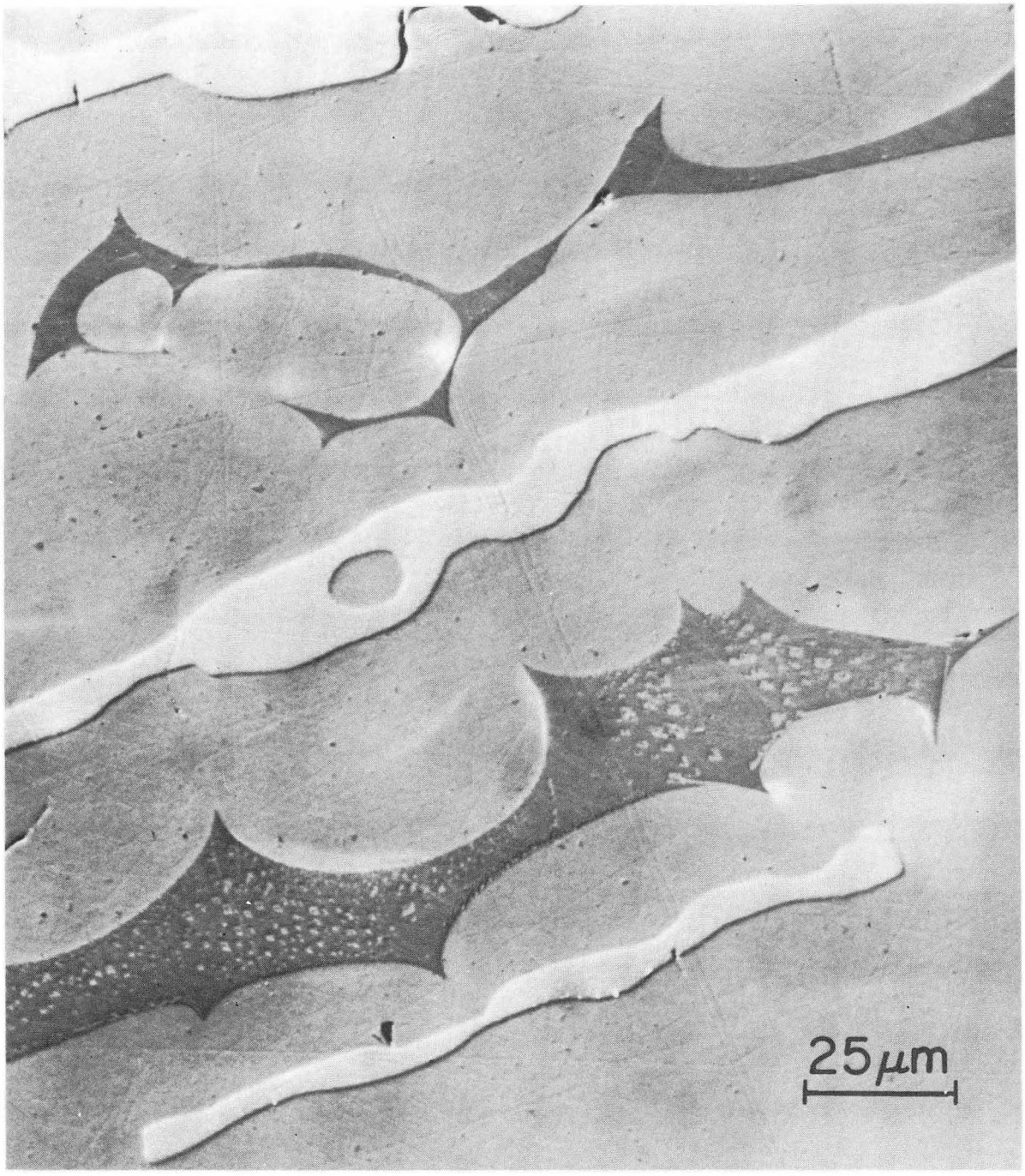

XBB 7210-5188

Fig. 23. Microstructure of the 71.8 wt% Al_2O_3 containing silicate melted in a sealed Mo crucible at 1953°C for 460 min, cooled to 1753°C in 30 min, annealed at 1753°C for 42,392 min (29.4 days), and quenched from 1753°C (9.70.2 and 8.71.8A). The light gray precipitates are alumina that are completely covered with a layer of mullite (gray). The glassy inclusions (dark gray) between the mullite layers also contain fine precipitates of mullite.

throughout the specimen. The microstructure around each alumina precipitate of Fig. 23, then, actually represents a sapphire-mullite-liquid diffusion couple (Fig. 16B), except that in this case alumina is grown in situ.

Typical microstructures of the silicate mixtures of 78.3 and 80.0 wt% Al_2O_3 that were homogenized above the alumina liquidus, at 2003°C, are shown in Figs. 24-26. As illustrated in these microstructures, the degree of mullite and/or alumina precipitation in the melts was highly dependent on the cooling rate followed. A rapid quench through the alumina-liquid field always resulted in the precipitation of only mullite with compositions varying up to 83.2 wt% Al_2O_3 (Fig. 24). Some residual high-silica glass was always present between the mullite grains. Occasional precipitation of alumina could only be observed around the sharp edges of the crucibles that apparently acted as nucleation sites for alumina precipitation. When the melts were not quenched but cooled slowly, alumina precipitated readily. The microstructure shown in Fig. 25 was typical of a specimen that was furnace-cooled at a moderate rate by just turning off the power to the furnace. Incrustation of alumina precipitates by a mullite matrix with glassy inclusions is again indicative of an incomplete incongruent reaction.

The microstructure shown in Fig. 26 which was typical of a very slowly cooled specimen containing 78.3 or 80.0 wt% Al_2O_3 is a unique one since it contains no mullite but only alumina surrounded by a glassy matrix. The needles embedded in the glassy matrix were in generally only a few microns thick and thus were too small for electron

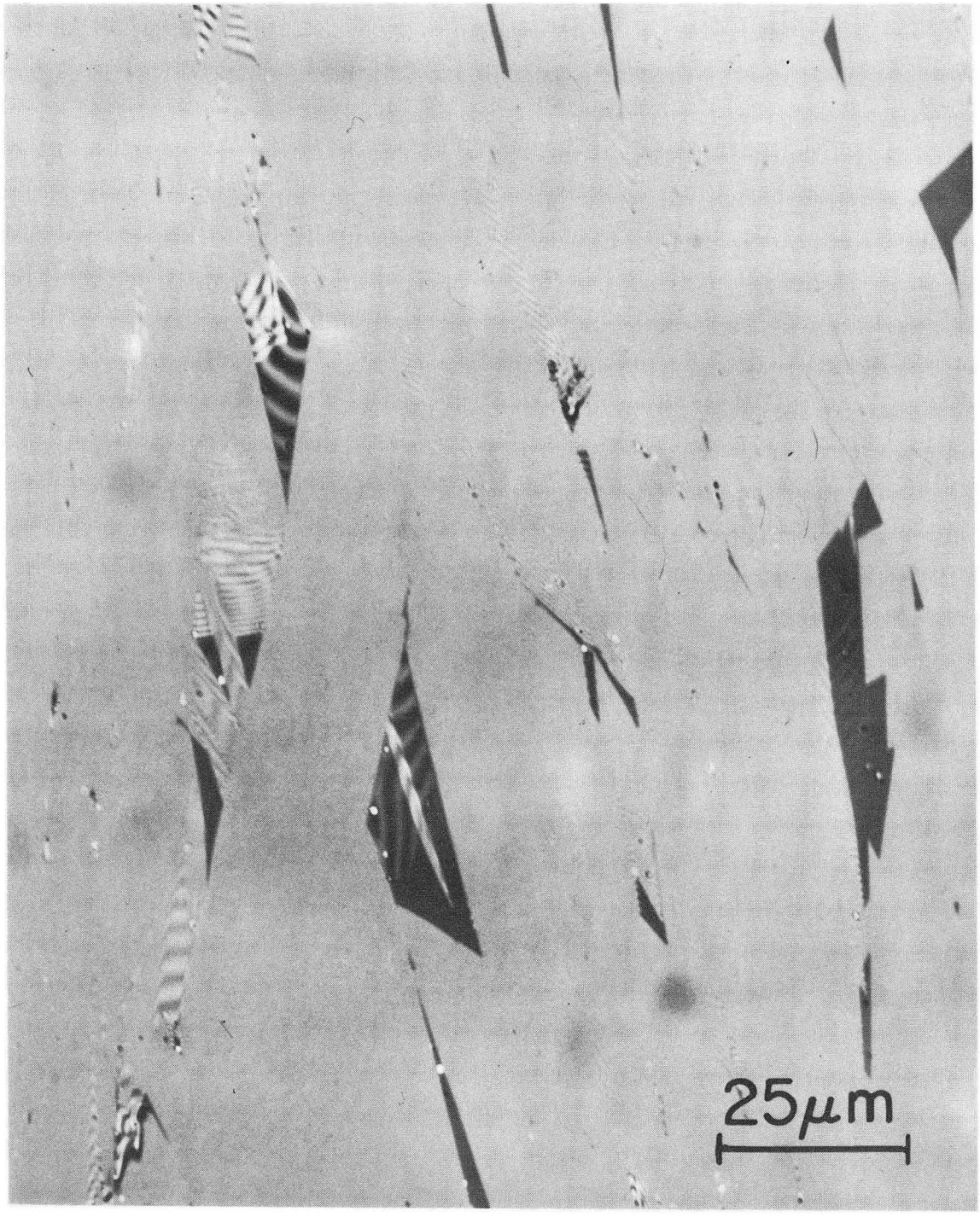

XBB 7210-5185

Fig. 24. Microstructure of the 78.3 wt% Al_2O_3 containing silicate melted in a sealed Mo crucible at 2003°C for 30 min and quenched in He (12.71.2). The matrix is mullite with glassy inclusions (dark gray).

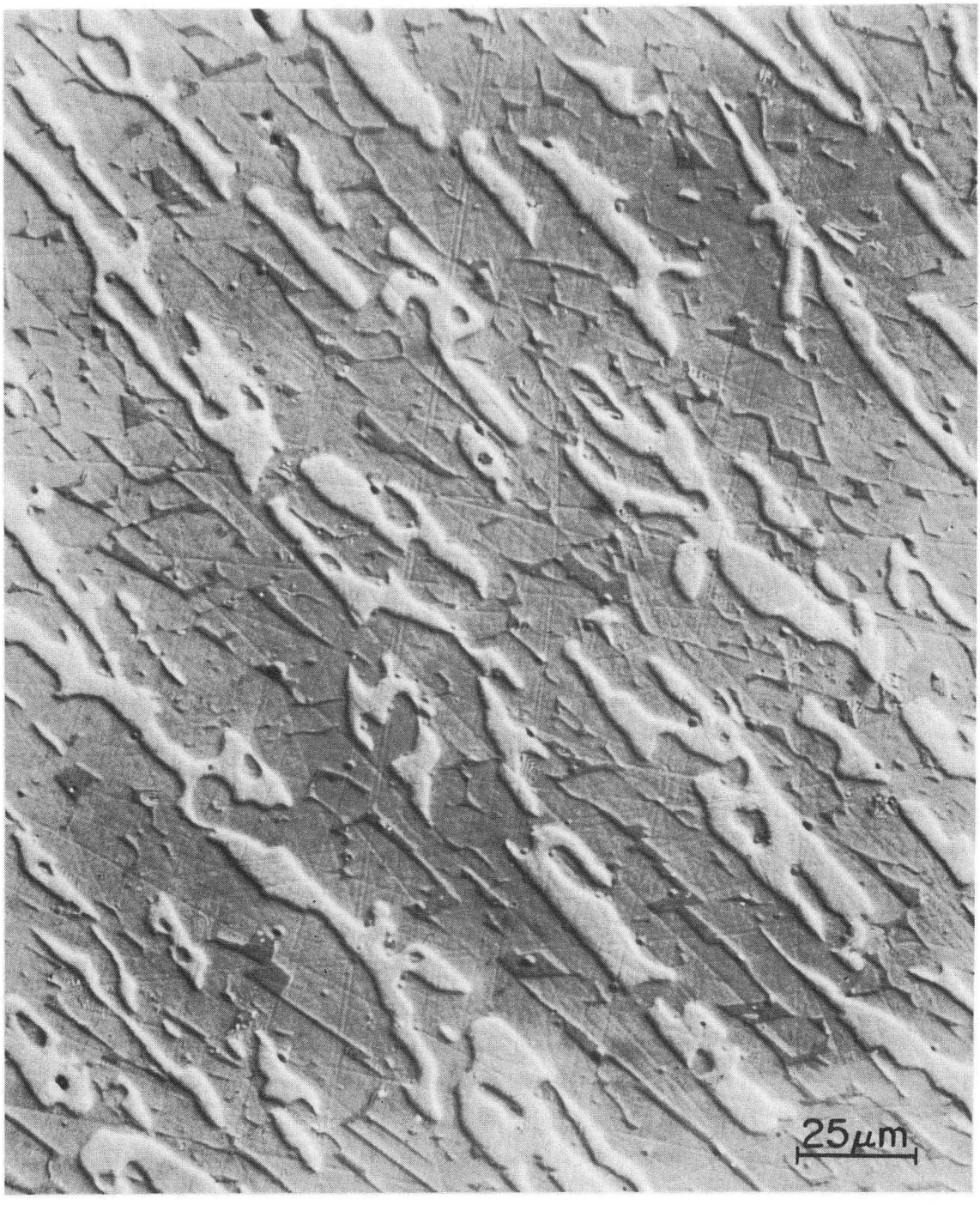

XBB 7210-5187

Fig. 25. Microstructure of the 80.0 wt% Al_2O_3 containing silicate melted in a sealed Mo crucible at 2003°C for 30 min and cooled at a moderate rate in vacuum by turning off the power to the furnace (12.71.4(2)). The light gray precipitates are alumina that are surrounded by mullite (gray). The dark gray inclusions are glass.

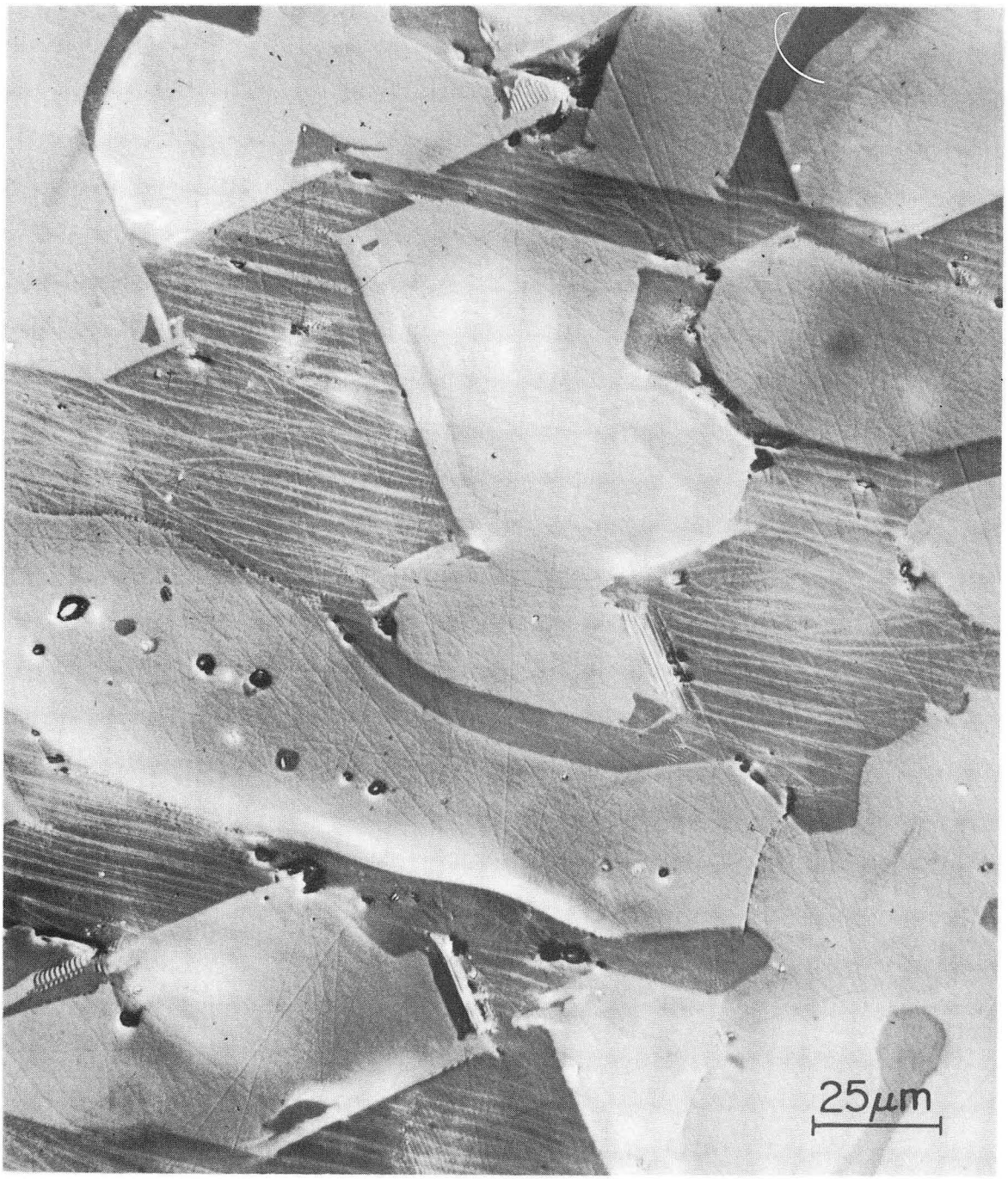

XBB 7210-5186

Fig. 26. Microstructure of the 80.0 wt% Al_2O_3 containing silicate melted in a sealed Mo crucible at 2003°C for 90 min, cooled to 1753°C in 60 min, and quenched in He from 1753°C (12.71.4(1)). The light gray, large precipitates and the needles are alumina surrounded by a glassy matrix.

microprobe analysis. X-ray diffraction analysis of such surfaces, however, indicated α-Al_2O_3 as the only crystalline phase; thus, these needles were indirectly identified as the secondary alumina that precipitated out during quenching from 1753°C. The overall composition of the matrix surrounding the primary alumina precipitates, as determined by scanning-beam electron microprobe analysis, was ∿48 wt% Al_2O_3. This composition is identical to that of alumina liquidus at 1753°C when it is extended below the transition temperature (Fig. 17) and provides a direct proof for the existence of a metastable SiO_2-Al_2O_3 binary diagram without any mullite phase.

E. Melting Behavior of Mullite

The melting temperature of stoichiometric mullite of 71.8 wt% Al_2O_3 composition was consistently determined to be 1880°C. Exactly the same melting temperature was also determined, independently by Mazdiyasni and Brown[58] using an identical material and similar experimental conditions. This value is considerably higher than the peritectic melting temperature of 1828°C as determined from the diffusion studies (Fig. 17). Furthermore, the microstructure of a partially melted specimen (Fig. 27) showed no alumina formation in the molten portion but only mullite that resolidified during cooling. Thus, stoichiometric mullite melted congruently at 1880°C but not incongruently at 1828°C, as expected on the basis of the results reported in the previous sections.

According to the stable phase diagram presented in Fig. 17, a mullite of 71.8 wt% Al_2O_3 composition becomes unstable at 1816°C and will dissociate to a mixture of a silica rich liquid phase and a higher

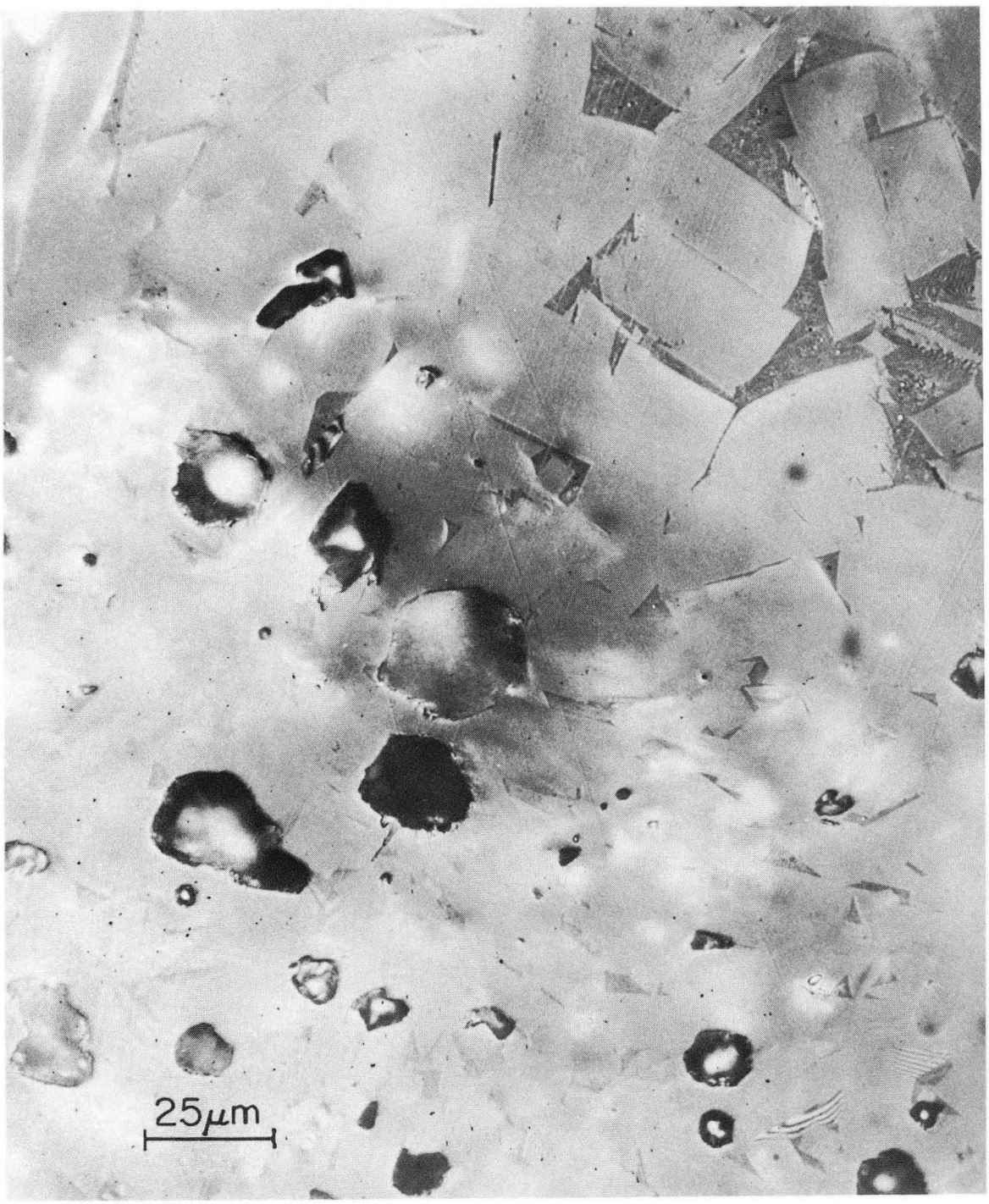

XBB 7210-5302

Fig. 27. Microstructure of stoichiometric mullite (71.8 wt% Al_2O_3) after partial melting at 1880°C and quenching in He (3.72.6). Unmolten section (bottom) is the porous (pull-outs) portion of the specimen where glassy inclusions (dark gray) are present between the mullite grains. The large precipitates that formed in the molten portion (top) are also mullite surrounded by a glassy matrix.

alumina mullite as temperature is increased above 1816°C. The specimens used in this study had submicron size grains and contained no liquid phase.[58] The unmolten portion of such a specimen after heating to 1880°C (Fig. 27) shows a mixture of ∿5-10 μm size mullite grains and a glassy phase indicating that in addition to the formation of a liquid phase, considerable amount of grain growth also took place above 1816°C. The composition of these mullite grains as determined by point-beam microprobe analysis was consistently 75.8 wt% Al_2O_3. Similarly, mullite that resolidified in the molten portion (top) corresponded to the same composition.

Eitel[38] has pointed out that incongruently melting silicates can be superheated above the peritectic temperature with the metastable prolongation of the corresponding liquidus. The result of this prolongation, then, is the metastable congruent melting of that compound at a higher temperature than the peritectic temperature. It is interesting to note that the mullite liquidus of Fig. 17 when extended beyond the peritectic temperature intersects the 71.8 wt% Al_2O_3 composition line at ∿1880°C which corresponds to the congruent melting temperature measured in this study. Such metastable congruent melting of mullite would also necessitate the extension of the mullite solidus above the transition temperature to higher alumina contents and thus provides the explanation for the shift in alumina content of mullite to 75.8 wt% Al_2O_3.

F. Stable and Metastable Phase Equilibria

The results of the last two sections on metastable equilibria are now outlined in Fig. 28. The diagram shown in this figure is simply the composite of two binary eutectic diagrams between silica-mullite and silica-alumina. When superimposed, the outcome is the stable phase diagram outlined with the solid lines, which shows a peritectic at the intersection of mullite and alumina liquidus lines. The upper limit of the mullite solid solution range with respect to alumina has been set at 83.2 wt% Al_2O_3 since this was the highest alumina content detected in any mullite during this study. The maximum temperature for this composition has been tentatively set at ∿1890°C and is subject to change as more data become available on the metastable extensions of the liquidus and solidus lines. However, on the basis of the liquidus temperature determined at 71.8 wt% Al_2O_3 (Section IVE), it may be stated that this maximum temperature is definitely not below 1880°C. This upper limit agrees well with the compositions of mullite single crystals grown from a melt by Bauer, et al.[11,86] (82.57 wt% Al_2O_3) and Neuhaus and Richartz[87] (77.5 wt% Al_2O_3). The metastable silica-mullite equilibrium diagram, as presented in Fig. 28, then effectively explains the formation of high-alumina mullites only when they are solidified from a melt. In the presence of alumina, the solid solution range is limited to a narrow range; thus the highest alumina content that can be incorporated into mullite by solid state reactions is 74.0 wt% Al_2O_3.

The only shortcoming of the diagram presented in Fig. 28 is that it does not provide an explanation for the precipitation of alumina-rich mullite in the diffusion zone of the couples annealed at 1678°C

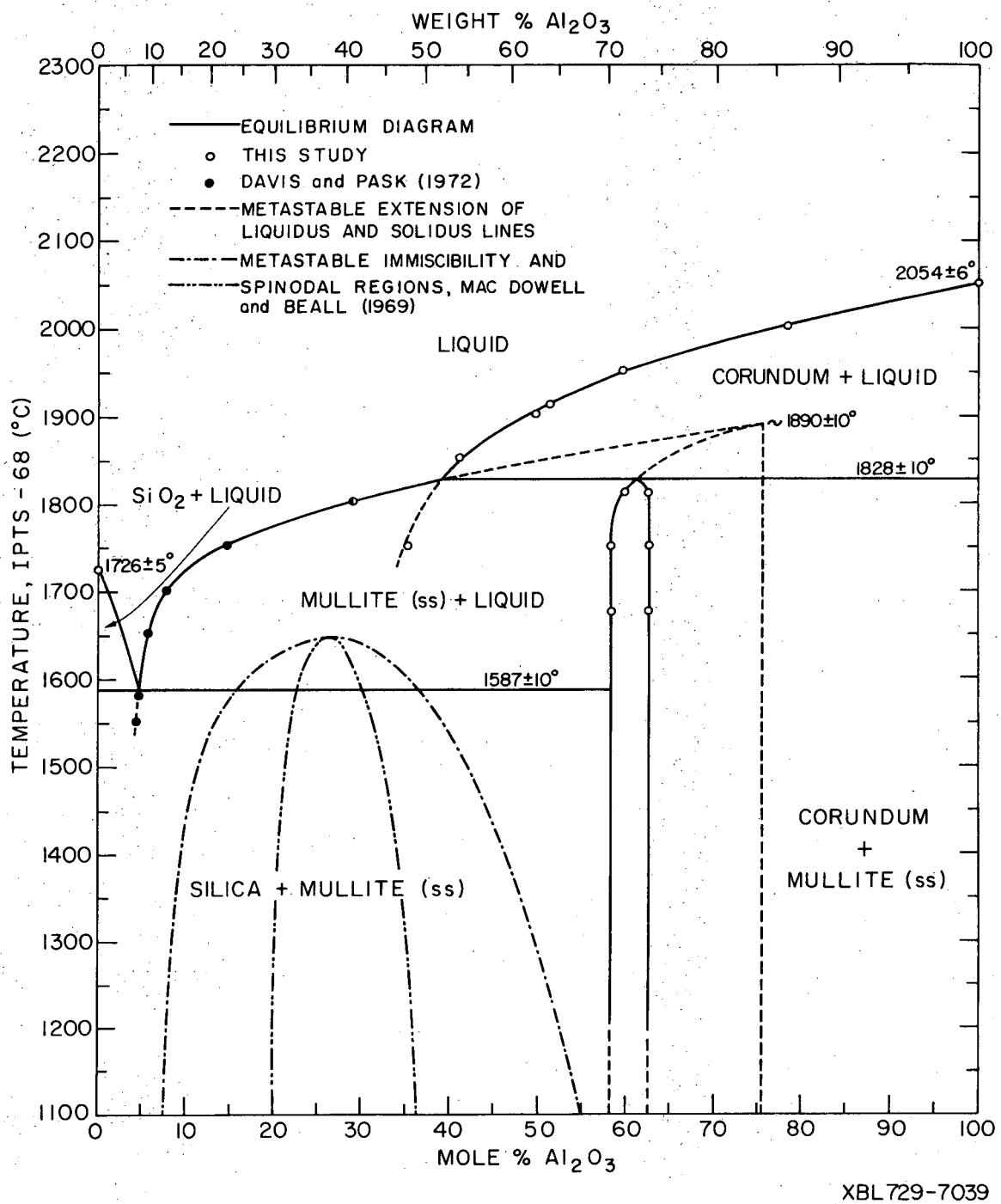

Fig. 28. Metastable extension of the silica-mullite equilibrium diagram superimposed on the equilibrium silica-alumina diagram.

to 1813°C (Section IVB2). The composition of the melts in this diffusion couples ranged from 10.9 to 42.2 wt% Al_2O_3, and they were at equilibrium with mullite at the stated temperatures. Any mullite to precipitate out in these melts, under equilibrium conditions, could not be any richer than 71.5 wt% Al_2O_3 at 1813°C and 70.5 wt% Al_2O_3 below 1753°C. A possible explanation for the precipitation of an alumina-rich phase in these high-silica melts would then be the existence of a disordered mullite phase as illustrated by the free energy of mixing vs composition curves in Fig. 29.

Aramaki and Roy[26] by X-ray studies, observed that heat treatment of mullite caused nearly as much change in its lattice parameters as composition and suggested Al-Si order-disorder as a possible explanation. Later, similar observations have also been made by Majumdar and Welch[88] and Mazdiyasni and Brown[58] in support of Al-Si order-disorder in mullite. A disordered mullite phase, as shown in Fig. 29, will have a broad free energy of mixing vs composition curve and may easily vary in composition to higher alumina contents when precipitated from a melt. At the present, however, no definite proof for the existence of such a disordered phase is provided.

G. Diffusion Data

1. Diffusion in SiO_2-Al_2O_3 Melts

Diffusivity values as a function of aluminum concentration in the melt were determined by the Boltzmann-Matano analysis, utilizing the diffusion profiles as presented in Fig. 12. Diffusivities varied exponentially with aluminum concentration at 1803° and 1853°C. At

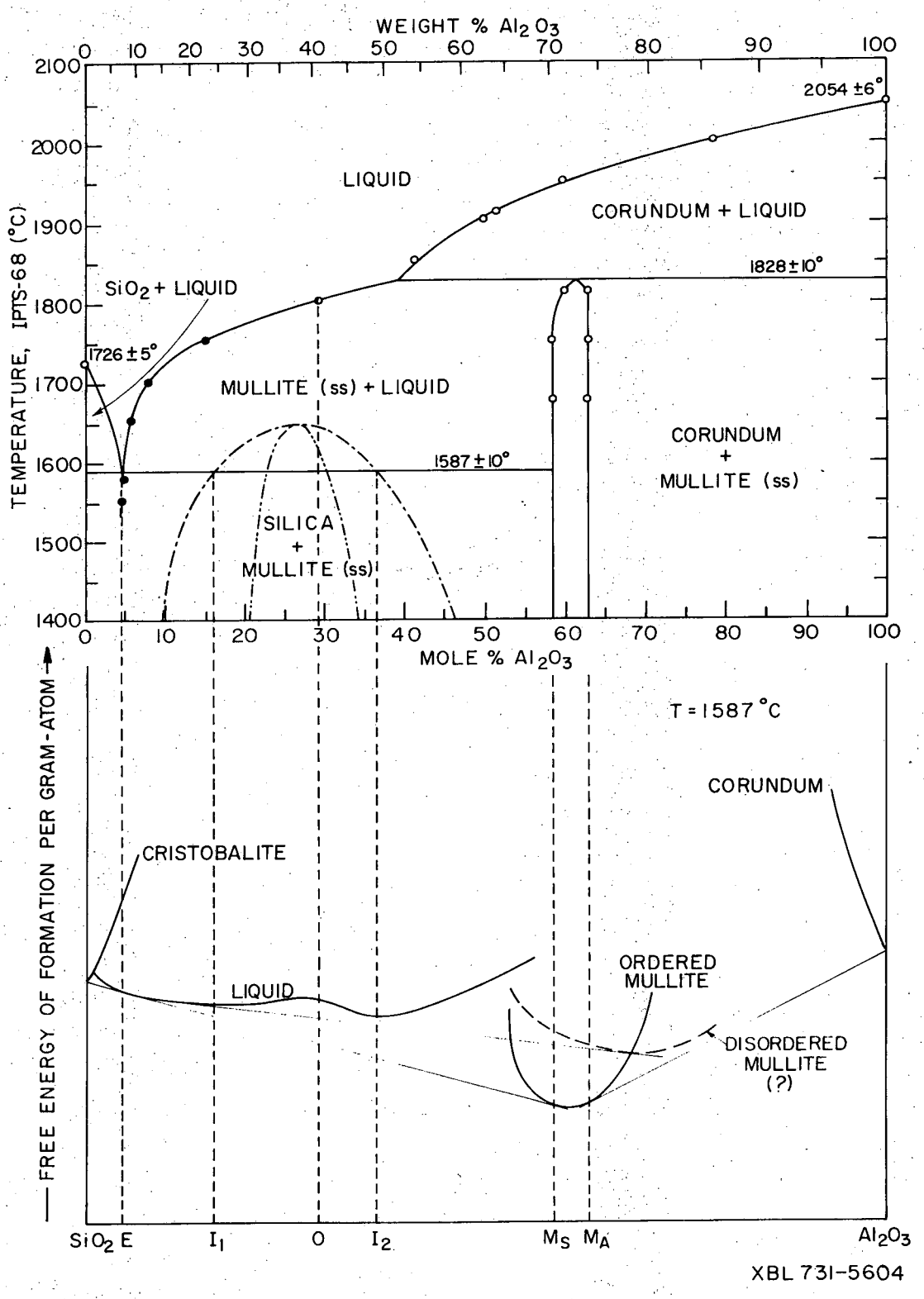

Fig. 29. Hypothetical free energy of mixing vs concentration curves in SiO_2-Al_2O_3 system at the eutectic temperature.

1903° to 2003°C, however, the concentration range covered was wider (e.g. 0-80.0 mole% Al_2O_3 at 2003°C), and it was necessary to express the diffusivity-concentration relationships with two exponential functions. Such computer drawn diffusivity-concentration plots, representative of various runs conducted at a temperature, and the corresponding exponential equations are given in Fig. 30. Similar diffusivity-concentration relationships were determined by Davis and Pask[42] in the temperature range of 1653° to 1803°C. For comparison, their data have been replotted in Fig. 31 along with the data obtained in this study. In both Figs. 30 and 31, the termination of the solid portion of a line represents the solubility limit of the liquid in contact with mullite or alumina (Fig. 17).

In order to determine the temperature dependence of diffusivity (Eq. 28), lnD values at a certain composition were determined and plotted as a function of inverse temperature in Fig. 32. The D_o and Q values were determined from these Arrhenius plots by least-squares analysis and are tabulated in Table IV. Due to an apparent change in diffusion mechanism, the entire temperature range could not be covered by a single Arrhenius equation, and it was necessary to show a break at ∿1870°C. However, such a break at a specific temperature is only for convenience in analytical analysis, and any change in diffusion mechanism over this temperature range should rather be considered more gradual. This topic will be discussed further in Section V.

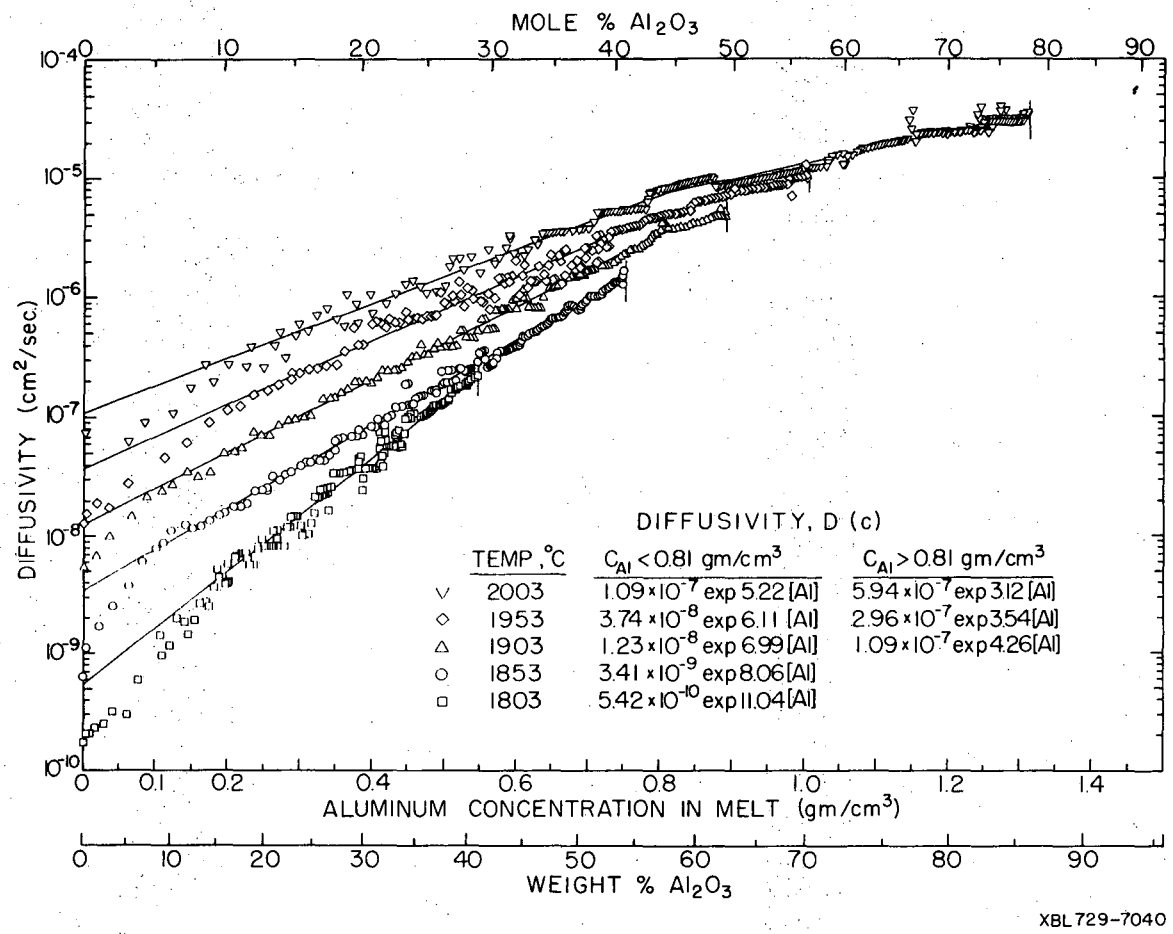

Fig. 30. Computer drawn diffusivity-concentration plots for diffusion in the SiO_2-Al_2O_3 melts in the temperature range of 1803° to 2003°C.

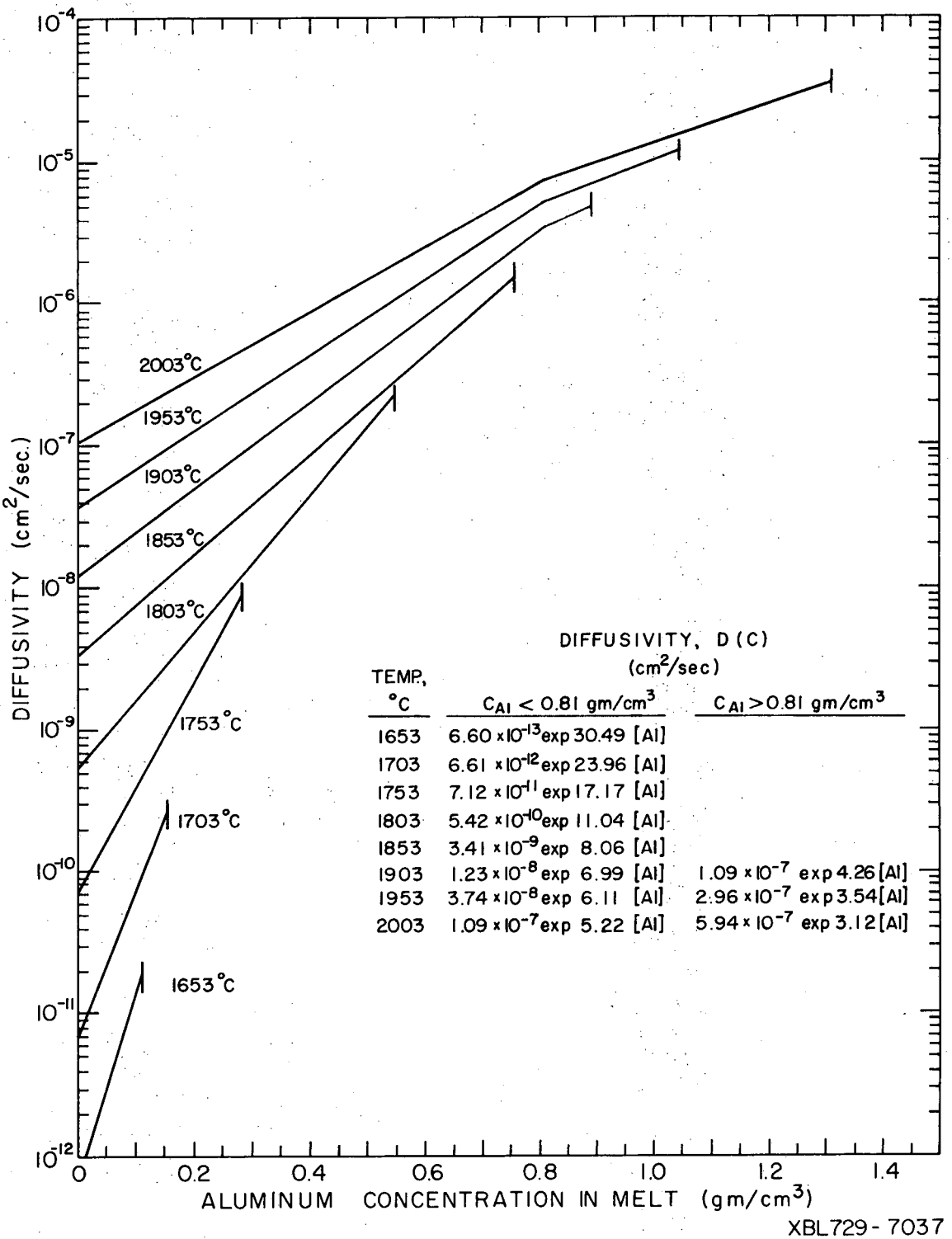

Fig. 31. Diffusivity-concentration plots for diffusion in the SiO_2-Al_2O_3 melts in the temperature range of 1653° to 2003°C.

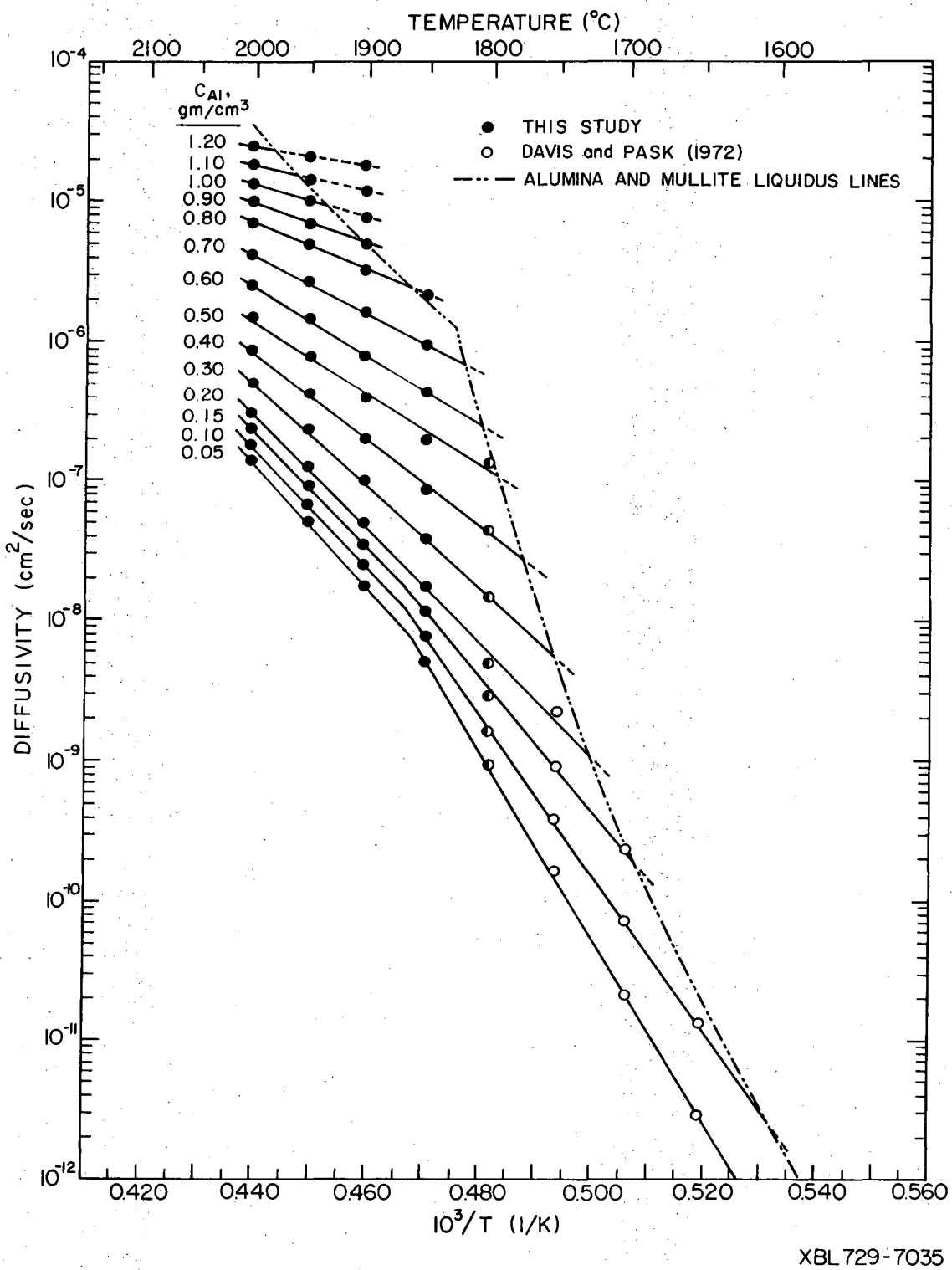

Fig. 32. Arrhenius plots of diffusivity vs reciprocal of absolute temperature at constant aluminum concentrations in the melt.

Table IV. Diffusion data for the SiO_2-Al_2O_3 melts.

C_{Al} (gm/cm^3)	$C_{Al_2O_3}$ (mole%)	<∿1870°C		>∿1870°C	
		D_o (cm^2/sec)	Q (kacl/mole)	D_o (cm^2/sec)	Q (kcal/mole)
0.05	2.53	8.03×10^{22}	303.3±1.6	7.00×10^{12}	205.2±0.1
0.10	5.10	1.55×10^{18}	256.0±1.3	1.33×10^{12}	196.4±0.1
0.15	7.66	5.86×10^{13}	211.5±3.7	2.51×10^{11}	187.7±0.2
0.20	10.25	2.07×10^{11}	185.6±2.5	2.07×10^{11}	185.6±2.5
0.30	15.51			5.87×10^{9}	167.1±0.8
0.40	20.87			3.25×10^{7}	141.4±2.0
0.50	26.37			1.80×10^{5}	115.8±4.0
0.60	32.00			1.47×10^{5}	112.1±0.9
0.70	37.81			4.53×10^{3}	94.0±0.8
0.80	43.81			1.40×10^{2}	76.0±0.7
0.90	50.00			16.9	64.9±0.7
1.00	56.45			1.89	53.6±0.1
1.10	63.10			0.21	42.4±0.8

2. Diffusion in Mullite

Concentration independent diffusivities for diffusion in mullite were determined by utilizing the data reported in Table III and Eq. 26. The constants γ_A and γ_B needed for the calculation of the diffusivities by Eq. 26 were obtained by solving Eqs. 24A and 24B graphically. The values for $(\gamma_B-\gamma_A)$ and diffusivity are tabulated in Table V. As discussed in Section IIC, the use of Eq. 26 assumes a concentration independent diffusivity. The validity of this assumption was checked by the Boltzmann-Matano analysis of the layer grown at 1813°C; and exactly the same diffusivity with no concentration dependence was also obained by this method. An Arrhenius plot of these diffusivities is shown in Fig. 33 along with the low-temperature and low-concentration portion of the diffusion data for the SiO_2-Al_2O_3 melts. An apparent activation energy of 168.1±7.0 kcal/mole was obtained for diffusion in the mullite phase.

Table V. Data for diffusion in mullite.

Temp. IPTS-68 (°C)	γ_A	γ_B	$\gamma_B-\gamma_A$	Diffusivity, D (cm^2/sec)
1678	-0.140	0.112	0.252	5.39×10^{-12}
1678	-0.140	0.112	0.252	4.49×10^{-12}
1703	-0.140	0.115	0.255	8.10×10^{-12}
1703	-0.140	0.115	0.255	8.12×10^{-12}
1703	-0.140	0.115	0.255	8.82×10^{-12}
1703	-0.140	0.115	0.255	9.23×10^{-12}
1753	-0.135	0.126	0.261	1.56×10^{-11}
1813	-0.135	0.130	0.235	9.76×10^{-11}

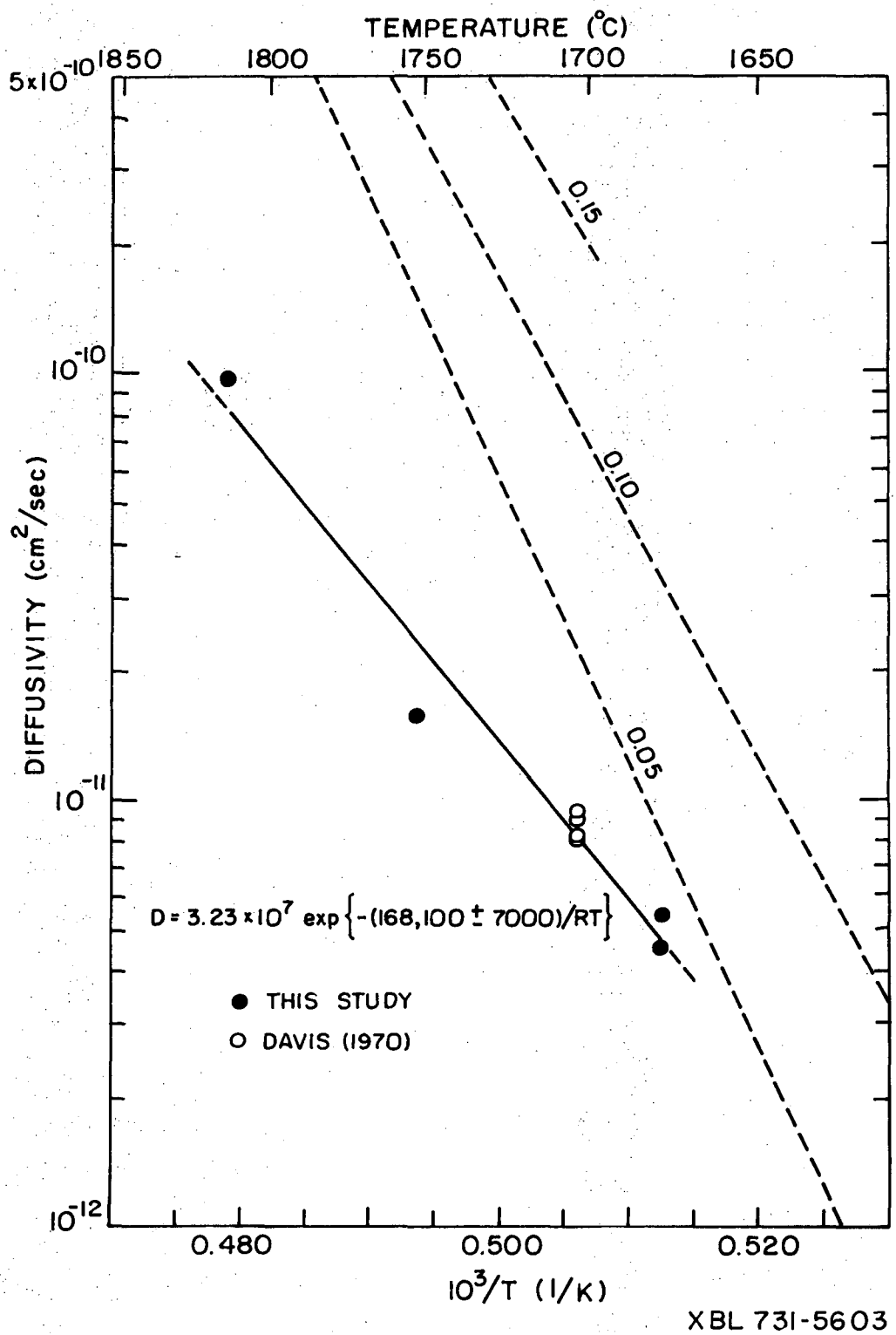

Fig. 33. Arrhenius plot of diffusivity vs reciprocal of absolute temperature for diffusion in mullite. Broken lines correspond to low temperature regions of Fig. 32.

V. DISCUSSION

A. Structure of SiO_2-Al_2O_3 Melts

The parameters reported in Table IV for diffusion in the SiO_2-Al_2O_3 melts correspond to a wide composition range extending from pure SiO_2 to compositions as high as 60 mole% Al_2O_3. The correlation of these parameters to operative diffusion mechanisms in these melts requires a prior knowledge of the fused silica structure and the changes brought about by the addition of alumina.

An acceptable interpretation of the fused silica structure follows the principles set down by Zachariasen[89] some 40 years ago and supported by the experimental work of Warren, et al.[90] Zachariasen's model draws an analogy to the structure of crystalline silicates where the structural backbone consists of oxygen tetrahedra sharing corners. In crystalline silicates, silicon lies in the center of such tetrahedra with a resulting Si-O-Si bond angle of $\sim 180°$. Fused silica, although consisting of a similar structural backbone of oxygen tetrahedra joined at the corners, lacks the systematic packing of the crystalline phases. Its structure is described as a random network where the Si-O-Si bond angle can range from 180 down to at least 150°.

The random network model of Zachariasen and Warren, however, has not been free of criticism[91-93] because the radial distribution function method of Warren, et al., used in their experimental work is inadequate in describing the average coordination numbers of the atoms beyond the first or second coordination spheres. Most recent studies[92,93] support a short-range order cyrstallite structure in which tridymite-like regions

of up to ∿20Å or more are bonded together in essentially random orientations.

For the purposes of this study, either model is equally acceptable since the discussion of diffusion mechanisms will only consider the degree of Si-O-Si continuity in the melt structure but not the degree of ordering.

In binary silicates, the continuity of the network structure of fused silica is dependent on the nature and the amount of metal oxide addition. Alkali and alkaline-earth metals with low M-O bond strength and high coordination number (modifiers) are incapable of replacing tetrahedrally coordinated silicon and instead fit into the interstices. A continuous silica network model is generally accepted at high-silica contents when the O/Si ratio (determined by the amount of modifier oxides) is high enough to result in at least two of the oxygens of a tetrahedra being shared with two other tetrahedra (bridging oxygens).

The role of the aluminum ion in the silica network differs from that of the modifiers since it can either participate in network formation by replacing silicon isomorphously or go into six-fold coordination, as predicted from an oxygen/aluminum ionic ratio of 0.41.[94] In the polymorphs of Al_2SiO_5, for instance, the observed ligancies are four and six in sillimanite, five and six in andalusite, and only six in kyanite. Similarly, in mullite, the ligancies are four and six.

Extensive studies concerning the coordination of aluminum ion in silicate glasses and melts, thus far, have been limited to alkali aluminosilicates. Isard[95] measured electrical conduction in sodium aluminosilicate glasses and observed a pronounced minimum in activation

energy at compositions having a sodium to aluminum ion ratio of one. He proposed that up to the limit where the Na/Al ratio equals one, aluminum is directly substituted for silicon in tetrahedral coordination; thus, the coordination shell around the sodium ions expands a non-bridging oxygens are eliminated, and the activation energy decreases. Beyond this limit, all the aluminum ions in excess of sodium ions are assumed to go into six-fold coordination as a network modifier, allowing the coordination shell of the sodium ion to decrease again. This structural model was further supported by the more systematic studies of Day and Rindone [96] who measured refractive index, density, infrared absorption, internal friction and X-ray fluoresence shifts of the AlK_{α} peaks for similar sodium aluminosilicate glasses and observed analogous changes in these properties with composition. An implication of this model then is that in the total absence of alkali ions, i.e., in binary aluminum-silicate melts or glasses, all the aluminum ions would be in octahedral coordination.

The dependence of density, index of refraction, and internal friction on the Li/Al ratio in lithium aluminosilicate glasses has been studied by Dei and Steinkamp.[97] The similarity between the property dependences on the R/Al ratio has been related to the structural similarities of both sodium and lithium aluminosilicate glasses.

Lacy,[98] on the other hand, has argued that in glasses and melts with a high proportion of basic oxides, the formation of AlO_6 groups would be unlikely since this requires the sharing of oxygens with other tetrahedral or octahedral groups and thus constitutes a spatically and energetically unfavorable configuration. He therefore suggests

that a proportion of individual oxygen atoms may be shared between an AlO_4 group and two SiO_4 groups or between an SiO_4 group and two AlO_4 groups, i.e., "tricluster". He also pointed out that due to the formation of tricluster, oxygen may be made available for incorporation in octahedral groups in compositions where this otherwise would be impossible.

Similarly, Riebling,[99] who based his arguments on molar volume models, viscosity and density data of sodium aluminosilicate melts, suggested that when the Al/Na ratio is greater than one, <u>some</u> AlO_6 octahedra <u>may</u> exist in the melts, but <u>not every</u> aluminum ion in excess of the sodium ion total finds itself in an octahedral configuration. He also noted that this model for the high-temperature liquid state would agree with the corresponding high-temperature crystalline-state information, especially for melts close to the SiO_2-Al_2O_3 binary system.

This background information on alkali aluminosilicates may now be extended to the binary SiO_2-Al_2O_3 system in order to explain the changes brought about in the fused silica structure by the addition of alumina. The activation energy for diffusion in the SiO_2-Al_2O_3 melts above ∿1870°C dropped drastically from 205 to 42 kcal/mole as the alumina content increased from 2.53 to 63.10 mole% Al_2O_3 (Table IV). Similarly, the activation energy for viscous flow[100,101] in the SiO_2-Al_2O_3 melts, above 1860°C, drops from ∿120 kcal/mole to ∿40 kcal/mole as the composition ranges from pure silica to alumina. When plotted as a function of alumina content (Fig. 34), it is noted that the large changes in activation energy are actually confined to the composition range up to ∿45 mole% Al_2O_3 while the changes beyond that composition are more gradual. As discussed in Section IVA, the densities of these

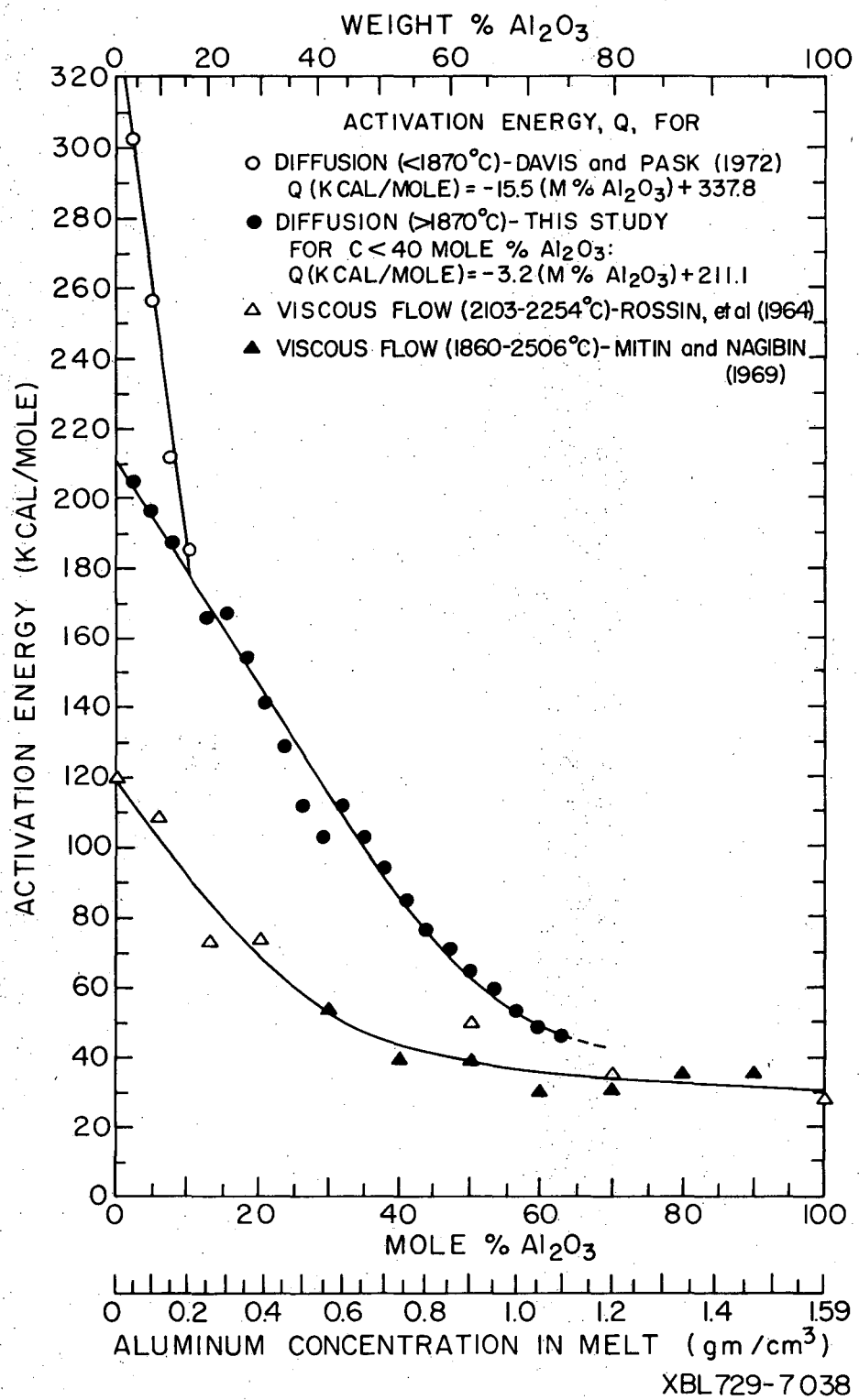

Fig. 34. Concentration dependence of activation energy for diffusion and viscous flow[100,101] in SiO_2-Al_2O_3 binary melts.

aluminum-silicate melts increase linearly up to ∿45 mole% Al_2O_3 and show a negative deviation from linearity beyond that composition. Such anomalous changes in activation energy for transport and density then are indicative of a fundamental change in the structure of these melts at ∿45 mole% Al_2O_3. Studies[81,102,103] on alkali and alkaline-earth binary silicates have indicated analogous changes in properties over the composition range of 10-20 mole% metal oxide. Activation energy for viscous flow,[102] for instance, decreases from ∿120 kcal/mole for pure silica to ∿50 kcal/mole at 10 and 20 mole% M_2O and MO, respectively. Changes beyond this composition, as in the SiO_2-Al_2O_3 system, become more gradual. In an attempt to explain these anomalous changes in properties, Bockris and co-workers,[103,104] have postulated an ionic model which assumes that at a certain metal oxide content the continuous network structure of fused silica becomes unstable with respect to discrete ionic silicate groups. These silicate groups vary in size and complexity depending on the nature of the cations and the overall composition. The range 10-20 mole% M_2O or MO corresponds to the stability limit where the continuous network structure is completely broken down in the presence of modifying cations. In comparison, then, the fact that this stability limit is considerably higher (∿40 mole% Al_2O_3) in the SiO_2-Al_2O_3 system indicates that aluminum itself acts as a network former and is present mainly in tetrahedral coordination, at least at high silica contents.

More direct evidence for the presence of aluminum ion in tetrahedral coordination, in binary SiO_2-Al_2O_3 glasses, has been provided by Davis[84] utilizing X-ray fluorescence measurements. He showed that AlK_α

wavelength of aluminum-silicate glasses quenched from ∿1200°C, when compared to the X-ray emission spectra of metallic aluminum, corresponded to that of a tetrahedrally coordinated aluminum at 3.0 mole% Al_2O_3 and octahedrally coordinated aluminum at and above 6.2 mole% Al_2O_3. Wardle and Brindley[105] have recently pointed out that although the X-ray fluoresence technique provides a means for determining coordination numbers, when more than one coordination state occurs simultaneously, the results reflect the weighted average of the two coordinations. Thus, the findings of Davis do not necessarily indicate a sudden change from four-fold to six-fold coordination at 6.2 mole% Al_2O_3 but could also indicate a gradual change from a predominantly four-fold coordinated structure to a predominantly six-fold coordinated one. Furthermore, these findings reflect the coordination states at room temperature after some of the glasses were cooled into the immiscibility region and microsegregated (Fig. 28). The lower limit of the immiscibility region, at 1200°C, is 7.0 mole% Al_2O_3 and corresponds closely to the transition range determined by Davis. Therefore, it is suggested that, above the immiscibility region, in the melts, aluminum ion is predominantly in tetrahedral coordination up to ∿45 mole% Al_2O_3 content, as indicated by the activation energy and density data. Glasses that form from these melts, however, would contain AlO_6 groups at a higher proportion due to microsegregation during cooling.

B. Diffusion Mechanism in SiO_2-Al_2O_3 Melts

On the basis of the structural information outlined above, the discussion of the diffusion mechanism in aluminum-silicate melts, over the composition range covered in this study, has to consider two types of end-structures: (1) at high silica contents, a silica tetrahedra network structure that is very much like the crystalline phases of silica, and (2) at alumina contents above ∿45 mole% Al_2O_3, a structure that consists of isolated silica tetrahedra and is ionic in nature. Diffusion in fused silica and high silica melts would compare to diffusion in highly disordered ionic solids where transport is by interdiffusion of individual ions involving the rupture of M-O bonds. Diffusion in high alumina liquids, on the other hand, would be by mutual rotation of anionic groups involving only coulombic interaction.

Let us first consider the diffusion in fused silica and high silica melts. In this case, the interpretation of the activation energies for diffusion may follow one of two fundamental approaches. In the first approach, as discussed by Mott and Gurney,[106] diffusion occurs exclusively by the vacancy mechanism. Ions may diffuse by jumping from a lattice position into an adjoining vacancy, or empty lattice site. The experimentally determined activation energy, Q, is expressed in two parts as the energy necessary for the formation of the defect and the energy necessary for its migration. In order to maintain charge neutrality, two kinds of defects of opposite charge must be formed. This may be accomplished either by the formation of an equal number of vacant sites and interstitial ions (Frenkel defects) or by the formation of vacancies in both the anion and cation lattices (Schottky defects).

In the second approach,[107] the diffusion process is expressed in terms of the absolute reaction rate or transition state theory. Diffusion is characterized as an activated jump process over an energy barrier, or saddle point, separating two equilibrium lattice sites. Only a certain fraction of the diffusing units attain this "activated state" or"transition state" and move from one site to the next. According to the theory of absolute reaction rates, the activated complex can be treated as any other atomic species, possessing the usual thermodynamic properties. Heat of formation of this complex then is equal to the experimentally determined activation energy for diffusion.

In either approach, it is difficult to estimate quantitatively the activation energy for diffusion. However, since diffusion of ions in a continuous oxygen network structure first requires the rupture of cation-anion bonds, the measured activation energies, to a first approximation, have to be consistent with the bond energies. Secondly, the measured activation energies have to relate to the openness of the structure since the energy needed for the subsequent motion of the ion to the next site depends mainly on the energy needed to squeeze through the "doorways" between sites.

The activation energy for alumina diffusion into fused silica, as obtained by extrapolation of the activation energy vs concentration plots of Fig. 34 to pure silica composition, is 211 kcal/mole above ∿1870°C and 338 kcal/mole below ∿1870°C. The M-O bond strengths of tetrahedrally coordinated silicon and aluminum ions are 106 and 101-79 kcal/mole, respectively, and that of octahedrally coordinated aluminum

is ∿60 kcal/mole.[108] Thus, although the measured activation energies are quite high, they are certainly consistent with the high M-O bond energies of tetrahedrally coordinated aluminum and silicon. The rupture of only two Si-O bonds would require an activation energy of 216 kcal/mole. Thus, these activation energies are comparable with what one would expect from the interdiffusion of tetrahedrally coordinated aluminum and silicon ions in an oxygen network structure. Due to the lack of self-diffusion data, however, a detailed analysis of the interdiffusion mechanism, at this point, would only be speculative in nature.

The change in activation energy for diffusion from 338 to 211 kcal/mole with increasing temperature is indicative of a structural change in fused silica. This premise is further supported by the fact that a similar shift in the activation energy for viscous flow has been observed over the same temperature range, from 122 kcal/mole in the high-temperature range (Fig. 34) to 160 kcal/mole in the low-temperature range.[109] The viscosity of fused silica,[109] in the temperature range of 1650° to 2000°C, varies from 10^8 to 10^6 poise, respectively. By definition,[110] the softening point of a glass corresponds to a viscosity of $\sim 10^{7.6}$ poise. For fused silica, this temperature is ∿1750°C.[109] A check on the specific volume data of fused silica[109] reveals that, below the softening point, the volume is almost temperature independent and varies from ∿0.454 cm^3/gm at room temperature to only ∿0.456 cm^3/gm at ∿1800°C. Above 1800°C, however, the volume increases significantly reaching a value of ∿0.500 cm^3/gm at 2000°C. Thus, the loosening of the network structure above the softening point relates closely to the changes in activation energy both for viscous flow and diffusion; the

formation of an open structure would be the primary cause of the decrease in the activation energies.

The decrease in activation energy with increasing alumina content, however, cannot be attributed to the formation of a looser structure since, on the contrary, with formation of triclusters and AlO_6 groups a closer mode of oxygen packing is realized. It may then only be suggested that the lowering of the activation energy with alumina addition appears to be related to the continual increase of the octahedrally coordinated aluminum and thus the formation of non-bridging oxygens.

Let us now consider the diffusion in high alumina melts ($>\sim 45$ mole% Al_2O_3) where the continuous oxygen network structure of silica is completely broken down. Just as the structure of fused silica is closely related to that of its crystalline forms, it is possible to postulate that the structure of a melt containing 60 mole% Al_2O_3 is a randomized version of mullite structure. The characteristic feature of the mullite structure consists of columns of edge-sharing AlO_6 units linked through AlO_4 and SiO_4 tetrahedra, similar to that of sillimanite shown in Fig. 35. The structure of the corresponding liquid phase, then, may be visualized as a dissociated structure consisting of chains of edge-sharing AlO_6 groups and discrete anionic groups of tetrahedrally coordinated aluminum and silicon. Diffusion in this structure does not necessarily have to involve the breaking of the M-O bonds but could easily take place by the cooperative movement of AlO_4 and SiO_4 groups through a ring mechanism involving only coulombic interaction. The activation energies as low as 42 kcal/mole at 63 mole% Al_2O_3, then, are in agreement with this model. Increase in silica content causes

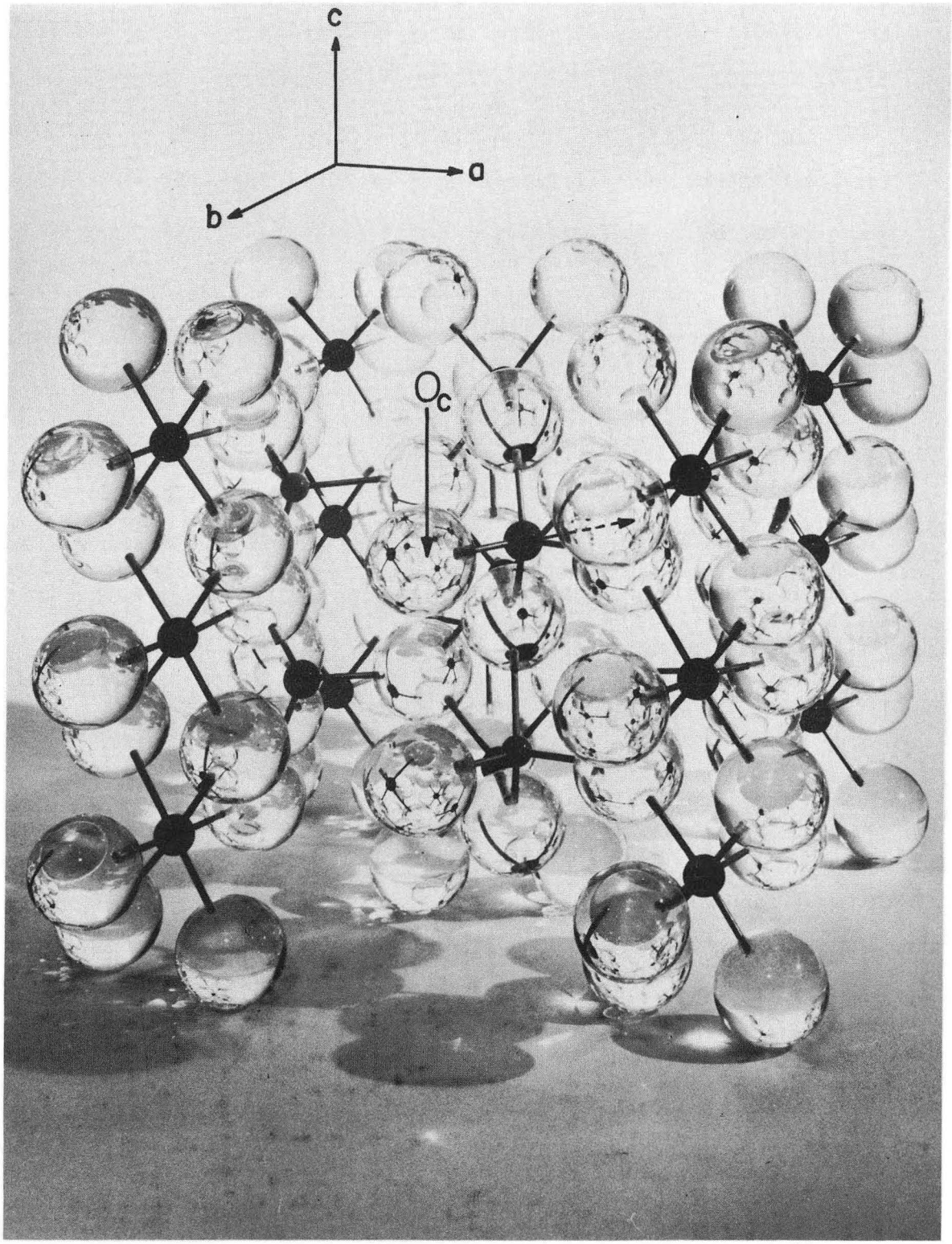

XBB 729-4749A

Fig. 35. Model of sillimanite ($Al_2O_3 \cdot SiO_2$) unit cell. Light gray and small spheres represent silicon.

the polymerization of the SiO_2^{2-} tetrahedra to form larger units of $Si_3O_9^{6-}$, $Si_4O_{12}^{8-}$, etc.[103] and subsequently a continuous three-dimensional network type structure. The gradual increase of activation energy with silica content, then, is also in agreement with the gradual increase in size of the diffusing anionic units.

C. Diffusion Mechanism in Mullite

The structure of mullite[111-113] is a derivative of the sillimanite ($Al_2O_3 \cdot SiO_2$) structure. The sillimanite structure[114] (Fig. 35) consists of chains of slightly distorted Al-O octahedra which run parallel to the c axis and are linked by double chains of Al-O and Si-O tetrahedra. The distribution of the tetrahedrally coordinated aluminum and silicon atoms is ordered, and each double chain may be thought of as a continuous series of four-membered rings, with each ring containing two silicon and two aluminum tetrahedra in the sequence Si-Al-Si-Al.

To derive the mullite structure from that of sillimanite and thus adjust the alumina/silica ratio from 1:1 to 3:2, an average of 0.5 silicon atom per sillimanite unit cell is replaced by 0.5 aluminum atom at random. The preservation of electro-neutrality demands the removal of 0.25 oxygen atoms from the positions O_C, linking the Si and Al tetrahedra (Fig. 35). Since the adjoining tetrahedra would then remain open, the corresponding central atoms are transferred from their original Al, Si positions into new tetrahedral sites previously unfilled in sillimanite. The direction of this shift is indicated by the broken arrow in Fig. 35.

The "derivation" of the mullite structure from that of sillimanite is illustrative of the possible diffusion mechanism in a mullite layer ranging in composition from 70.5 to 74.0 wt% Al_2O_3. Under such a concentration gradient, the diffusion of aluminum from a high-alumina structure to a low-alumina one requires the replacement of tetrahedrally coordinated silicon by aluminum. In order to maintain charge-neutrality, the substitution of four Al^{3+} for three Si^{4+} results in the formation of one cation vacancy. Due to the lack of self-diffusion data on the individual ions, it is difficult to postulate the exact diffusion mechanism. In either case, however, the apparent activation energy of 168 kcal/mole, again, reflects the high bond energies of tetrahedrally coordinated silicon and aluminum. Furthermore, this activation energy for diffusion is in excellent agreement with the activation energy for creep of mullite.[115,116]

VI. CONCLUSIONS

Diffusion studies in the SiO_2-Al_2O_3 system, in the temperature range of 1678° to 2003°C, yielded information on (1) stable and metastable phase equilibria and (2) diffusion kinetics in aluminum-silicate melts and mullite ($3Al_2O_3 \cdot 2SiO_2$).

The dissolution of alumina in fused silica and the growth of interfacial mullite were diffusion-controlled. The interfacial compositions of the phase boundaries, thus, corresponded to the equilibrium liquidus and solidus compositions and were used to construct the equilibrium SiO_2-Al_2O_3 phase diagram. The equilibrium phase diagram indicates the incongruent melting of mullite at 1828±10°C, as originally determined by Bowen and Greig.[10] The incongruency of mullite was also supported by the static method of quenching experiments.

The stable solid solution range of mullite was at 70.5 to 74.0 wt% Al_2O_3 below 1753°C and at 71.8 to 74.0 wt% Al_2O_3 at 1813°C.

The examination of the diffusion zone microstructures and the microstructures of the specimens heat treated by the static method of quenching yielded additional information on the metastable equilibria. Due to the supercooling of the aluminum-silicate melts below the alumina liquidus and the peritectic temperature, precipitation of only mullite was realized, without any alumina precipitation. When the specimens were cooled slowly or sites for heterogeneous nucleation of alumina were available, alumina did precipitate as predicted by the stable SiO_2-Al_2O_3 phase diagram. The extension of the alumina liquidus below the transition temperature provided direct evidence for the

metastable existence of a SiO_2-Al_2O_3 binary phase diagram without any mullite phase.

Stoichiometric mullite of 71.8 wt% Al_2O_3 composition melted congruently at 1880±10°C due to the metastable extension of the silica-mullite binary equilibrium above the peritectic transition temperature. This metastable extension of the silica-mullite binary diagram above the incongruent melting temperature of mullite successfully explains the formation of high-alumina mullites, ranging in composition up to 83.2 wt% Al_2O_3, only when they are precipitated from a melt.

The activation energy for diffusion in the aluminum-silicate melts, above the softening temperature of fused silica, decreased from 211 kcal/mole for pure silica to 42 kcal/mole at 63 mole% Al_2O_3. This substantial change in activation energy for diffusion is attributed to the gradual increase in the ratio of AlO_6/AlO_4 groups with increasing alumina content and thus the formation of non-bridging oxygens. Below the softening point, the activation energy for diffusion in fused silica increases to 338 kcal/mole due to the tightening of the network structure. At 45 mole% Al_2O_3 content, the continuous network structure of fused silica is completely broken down to form discrete anionic groups. High activation energies in fused silica and high-silica melts are attributed to the rupture of M-O bonds of tetrahedrally coordinated silicon and aluminum. Diffusion in high alumina liquids, on the other hand, is by mutual rotation of anionic groups involving only coulombic interaction and thus requires a lower activation energy. The structural model for the SiO_2-Al_2O_3 melts is further supported by the viscosity and density data.

An activation energy of 168±7 kcal/mole was determined for diffusion in mullite.

ACKNOWLEDGEMENTS

Professor Joseph A. Pask supervised the project and, throughout the author's graduate studies, acted as a constant source of inspiration and encouragement for which the author is very grateful. Colleagues and friends, in particular, Robert F. Davis and Carl E. Hoge were always helpful in the discussion of problems at hand.

Professors Leo Brewer, Alan W. Searcy and John Chipman critically read and commented on the manuscript.

Grateful acknowledgements are extended to the support staff of the Inorganic Materials Research Division of Lawrence Berkeley Laboratory who assisted the project in many ways. Special thanks are due George J. Georgakopoulos (electron beam microprobe analysis), Donald K. Whitaker and Wilbur Bullis (cricible fabrication and equipment design), Jack N. Wodei (electronic equipment), Neal W. Holding and Lee R. Johnson (ceramography), Gloria C. Pelatowski (technical drawing), Phila J. Witherell and Douglas P. Kreitz (photography), Norman Gardner and Victor F. Draper (data reduction), Kelly Radmilovic and Jean A. Wolslegel (manuscript preparation).

This research was performed under the auspices of the U. S. Atomic Energy Commission through the Inorganic Materials Research Division of the Lawrence Berkeley Laboratory.

APPENDIX: COMPUTER PROGRAM FOR BOLTZMANN-MATANO ANALYSIS

```
      PROGRAM SNARL (INPUT,OUTPUT,TAPE7,TAPE98,PLOT,TAPE99=PLOT)
      COMMON /CCPOOL/ XMIN,XMAX,YMIN,YMAX,CCXMIN,CCXMAX,CCYMIN,CCYMAX
      DIMENSION XX(1000), YY(1000)
      DIMENSION X(2000),Y(2000),ID(5)
      XRANGE = CCXMAX-CCXMIN
      CCXMAX = CCXMIN + 2.*XRANGE
  300 READ 10, K,N,ARBX,XIN,      ID
   10 FORMAT (I1,I9,2F10.5,5A8)
      PRINT 10, K,N,ARBX, XIN, ID
      IF (N.LE.0) GO TO 400
      READ100,T
  100 FORMAT(E12.5)
      READ30, (X(I),Y(I), I=1,N)
   30 FORMAT(12F6.0)
      IF (K.EQ.1) 90,1090
   90 CONTINUE
      M=0
      DO 13 I=1,N
      J=I+N
      X(J)=ABS(X(I)-ARBX)
      IF (X(I).LT.ARBX) 11,12
   11 Y(J) =2.098 - Y(I)
      M=M+1
      GO TO 13
   12 Y(J)=Y(I)
   13 CONTINUE
      K=2*N+1
      Y(K) =2.098 - Y(M+N)
      A1=.5*(Y(N+2)-Y(N+1))*(X(N+1)+X(N+2))
      A2=.5*(Y(K)-Y(N+M+1))*(X(M+N)+X(M+N+1))
      NNN=2*N
      MN1=M+N+1
      M2=N+M-1
      N1=N+1
      NN=(2*N)-1
      N3=(2*N)-2
      MM=M2-1
      DO 50 J=N1,M2
      A1=A1+.5*(Y(J+1)-Y(J))*(X(J+1)+X(J))
   50 CONTINUE
      DO 60 J=MN1,NN
      A2=A2+.5*(Y(J)-Y(J+1))*(X(J+1)+X(J))
   60 CONTINUE
      IF (A1.GE.A2) 70,80
   80 ARBX=ARBX+XIN
      GO TO 90
   70 PRINT75, ID,ARBX
   75 FORMAT(1H1,20X,5A8//,5X,*THE BOLTZMANN-MATANO INTERFACE IS LOCATED
     XAT X=*,F10.5,*       MICRONS*///)
      PRINT200, T
  200 FORMAT(5X,*TIME=*,E12.5,*      SECONDS*//)
      PRINT201
  201 FORMAT(7X,*INPUT DATA*/,7X,*MICRONS*,10X,*CONCENTRATION AL*//)
      DO 202 I=1,N
  202 PRINT203, X(I),Y(I)
  203 FORMAT(2(5X,F10.5))
      DO 5 J=N1,NNN
    5 X(J)=X(J)*1.E-4
      PRINT116
  116 FORMAT(1H1,5X,*DIST/INTERFACE        CONCENTRATION        DX/DC
     X  AREA              DIFFUSIVITY*/, 10X,*CM              AL ATOM*///)
```

```
      A3=.5*(Y(N+2)-Y(N+1))*(X(N+1)+X(N+2))
      A4=.5*(Y(K)-Y(N+M+1))*(X(M+N)+X(M+N+1))
      SNEW=(Y(N+1)-Y(N+2))/(X(N+2)-X(N+1))*(-1.)
      KN1=MM-N1+1
      WRITE(7,140) KN1
      IGO = 0
      I = 1
      DO 110 J=N1,MM
      A3=A3+.5*(Y(J+1)-Y(J))*(X(J+1)+X(J))
      SOLD=SNEW
      SNEW=(Y(J+1)-Y(J+2))/(X(J+2)-X(J+1))*(-1.)
      SL=2./(SOLD+SNEW)
      D=-.5*SL*A3/T
      RY =2.098 - Y(J)
      PRINT115, X(J),RY,SL,A3,D
  115 FORMAT(5(5X,E12.5))
      XX(I) = RY
      YY(I) = ALOG10(D)
      I = I + 1
      WRITE(7,130) RY,D
  130 FORMAT(2E12.5)
  140 FORMAT(I10)
  110 CONTINUE
 145  CONTINUE
      NY = I - 1
      XMIN = 0.
      XMAX = 1.5
      YMAX = -4.
      YMIN = YY(1)
      DO150 I=2,NY
      IF( YY(I) .LT. YMIN ) YMIN = YY(I)
 150  CONTINUE
      IF( YMIN .GT. -9. ) GO TO 155
      YMIN = -14.
      GO TO 160
 155  CONTINUE
      YMIN = -9.
 160  CONTINUE
      CALL CCGRID( 1, 15, 6HLABELS, 1 )
      XC = XMIN + .001*(XMAX-XMIN)
      NC = IFIX( YMAX-YMIN+.001 )
      DO164 I=1,9
      YC = YMIN + ALOG10( FLOAT(I) )
      DO163 J=1,NC
      CALL CCPLOT( XC, YC, 1, 6HNOJOIN, 2, 1 )
      YC = YC + 1.
 163  CONTINUE
 164  CONTINUE
      CALL CCPLOT( XX, YY, NY, 6HNOJOIN, 6, 1 )
      CALL CCNEXT
      IF( YMIN .LT. -10. ) GO TO 165
      YMIN = -14.
      GO TO 160
 165  CONTINUE
      PRINT401
  401 FORMAT(1H1,///)
      IF( IGO .EQ. 1 ) GO TO 1115
      SNEW=((Y(M+N+1)-Y(K))/(X(M+1)-X(M)))*1.E+4
      KN2=N3-MN1+1
      WRITE(7,140) KN2
      DO 120 J=MN1,N3
      A4=A4+.5*(Y(J)-Y(J+1))*(X(J+1)+X(J))
```

```
      A5=A2*1.E-4-A4
      SOLD=SNEW
      SNEW=(Y(J+2)-Y(J+1))/(X(J+2)-X(J+1))
      SL=2./(SOLD+SNEW)
      D=-.5*SL*A5/T
      RY=Y(J)
      PRINT115, X(J),RY,SL,A5,D
      WRITE(7,130) RY,D
  120 CONTINUE
      GO TO 300
CC
CC
CCC  THE FOLLOWING IS THE MIRROR IMAGE OF SNARL WHICH IS USED FOR PROFILES WHICH
CCCC  HAVE A POSITIVE SLOPE
CC
CC
 1090 CONTINUE
      M=0
      DO 1013 I=1,N
      J=I+N
      X(J)=ABS(X(I)-ARBX)
      IF (X(I).GE.ARBX) 1011,1012
 1011 Y(J) =2.098 - Y(I)
      GO TO 1013
 1012 Y(J)=Y(I)
      M=M+1
 1013 CONTINUE
      K=2*N+1
      Y(K) =2.098 - Y(M+N)
      A1=.5*(Y(N+2)-Y(N+1))*(X(N+1)+X(N+2))
      A2=.5*(Y(K)-Y(N+M+1))*(X(M+N)+X(M+N+1))
      NNN=2*N
      MN1=M+N+1
      M2=N+M-1
      N1=N+1
      NN=(2*N)-1
      N3=2*N-2
      MM=M2-1
      DO 1050 J=N1,M2
      A1=A1+.5*(Y(J+1)-Y(J))*(X(J+1)+X(J))
 1050 CONTINUE
      DO 1060 J=MN1,NN
      A2=A2+.5*(Y(J)-Y(J+1))*(X(J+1)+X(J))
 1060 CONTINUE
      IF (A1.GE.A2) 1070,1080
 1080 ARBX=ARBX+XIN
      GO TO 1090
 1070 PRINT75, ID,ARBX
      PRINT200, T
      PRINT201
      DO 1202 I=1,N
 1202 PRINT203, X(I),Y(I)
      DO 1005 J=N1,NNN
 1005 X(J)=X(J)*1.E-4
      PRINT116
      A3=.5*(Y(N+2)-Y(N+1))*(X(N+1)+X(N+2))
      A4=.5*(Y(K)-Y(N+M+1))*(X(M+N)+X(M+N+1))
      SNEW=(Y(N+2)-Y(N+1))/(X(N+2)-X(N+1))*(-1.)
      KN1=MM-N3+1
      WRITE(7,140) KN1
      I = 1
      IGO = 1
```

```
      DO 1110 J=N1,MM
      A3=A3+.5*(Y(J+1)-Y(J))*(X(J+1)+X(J))
      SOLD=SNEW
      SNEW=(Y(J+2)-Y(J+1))/(X(J+2)-X(J+1))*(-1.)
      SL=2./(SOLD+SNEW)
      D=.5*SL*A3/T
      RY=Y(J)
      PRINT115, X(J),RY,SL,A3,D
      WRITE(7,130) RY,D
      XX(I) = RY
      YY(I) = ALOG10(D)
      I = I + 1
 1110 CONTINUE
      GO TO 145
 1115 CONTINUE
      SNEW=((Y(K)-Y(N+M+1))/(X(M+1)-X(M)))*1.E+4
      KN2=N3-MN1+1
      WRITE(7,140) KN2
      DO 1120 J=MN1,N3
      A4=A4+.5*(Y(J)-Y(J+1))*(X(J+1)+X(J))
      A5=A2*1.E-4-A4
      SOLD=SNEW
      SNEW=(Y(J+1)-Y(J+2))/(X(J+2)-X(J+1))
      SL=2./(SOLD+SNEW)
      D=.5*SL*A5/T
      RY =2.098 - Y(J)
      PRINT115, X(J),RY,SL,A5,D
      WRITE(7,130) RY,D
 1120 CONTINUE
      GO TO 300
  400 ENDFILE 7
      CALL CCEND
      STOP
      END
```

```
      PROGRAM COREL (INPUT,OUTPUT,TAPE7)
      REAL KKN
      DIMENSION Y(2000),D(2000),DEV(2000),ID(10)
      DIMENSION DEVY(2000),T(500)
      DATA (T(I),I=1,500)/12.7,4.30,3.18,2.78,2.57,2.45,2.36,2.31,2.26,
     A2.23,2.20,2.18,2.16,2.14,2.13,2.12,2.11,2.10,2*2.09,2.08,2*2.07,
     B3*2.06,3*2.05,3*2.04,5*2.03,7*2.02,10*2.01,20*2.00,30*1.99,40*1.98
     C,50*1.97,305*1.96/
  800 READ100, NPROB,ID
  100 FORMAT(I10,10A7)
      IF (NPROB.LE.0) GO TO 900
      READ(7,200) KN
  200 FORMAT(I10)
      READ(7,300) (Y(I),D(I), I=1,KN)
  300 FORMAT(2E12.5)
      M=0
      KKN=FLOAT(KN)
      IF (KKN.GT.40.) 1,2
    1 KKN=KKN-10.
      NK=KN-5
      MK=6
      GO TO 700
    2 MK=1
      NK=KN
  700 CONTINUE
      NKN=NK-MK+1
      SDEVY=0.
      SIG2=0.
      SDEVSQ=0.
      SUMDEV=0.
      SUMY=0.
      SUMD=0.
      SUMYD=0.
      SUMYY=0.
      SUMDD=0.
      DO 400 I=MK,NK
      SUMY=SUMY+Y(I)
      SUMD=SUMD+D(I)
      SUMYD=SUMYD+Y(I)*D(I)
      SUMYY=SUMYY+Y(I)**2
      SUMDD=SUMDD+D(I)**2
  400 CONTINUE
      A=(SUMD*SUMYY-SUMYD*SUMY)/(KKN*SUMYY-SUMY**2)
      B=(KKN*SUMYD-SUMD*SUMY)/(KKN*SUMYY-SUMY**2)
      AVD=SUMD/KKN
      AVY=SUMY/KKN
      DO 1000 I=MK,NK
      SIG2=SIG2+(B*Y(I)+A-D(I))**2/KKN
      DEV(I)=ABS(AVD-D(I))
      SDEVSQ=SDEVSQ+DEV(I)**2
      DEVY(I)=ABS(AVY-Y(I))
      SDEVY=SDEVY+DEVY(I)**2
 1000 CONTINUE
      SIGB=SQRT(KKN*SIG2/(KKN*SUMYY-SUMY**2))
      SIGA=SQRT(SIG2*SUMYY/(KKN*SUMYY-SUMY**2))
      SDEVD=SQRT(SDEVSQ/(KKN-1.))
      SDEVY=SQRT(SDEVY/(KKN-1.))
      R=B*SDEVY/SDEVD
      TS=ABS(B)*SDEVY*SQRT(KKN-2.)/SDEVD/SQRT(1.-R**2)
      IF (M.EQ.0) 401,402
  401 PRINT500, ID,R,KN,AVD,SDEVD
```

```
  500 FORMAT(1H1/,10A7///,*CORRELATION COEFFICIENT FOR LINEAR RELATIONSH
     *IP =*,F10.5/,*NO. OF PAIRS OF POINTS INVOLVED =*,I10/,*AVERAGE DIF
     *FUSIVITY =*,E12.5/,*WITH STANDARD DEVIATION OF *,E12.5////)
      PRINT1100, A, SIGA,B,SIGB
 1100 FORMAT(*D=DIFFUSIVITY, Y=MOLE FRACTION OF DIFFUSING CATION*/,*IN T
     1HE FORMULA  D=A+BY*/,*A=*,E12.5,* PLUS OR MINUS*,E12.5/,*B=*,E12.5
     2,* PLUS OR MINUS*,E12.5)
      PRINT1200, TS,T(NKN-2)
 1200 FORMAT(*THE T-STATISTIC=*,E12.5/,*THE T-STATISTIC FOR A 5 PCT. SIG
     1NIFICANCE LEVEL=*,E12.5//////)
  402 M=M+1
      IF (M.EQ.1) 501,502
  501 CONTINUE
      DO 600 I=1,KN
      D(I)=ALOG(ABS(D(I)))
  600 CONTINUE
      GO TO 700
  502 PRINT503, R,KN
  503 FORMAT(*CORRELATION COEFFICIENT FOR EXPONENTIAL RELATIONSHIP =*,
     * F10.5/,*NO. OF PAIRS OF POINTS INVOLVED =*,I10)
      PRINT1101, A,SIGA,B,SIGB
 1101 FORMAT(////,*IN THE FORMULA  LN D=LN A + BY*/,*LN A=*,E12.5,* PLUS
     1 OR MINUS*,E12.5/,*B=*,E12.5,* PLUS OR MINUS*,E12.5)
      AA=EXP(A)
      PRINT1102,AA
 1102 FORMAT(*A=*,E12.5)
      PRINT1200, TS,T(NKN-2)
      GO TO 800
  900 STOP
      END
```

```
      PROGRAM DRIPY (INPUT,OUTPUT,TAPE7,TAPE98,PLOT,TAPE 99 = PLOT)
      DIMENSION D(2000),Y(2000)
      DIMENSION IBCD(7)
    5 READ10,NS,SAMPLE
   10 FORMAT(I5,A7)
      IF (NS.LE.0) GO TO 50
      ENCODE (20,1000,IBCD) SAMPLE
 1000 FORMAT(11HSAMPLE NO. ,A7)
      IBCD(7)=0
      READ(7,15)NO
   15 FORMAT(I10)
      READ(7,20)(Y(I),D(I),I=1,NO)
   20 FORMAT(2E12.5)
      CALL GRAPH (Y,D,NO,IBCD,13HCONCENTRATION,11HDIFFUSIVITY)
      GO TO 5
   50 CALL CCEND
      STOP
      END
```

```
      SUBROUTINE GRAPH(X,Y,N,RG,RX,RY)
      COMMON/CCPOOL/XMIN,XMAX,YMIN,YMAX,CCXMIN,CCXMAX,CCYMIN,CCYMAX
      DIMENSION ROUND(4),X(1),Y(1)
      DIMENSION YSC(2)
      DATA (ROUND(I),I=1,4)/1.,2.,2.5,5./
      DATA NROUND,PART/4,10./
      YSC(1)=Y(1)
      YSC(2)=Y(1)
      DO 101 I=1,N
      IF (Y(I).GT.YSC(1)) YSC(1)=Y(I)
      IF (Y(I).LT.YSC(2)) YSC(2)=Y(I)
  101 CONTINUE
      CCXMIN=200.$CCXMAX=3200.$CCYMIN=200.$CCYMAX=1000.
      WRITE (99,9900)
 9900 FORMAT (*$PLEASE POSITION PEN*/1H=)
      CALL LINEUP(X,N,ROUND,NROUND,PART,XMIN,XMAX)
      CALL LINEUP(YSC,2,ROUND,NROUND,PART,YMIN,YMAX)
      XMIN = 0
      XMAX = .150
      CALL CCGRID(1,IFIX(PART),6HNOLBLS,1,IFIX(PART))
      CALL CCLBL(IFIX(PART),IFIX(PART))
      CALL CCLTR(210.,50.,0,3,RG,18)
      CALL CCLTR(1300.,100.,0,3,RX,13)
      CALL CCLTR(230.,475.,1,3,RY,11)
      CALL CCPLOT(X,Y,N,6HNOJOIN,8,1)
      CALL CCPLOT(XMAX,YMIN,1,6HNOJOIN,0,1)
      CALL CCLTR(CCXMAX,0.,0,1,1H ,1)
      CALL CCNEXT
      RETURN
      END
```

```
      SUBROUTINE CCLBL(NX1,NY1)
      COMMON/CCPOOL/XMIN,XMAX,YMIN,YMAX,CCXMIN,CCXMAX,CCYMIN,CCYMAX
      COMMON/CCFACT/FACTOR
      ISZERO=0
      XD=XMAX-XMIN            $YD=YMAX-YMIN
      CCXD=CCXMAX-CCXMIN      $CCYD=CCYMAX-CCYMIN
      XI=XD/FLOAT(NX1)        $YI=YD/FLOAT(NY1)
    8 KSIZE = 2                  $KORIENT = 0
C     LABEL FROM RIGHT TO LEFT ALONG THE X-AXIS.
10    DO 16 NX=ISZERO,NX1
      CCX=CCXMAX-CCXD*FLOAT(NX)/FLOAT(NX1)
      X=(CCX-CCXMIN)*XD/CCXD+XMIN
C     SET X TO A TRUE ZERO IF X=0. TO WITHIN MACHINE ACCURACY.
      IF(ABS(X/XI).LT.1.0E-6)X=0.
      WRITE(98,27)X
16    CALL CCLTR(CCX-32.*FLOAT(KSIZE)/FACTOR,
     1CCYMIN-10.*FLOAT(KSIZE)/FACTOR,KORIENT,KSIZE)
   18 KSIZE = 2                  $KORIENT = 0
C     LABEL UPWARD ALONG THE Y-AXIS.
20    DO 26 NY=ISZERO,NY1
      CCY=CCYMIN+CCYD*FLOAT(NY)/FLOAT(NY1)
      Y=(CCY-CCYMIN)*YD/CCYD+YMIN
C     SET Y TO A TRUE ZERO IF Y=0. TO WITHIN MACHINE ACCURACY.
      IF(ABS(Y/YI).LT.1.0E-6)Y=0.
      WRITE(98,27)Y
26    CALL CCLTR(CCXMIN-70.*FLOAT(KSIZE)/FACTOR,CCY,KORIENT,KSIZE)
27    FORMAT(E10.2)
      RETURN
      END
```

REFERENCES

1. J. Crank, The Mathematics of Diffusion (Oxford University Press, London, 1967).
2. W. Jost, Diffusion in Solids, Liquids and Gases (Academic Press, New York, 1969).
3. P. G. Shewmon, Diffusion in Solids (McGraw Hill Book Co., Inc., New York, 1963).
4. L. A. Girifalco, Atomic Migration in Crystals (Blaisdell Publ. Co., New York, 1964).
5. J. R. Manning, Diffusion Kinetics for Atoms in Crystals (D. Van Nostrand Co., Inc., New Jersey, 1968).
6. C. P. Flynn, Point Defects and Diffusion (Oxford University Press, London, 1972).
7. J. E. Dorn, J. T. Gier, L. M. K. Boelter and N. F. Ward in Symposium on Surface Treatment of Metals (Am. Soc. Metals, Cleveland, Ohio, 1941) p. 166.
8. N. Swindells, J. Inst. Metals 90 [5], 167 (1962).
9. J. M. Short and R. Roy, J. Am. Ceramic Soc. 47 [3], 149 (1964).
10. N. L. Bowen and J. W. Greig, J. Am. Ceramic Soc. 7 [4], 238 (1924). [5], 410 (1924).
11. W. H. Bauer, I. Gordon and C. H. Moore, J. Am. Ceramic Soc. 33 [4], 140 (1950).
12. N. A. Toropov and F. Y. Galakhov, Doklady Akad. Nauk SSSR 78 [2], 299 (1951) (in Russian).

13. N. E. Filonenko and I. V. Lavrov, Doklady Akad. Nauk SSSR 89 [1], 141 (1953) (in Russian).

14. K. Konopicky, Bull. Fr. Ceram. Soc. [33], 3-6 (1956) (in French).

15. G. Trömel, L.-H. Obst, K. Konopicky, H. Bauer and I. Patzak, Ber. Dtsch. Keram. Ges. 34 [12], 397 (1957) (in German).

16. G. Trömel, The Physical Chemistry of Steel-Making, J. F. Elliott, ed.(MIT Press, New York, 1958).

17. J. H. Welch, Nature 186 [4724], 545 (1960).

18. J. H. Welch, Observations on Composition and Melting Behavior of Mullite, Trans. 7th Int. Ceramic Congress, London, 1960, p. 197.

19. K. Konopicky, Ber. Dtsch. Keram. Ges. 40 [5] 286 (1963) (in German).

20. H. R. Müller, Ber. Dtsch. Keram. Ges. 40 [5], 316 (1963) (in German).

21. T. Horibe and S. Kuwabara, Bull. Chem. Soc. Japan 40 [4], 972 (1967).

22. P. P. Budnikov, S. G. Tresvyatski and V. I. Kushakovski, Doklady Akad. Nauk SSSR 93 [2] 281, (1953) (in Russian).

23. F. Y. Galakhov, Bull. Fr. Ceramic Soc. [38], 11 (1958) (in French).

24. S. Aramaki and R. Roy, J. Am. Ceramic Society 42 [12], 644 (1959).

25. S. Aramaki and R. Roy, Nature 184 [4686], 631 (1959).

26. S. Aramaki and R. Roy, J. Am. Ceramic Soc. 45 [5], 229 (1962).

27. N. A. Toropov and F. Y. Galakhov, The Al_2O_3-SiO_2 System, Eksperiment V Tekhn. Mineralog. i Petrogr., po Materialam Soveshch., 7th, Lvov, 1966, p. 3 (in Russian).

28. G. Rehfeld and H. E. Schwiete, Ber. Dtsch. Keram. Ges. 48 [6] 258 (1971) (in German).

29. J. W. Greig, Am. J. Science 13, 1 and 133 (1927). Also, see the review by R. B. Rosman, The Phases of Silica (Rutgers University Press, New Jersey, 1965) p. 156.

30. S. J. Schneider and C. L. McDaniel, J. Res. NBS 71A [4], 317 (1967).

31. H. Salmang, Ceramics, Physical and Chemical Fundamentals (Butterworths, London, 1961) p. 105.

32. J. Grofcsik, Mullite, Its Structure, Formation and Significance, (Publ. House Hungarian Acad. Sci., Budapest, 1961) p. 31.

33. H. Müller-Hesse, Ber. Dtsch. Keram. Ges. 40 [5], 281 (1963) (in German).

34. W. Eitel, Silicate Science (Academic Press, New York, 1965) Vol. 3, p. 205.

35. R. F. Davis and J. A. Pask, High Temperature Oxides, A. M. Alper, ed. (Academic Press, New York, 1971) Vol. 4, p. 37.

36. J. B. Macchesney and P. E. Rosenberg, Phase Diagrams, Materials Science and Technology, A. M. Alper, ed. (Academic Press, New York, 1970) Vol. 1, p. 113.

37. N. L. Bowen, The Evolution of the Igneous Rocks (Dover Publications, Inc., New York, 1956) p. 25.

38. W. Eitel, Silicate Melt Equilibria (Rutgers University Press, New Jersey, 1951).

39. B. Chalmers, H. E. LaBelle, Jr. and A. I. Mlavsky, Mat. Res. Bull. 6 [8], 681 (1971).

40. T. P. Jones, J. Australian Ceramic Society 5 [2], 41 (1969).

41. R. F. Charvat, (Union Carbide Corp., Crystal Products, San Diego, Calif.), private communication, 1972.

42. R. F. Davis and J. A. Pask, J. Am. Ceramic Society 55 [10], 525 (1972).

43. L. S. Darken, Trans. AIME 175, 184 (1948).

44. A. R. Cooper, Jr. and J. H. Heasley, J. Am. Ceramic Society 49 [5], 280 (1966).

45. L. Boltzmann, Ann. der Phys. und Chem., Neue Folge 53 [13], 959 (1894) (in German).

46. C. Matano, Jap. J. Phys. 8 [3], 109 (1933).

47. W. Jost, Zeit. Physik 127 [3], 163 (1950) (in German).

48. M. Appel, Scripta Met. 2 [4], 217 (1968).

49. G. B. Gibbs, J. Nucl. Mater. 20 [3], 303 (1966).

50. C. V. Kidson, J. Nucl. Mater. 3 [1], 21 (1961).

51. S. L. Blank, Scripta Met. 4 [5], 349 (1970).

52. C. Wagner, presented in Ref. 2, Chapter 1, Appendix 4.

53. S. Arrhenius, Z. Physik. Chem. 4 [2], 226 (1889) (in German).

54. S. Glasstone, K. J. Laidler and H. Eyring, The Theory of Rate Processes (McGraw-Hill Book Co., New York, 1941).

55. F. D. Rossini, J. Chem. Thermodynamics 2, 447 (1970).

56. W. L. DeKeyser, Science of Ceramics, G. H. Stewart, ed. (Academic Press, London, 1965) p. 243.

57. W. G. Staley, Jr. and G. W. Brindley, J. Am. Ceramic Society 52 [11], 616 (1969).

58. K. S. Mazdiyasni and L. M. Brown, J. Am. Ceramic Society 55 [11], 548 (1972).

59. R. Theisen, Quantitative Electron Microprobe Analysis (Springer-Verlag, Inc., New York, 1965).

60. K. F. J. Henrich, ed., Quantitative Electron Probe Microanalysis, NBS Special Publication 298, Superintendent of Documents, U. S. Government Printing Office, Washington, D. C., 1968.

61. J. F. MacDowell and G. H. Beall, J. Am. Ceramic Society 52 [1], 17 (1969).

62. J. J. Rasmussen and R. P. Nelson, J. Am. Ceramic Society 54 [8], 398 (1971).

63. J. B. Conway and A. C. Losekamp. Trans. AIME 236 [5], 702 (1966).

64. J. Z. Frazer, R. W. Fitzgerald and A. M. Reid, Computer Programs EMX and EMX2 for Electron Microprobe Data Processing, Scripps Institution of Oceanography, University of California, San Diego, LaJolla, California.

65. M. Appel (Lawrence Berkeley Laboratory, University of California, Berkeley, California), personal communication, 1968.

66. J. L. Bates, C. E. McNeilly and J. J. Rasmussen, Materials Science Research, Vol. 5: Ceramics in Severe Environments, W. W. Kreigel and H. Palmour, III, eds. (Plenum Press, New York, 1971) p. 11.

67. H. V. Wartenbert, G. Wehner and E. Saran, Nachr. Ges. Wiss. Göttingen, Jahresber. Geschäftjahr, Math.-Physik. Klasse, Fachgruppen II, [N. F.] 2, 73 (1936).

68. W. D. Kingery, J. Am. Ceramic Society 42 [1], 6 (1959).

69. A. D. Kirshenbaum and J. A. Cahill, J. Inorg. Nucl. Chem. 14 [3-4], 283 (1960).

70. B. S. Mitin and Yu. A. Nagibin, Zh. Fiz. Khim. 44 [5], 1325 (1970), or Russ. J. Phys. Chem. 44 [5], 741 (1970).

71. J. J. Rasmussen and R. P. Nelson, J. Am. Ceramic Society 54 [8], 398 (1971).

72. J. B. Wachtman, Jr., T. G. Scuderi and G. W. Cleek, J. Am. Ceramic Society 45 [7], 319 (1962).

73. W. D. Kingery, Introduction to Ceramics (John Wiley and Sons, Inc., New York, 1960) p. 468.

74. J. F. Bacon, A. A. Hasapis and J. W. Wholley, Jr., Phys. and Chem. Glasses 1 [3], 90 (1960).

75. P. R. Bevington, Data Reduction and Error Analysis for the Physical Sciences (McGraw-Hill Book Co., New York, 1969).

76. M. L. Huggins and K.-H. Sun, J. Am. Ceramic Society 26 [1], 4 (1943).

77. Y. Bottinga and D. F. Weill, Am. J. Science 269 [2], 169 (1970).

78. M. L. Huggins, J. Op. Soc. Am. 30 [9], 420 (1940).

79. G. Heidtkamp and K. Endell, Glastech. Ber. 14, 89 (1936).

80. L. Shartsis, S. Spinner and W. Capps, J. Am. Ceramic Society 35 [6], 155 (1952).

81. J. O'M. Bockris, J. W. Tomlinson and J. L. White, Trans. Faraday Soc. 52, 299 (1956).

82. P. Tyrolerova and W.-K. Lu, J. Am. Ceramic Society 52 [5], 292 (1969).

83. P. Tyrolerova and W.-K. Lu, J. Am. Ceramic Society 52 [2], 77 (1969).

84. R. F. Davis, Diffusion Studies in the Alumina-Silica System (Ph. D. Thesis), UCRL-19644, July 1970.

85. J. F. Schairer and N. L. Bowen, Am. J. Science 253 [12], 681 (1955).

86. W. H. Bauer and I. Gordon, J. Am. Ceramic Society 34 [8], 250 (1951).

87. A. Neuhaus and W. Richartz, Ber. Dtsch. Keram. Ges. 35 [4], 108 (1958) (in German).

88. A. J. Majumdar and J. H. Welch, Trans. Brit. Ceramic Society 62 [8], 603 (1963).

89. W. H. Zachariasen, J. Am. Chem. Soc. 54 [10], 3841 (1932).

90. B. E. Warren, H. Drutter and O. Morningstar, J. Am. Ceramic Society 19 [7], 202 (1936).

91. S. Urnes, Modern Aspects of the Vitreous State, J. D. MacKenzie, ed. (Butterworth, Inc., Washington, D. C., 1960) Vol. 1, p. 10, and J. Zarzycki, Chemical and Mechanical Behavior of Inorganic Materials, A. W. Searcy, D. V. Ragone and U. Colombo, eds. (John Wiley and Sons, Inc., New York, 1970) p. 443-74 give reviews of early critisms.

92. A. J. Leadbetter and A. C. Wright, J. Non-Cryst. Solids 7 [1], 23 (1972).

93. J. H. Konnert, J. Karle and G. A. Ferguson, Science 179 [4069], 177 (1973).

94. L. Pauling, The Nature of the Chemical Bond (Cornell University Press, New York, 1960) p. 546.

95. J. O. Isard, J. Soc. Glass Tech. 43, 113T (1959).

96. D. E. Day and G. E. Rindone, J. Am. Ceramic Society 45 [10], 489 (1962).

D. E. Day and G. E. Rindone, J. Am. Ceramic Society 45 [10], 496 (1962).

D. E. Day and G. E. Rindone, J. Am. Ceramic Society 45 [12], 579 (1962).

97. D. E. Dei and V. E. Steinkamp, Stekloobrazn. Sostoyanie, p. 294-98 and p. 349 (1971) (in Russian). From Ref. Zh., Khim. 1972, Abstr. No. 10B671 and Chem. Abstr., 78 [6], 221 (1973), Abstr. No. 33319Z.

98. E. D. Lacy, Phys. Chem. Glasses 4 [6], 234 (1963).

99. E. F. Riebling, J. Chem. Phys. 44 [8], 2857 (1966).

100. R. Rossin, J. Bersan and G. Urbain, Comptes Rendus Acad. Sc. Paris 258 [2], 562 (1964).

101. B. S. Mitin and Yu. A. Nagibin, Izv. Vyssh. Ucheb. Zaved., Chern. Met. 12 [7], 8 (1969) (in Russian).

102. J. D. MacKenzie, Chem. Review 56 [3], 455 (1956).

103. J. O'M. Bockris, J. D. MacKenzie and J. A. Kitchener, Trans. Faraday Society 51 [12], 1734 (1955).

104. J. D. MacKenzie, Modern Aspects of the Vitreous State, J. D. MacKenzie, ed. (Butterworth, Inc., Washington, D. C., 1960) p. 188-218 provides a detailed review.

105. R. Wardle and G. W. Brindley, Am. Miner. 56 [11/12], 2123 (1971).

106. N. F. Mott and R. W. Gurney, Electronic Processes in Ionic Crystals (Dover Publ., Inc., New York, 1964).

107. S. Glasstone, K. J. Laidler and H. Eyring, The Theory of Rate Processes (McGraw-Hill Book Company, Inc., New York, 1941).

108. K.-H. Sun, J. Am. Ceramic Society 30 [9], 277 (1947).

109. R. Brückner, J. Non-Cryst. Solids 5 [3], 177 (1971).

110. H. R. Lillie, J. Am. Ceramic Society 35 [6], 149 (1952).

111. S. Durović, Kristallografiya 7 [3], 339 (1962) or Soviet Phys.-Crystallography 7 [3], 271 (1962).

S. Durović, Chem. Zvesti 23 [2], 113 (1969).

112. R. Sadanaga, M. Tokonami and Y. Takéuchi, Acta Cryst. 15 [1], 65 (1962).

113. C. W. Burnham, Year-book Carnegie Inst. 62, 158 (1963)
63, 223 (1964).

114. C. W. Burnham. Zeit. Kristal. 118 [1/2], 127 (1963).

115. C. O. Hulse and J. A. Pask, J. Am. Ceramic Society 49 [6], 312 (1966).

116. R. A. Penty and D. P. H. Hasselman, Mat. Res. Bull. 7 [10], 1117 (1972).

LEGAL NOTICE

This report was prepared as an account of work sponsored by the United States Government. Neither the United States nor the United States Atomic Energy Commission, nor any of their employees, nor any of their contractors, subcontractors, or their employees, makes any warranty, express or implied, or assumes any legal liability or responsibility for the accuracy, completeness or usefulness of any information, apparatus, product or process disclosed, or represents that its use would not infringe privately owned rights.

TECHNICAL INFORMATION DIVISION
LAWRENCE BERKELEY LABORATORY
UNIVERSITY OF CALIFORNIA
BERKELEY, CALIFORNIA 94720

AAF421
LBL Libraries